University of Alberta

Application of PBI Membrane Polymer Fuel Cell for Conversion of Hydrocarbon

by

Chin Kui Cheng ©

A thesis submitted to the Faculty of Graduate Studies and Research in partial fulfillment
of the requirements for the degree of Master of Science

in

Chemical Engineering

Department of Chemical and Materials Engineering

Edmonton, Alberta, Canada
Fall, 2004

Canadä

ACKNOWLEDGEMENTS

I would like to take this opportunity to express my sincere gratitude to my supervisors, Professors Karl T. Chuang and Jingli Luo, for their patience, technical guidance as well as financial support throughout my studies in University of Alberta.

I would like to thank Dr. A. R. Sanger for taking some time off to proof-read my thesis and giving me valuable advice and guidance during the writing.

I am also extremely indebted to the following colleagues in Fuel Cell Group: Mr. Jianjun Chen, Ms. Weizhu An, Dr. Guolin Wei, Dr. Juri Melnik and Dr. Man Liu for being so helpful and always giving me constructive ideas.

And finally, I would like to thank my family who always support and encourage me. Without their moral support, this work would never be possible to be completed.

LIST OF SYMBOLS

A	Area of tested membrane
E_{cell}	Measured cell potential (V)
F	Faraday constant (96,467 C)
i_L	Limiting current density (mA/cm^2)
i_o	Exchange current density (mA/cm^2)
i	Current density (mA/cm^2)
l	Thickness of membrane
n	Number of electrons transported
pK_a	Acid dissociation constant in logarithmic value
Q	Heat transfer (J/mol)
Q	Reaction quotient
R	Gas constant (8.314 x 10^{-3} kJ/mol.K)
$R_{measured}$	Resistance measured (Ohm)
R_{PBI}	Resistance by PBI polymer (Ohm)
$R_{external}$	External resistance (Ohm)
R_{wires}	Resistance caused by external electrical wire (Ohm)
$R_{bipolar\ plates}$	Resistance caused by bipolar plates (Ohm)
R_{mesh}	Resistance caused by mesh (Ohm)
$R_{carbon\ cloth}$	Resistance caused by carbon cloth (Ohm)
R	Reference material
R	Ohmic resistance (Ohm)
S	Sample
T	Absolute temperature (K)
T_g	Glass transition temperature (^{o}C)
V_{anode}	Half-cell potential at anode (V)
$V_{cathode}$	Half-cell potential at cathode (V)
W	Work done by system (J/mol)
ΔG	Changes in Gibbs energy (J/mol)
ΔG^o	Changes in Gibbs energy at standard conditions (J/mol)

ΔH	Changes in enthalpy (J/mol)
ΔS	Changes in entropy (J/mol.K)
ΔU	Theoretical reversible potential (V)
ΔU°	Theoretical reversible potential at standard conditions (V)
ΔV	Difference in cell potential (V)
α	Constant of electron transfer coefficient of reaction at the electrode
λ	Membrane hydration state ($N(H_2O)/N(SO_3H)$)
η_{act}	Activation overpotential (V)
η_{ohmic}	Ohmic overpotential (V)
η_{mass}	Mass limitation overpotential (V)
σ_{PBI}	Ionic conductivity of PBI membrane (S/cm)

LIST OF ABBREVIATIONS

AFC	Alkaline fuel cell
a.u.	Atomic unit
CWRU	Case Western Reserve University
DMAc	Dimethylacetamide
DMFC	Direct methanol fuel cell
DMSO	Dimethylsulfoxide
DSC	Differential scanning calorimetry
EIS	Electrochemical Impedance Spectroscopy
E.W.	Equivalent weight
G.C.	Gas chromatography
H_3PO_4	Phosphoric acid
H_2SO_4	Sulfuric acid
h	Hour
I.R.	Internal resistance
MCFC	Molten carbonate fuel cell
MEA	Membrane electrode assembly
M.W.	Average molecular weight of polymer
min.	Time (minute)
OCV	Open circuit voltage
PAFC	Phosphoric acid fuel cell
PBI	Polybenzimidazole
PEMFC	Polymer electrolyte membrane fuel cell
PTFE	Polytetrafluoroethylene
ppm	Parts per million
R.H.	Relative humidity
SOFC	Solid oxide fuel cell
STP	Standard temperature and pressure
vol%	Volume percentage
wt%	Weight percentage

TABLE OF CONTENTS

LIST OF FIGURES

LIST OF TABLES

CHAPTER 1

INTRODUCTION

1.1 OUTLINE OF THESIS

There is a strong demand for alternative cost effective and environmentally friendly power sources. A considerable effort has been made into exploring and implementing new methods of power production, and in particular into development of fuel cells. Fuel cells show promise as versatile options for mobile and standing engines for electrical energy generation. A detailed description and the principle of fuel cells operation are presented in Section 2.1.

To date, applications of fuel cells, especially for converting light hydrocarbon fuels to value-added products at low operating temperatures using polymer membranes, is an area that has received relatively little attention [1]. Previous reports show conflicting ideas and results on the application of polymer fuel cells in converting hydrocarbons [2, 3]. Furthermore, the majority of the hydrocarbon fuel cell studies done in 1960s utilized strong acids as liquid electrolytes, and operated at low temperatures [4–7]. Hence, the parameters and methods of operation of the present polymer-electrolyte fuel cells are distinct from the prior research (Section 2.2). The membranes of interest here are based on polybenzimidazole (PBI), an amorphous hydrocarbon chain polymer that, upon doping with H_3PO_4, can be used at elevated temperature (> 200°C), which provides an ideal condition for thermal dehydrogenation of light paraffins. This is incorporated in Section 2.3.

Chapter 3 focuses on the preparation and characterization of the PBI membranes used in this study, including PBI membranes preparation procedure, membrane morphology, gas permeation, and differential scanning calorimetry (DSC) studies. The latter tests were conducted to determine the thermal stability of PBI polymer membranes

1

after prolonged high temperature operation of PBI-based H_2-O_2 fuel cells, as it was anticipated that there could be changes in PBI properties as a function of time after exposure to temperatures as high as 250°C. While use of PBI membranes in fuel cells is well known, it is recognized that the raw PBI powders from which the membranes were made can have a range of molecular weights and, consequently, their properties differ [8]. Thus it was necessary to determine the impact of the preparation procedure on PBI properties.

The fuel cell apparatus and the results obtained using hydrogen and oxygen as reactants in a PBI fuel cell are described in Chapter 4. Chapter 5 describes the use of PBI-based membranes in hydrocarbon fuel cells. A detailed discussion of the results follows. Packed-column gas chromatography was used to analyze the inlet and effluent gas streams, and thereby determine the products of electrochemical conversion of hydrocarbon fuels in PBI polymer fuel cells. The implications for the concept of hydrocarbon fuel cells are presented. The results will show that the direct feeding of primary hydrocarbon fuels into the PBI fuel cells produces high cell potential, and can generate significant amounts of electrical energy. Furthermore, the concentration of electrochemical products was shown to be proportionate to the current flow observed.

Chapter 6 presents the conclusions derived from this work, and recommendations for future work.

1.2 OBJECTIVES

The Fuel Cells Research Group at the University of Alberta is developing fuel cells for chemical conversion processes and for clean energy production. Currently, particular emphasis is placed on the conversion of hydrocarbon fuels since there were conflicting ideas and results on the application of polymer fuel cells in converting hydrocarbons. The research to be described herein has targeted development of systems based on PBI polymer membranes. PBI membranes were developed as proton conductors that would operate under minimal influence from water vapor activity at temperatures greater than 200°C. The primary goal of the present research is to apply H_3PO_4 doped PBI membranes in proton-conducting fuel cells for conversion of hydrocarbons to value-added products. This involved the following concept that is to be developed.

2

$$\text{At anode: } C_3H_8 \text{ (g)} \rightarrow C_3H_6 \text{ (g)} + 2\,H^+ + 2\,e^-$$

$$\text{or}$$

$$C_2H_6 \text{ (g)} \rightarrow C_2H_4 \text{ (g)} + 2\,H^+ + 2\,e^-$$

$$\text{At cathode: } \tfrac{1}{2}\,O_2 \text{ (g)} + 2\,H^+ + 2\,e^- \rightarrow H_2O \text{ (g)}$$

$$\text{Overall reactions: } C_3H_8 \text{ (g)} + \tfrac{1}{2}\,O_2 \text{ (g)} \rightarrow C_3H_6 \text{ (g)} + H_2O \text{ (g)}$$

$$C_2H_6 \text{ (g)} + \tfrac{1}{2}\,O_2 \text{ (g)} \rightarrow C_2H_4 \text{ (g)} + H_2O \text{ (g)}$$
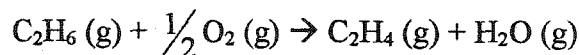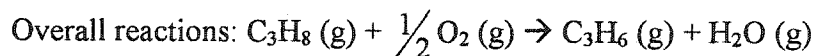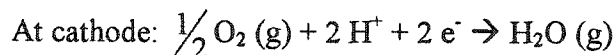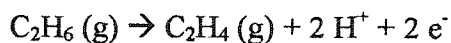
The above hydrocarbon fuel cells concept, if successful, will enable the utilization of fuel cells to co-generate electrical energy and olefins from paraffins while producing only water vapor as a clean by-product.

REFERENCES

[1]   Mazanec, T.J., and T.L. Cable, "Electrocatalytic oxidative dehydrogenation of saturated hydrocarbon to unsaturated hydrocarbon", U. S. Patent #4,933,054 (1990).

[2]   Petrovic, S., J.C. Donini, S.S. Thind, S. Tong and A.R. Sanger, "Electrochemical conversion of hydrocarbon", U. S. Patent #6,294,068 (2001).

[3]   Savadogo, O., and F.J.R. Varela, "Low-temperature direct propane polymer electrolyte membranes fuel cell (DPFC)", J. New Mat. Electrochem Systems, 4, 93 – 97 (2000).

[4]   Oswin, H.G., A.J. Hartner and F. Malaspina, "A direct hydrocarbon/air fuel cell", Nature, 200, 256 – 257 (1963).

[5]   Cairns, E.J., "High-performance hydrocarbon fuel cells with fluoride electrolytes", Nature, 210, 161 – 162 (1966).

[6]   Niedrach, L.W., "The performance of hydrocarbon in ion exchange membranes fuel cells", J. Electrochem. Soc., 109, 1092 – 1096 (1962).

[7]   Brummer, S.B., and M.J. Turner, "The adsorption and oxidation of hydrocarbon on Noble Metal", J. Phys. Chem., 71, 3902 – 3906 (1967).

[8]   Sansone, M.J., F.J. Onorato and N. Ogata, "Acid-modified polybenzimidazole fuel cell elements", U. S. Patent #5,599,639 (1997).

3

CHAPTER 2

BACKGROUND

2.1 FUEL CELLS BACKGROUND

2.1.1 Introduction

Over the past 20 years, one of the most important challenges facing industry in any country of the world is the search for a technology that can provide an answer to the three E's energy policy, Energy security, Economic growth and Environmental protection [1]. As natural resources like hydrocarbons have become fast depleting and the environmental constraints on industry grow tighter, it is imperative to search for an environmentally friendly and cost effective alternative to substitute for the traditional power production methods. One of the envisaged technologies is fuel cell.

Fuel cells technology has been around for a long time. So, it comes as a complete surprise to many people new to the subject of fuel cells that although they were invented some 160 years ago by Sir William Grove, a lawyer and physicist, they have taken so long to come to the forefront of energy and environmental considerations [2]. This has risen as a result of the technical challenges plaguing their introduction as a viable power system, for example limited current.

The relationship between chemistry and electricity is an old and long story, dating back as early as 1793. Allesandro Volta (1745–1827) was responsible for firmly placing the observation of the electrical phenomena on a scientific footing [3]. He discovered that electricity can be induced by simply placing two unidentical metals on opposite sides of moistened paper. By the early 19th century, the fuel cells phenomenon had already been discovered. Sir William Grove and Professor Christian Friedrich Schönbein were both instrumental in discovering the full potential of fuel cells [4].

4

The features that have now brought fuel cells to the forefront of research efforts for the automotive industry and power generation sector are:

(i) In fuel cells applications, the efficiency is not limited by temperature. In fact, there are several types of fuel cells which can operate at different operating temperatures ranging from 100 to 1000°C depending on the electrolytes used. The efficiency of a conventional heat engine is limited by Carnot efficiency, which never exceeds 50% [5]. On the other hand, fuel cells have efficiencies up to 50 – 70% and reaching nearly 90% with heat recovery. This has reduced fuel cell costs and conserves natural resources [1].

(ii) Fuel cells feed gases such as H_2-O_2 only produce water as the end product; this eliminates any hazardous effluents from polluting the mother earth [1].

(iii) Fuel cells have been used to convert hazardous industrial pollutant like H_2S into environmentally friendly products (e.g. H_2, S_2, S_3, S_4, S_5, S_6, S_7, S_8, S). Operation of such fuel cells enables rapid reactions at high temperatures, and overcomes theoretical equilibrium conversion limitations. Thus a H_2S-O_2 fuel cell is capable of total conversion of H_2S instead of being equilibrium limited to 14% at 850°C, while co-generating electricity and high quality steam [6, 7].

(iv) Contrary to conventional heat engines, fuel cells can operate with minimal mechanical action for feed of fuel and removal of products, thus minimizing noise pollution.

(v) Compared to conventional heat engines, fuel cell design is much simpler and construction costs are moderate. Besides that, fuel cells are relatively easy to maintain.

(vi) A variety of fuels can be selected. Of particular interest, hydrogen can be extracted from natural gas, propane, methanol, ethanol and also gasoline.

Fuel cells are commonly classified according to the operating temperature, type of electrolyte, and type of fuel being used. The major types of fuel cell which have found applications are [8]:

(i) Phosphoric acid fuel cell (PAFC)

(ii) Alkaline fuel cell (AFC)

(iii) Molten carbonate fuel cell (MCFC)

5

(iv)   Solid oxide fuel cell (SOFC)

(v)   Polymer electrolyte membrane fuel cell (PEMFC)

(vi)   Direct methanol fuel cell (DMFC)

Recently, PEMFC have been tipped as a future electrical source for automobile applications, laptops, hand phones etc. because of their low operating temperature as well as high energy density when operated using hydrogen (or methanol) and oxygen as reactants.

2.1.2 Fuel Cells – An Electrochemical Device

In a conventional battery, the chemical energy has to be stored beforehand. This type of power supply adopts exactly the same operating principle of an electrochemical cell, where operation is carried out spontaneously and delivers certain amount of work to the surroundings. As the reaction continues, the free energy of the system declines. So as time elapse, less energy remains to be covered. Eventually, the cell reaction will come to equilibrium when ΔG is zero and no further work can be extracted [3].

In reality, fuel cells are related to batteries. But, unlike conventional batteries, fuel cells operate on continuously fed reactants. Thus, fuel cells can keep operating and supplying useful electrical energy as long as fuel is supplied [8]. This involves conversion of chemical energy directly to electrical energy, unlike traditional thermo-mechanical system, thus extracting more electricity from the same amount of fuel due to the higher efficiency.

In order to fully understand the operating fundamentals of fuel cells, it is important to understand the functions of an electrochemistry cell and the parameters governing the operations.

2.1.2.1 Principles of Electroneutrality [3]

The principle of electroneutrality dictates clearly that every reaction involving charge transfer will have thermodynamic limitations. Work is always needed to separate opposite charges, or even to bring like charges into closer contact. This in return will create charge imbalance. Additional work is needed to create a larger degree of charge

6

imbalance, which will further raise the Gibbs free energy of the process, making it less and less spontaneous. The increment of Gibbs free energy in any reaction, from reactant to product, will result in non-spontaneous reaction, while any decrement in Gibbs free energy is deemed as spontaneous reaction.

If we have hydrogen gas contacting a metallic electrode, a small amount of hydrogen atoms will be split into protons, H^+ ions, leaving their electrons behind in the electrode:

$$H_2 \rightarrow 2\,H^+ + 2\,e^- \hspace{4cm} (2.1)$$

As this process proceeds, the electrons which remain in the electrode create a negatively charged environment. This buildup of electrons makes it increasingly difficult for reaction (2.1) to proceed. A similar buildup of positive charges in the proximity further inhibits this ionization reaction.

Contrary to this situation, if we withdraw the electrons from the metallic electrode as the protons are being generated, there will be no buildup of charge. One way to implement this idea is to drain off the excess electrons through an external circuit that forms part of a complete electrochemical cell, or an alternative way is to introduce a good electron acceptor. Both methods drive the reaction in Eqn. (2.1) forward, and this will restore the electroneutral environment to the two phases. Obviously, these require redox reactions.

Redox reactions involve the donation of electrons from a reducing agent and the acceptance of electrons by a chemical species that possesses a great affinity towards electrons in a simultaneous process. As a consequence, the transformation of hydrogen to protons is no longer inhibited by buildup of negative charge in the electrode because the excess electrons are removed from the electrode by an oxidizing agent with which they come into contact. At the same time, the electroneutrality condition can be preserved since all electrons released by hydrogen atoms couple with the oxidizing agent.

7

2.1.2.2 Thermodynamic Fundamentals

The energy conversion process in a fuel cell, like in any other energy converter, is governed by the First and Second Laws of Thermodynamic. According to the First Law of Thermodynamic, for an open system under steady-flow conditions, the conservation of energy is given by Eqn (2.2) [9]:

$$Q - W = \Delta H \tag{2.2}$$

where Q   = Heat transfer.

W   = Work done.

ΔH = Changes in enthalpy.

The Second Law of Thermodynamic defines that a process in which there is no entropy generation is called a reversible process where both the system and its surroundings can be returned to their original states at any point. For any reversible isothermal heat transfer, the entropy change corresponding to the amount of heat generated is given by Eqn. (2.3) [9]:

$$Q = T\Delta S \tag{2.3}$$

where ΔS = Changes in entropy.

T   = Absolute temperature.

In the case of a fuel cell where chemical reactions occur at constant temperature and pressure, the equation below relates changes in Gibbs free energy to the total energy of a system:

$$\Delta G = \Delta H - T\Delta S \tag{2.4}$$

in which ΔG is the measurement of the energy that is available or free for conversion into usable work. The amount of heat that is produced by a fuel cell operating reversibly is given by the term $T\Delta S$, which is unavailable for work because of the disorder or entropy of the system. Thus, even in a reversible fuel cell, there is a portion of heat that cannot be recovered and lost. Reactions in fuel cells that have negative entropy change generate heat, while those with positive entropy change extract heat from the surroundings [5].

8

2.1.2.3 Nernst Equation

The Nernst equation is especially useful for electrochemistry systems because it relates standard potential (U^o) at pressure of 1 atm and temperature of 25°C to equilibrium potential (U) at other temperatures and pressures of reactants and products. This dependency happens as a result from the dependency of Gibbs free energy on temperature and concentration, as shown here by van't Hoff Isotherm [10]:

$$\Delta G = \Delta G^o + RT \ln (Q) \qquad (2.5)$$

where ΔG^o = Changes in Gibbs free energy at standard conditions.

R = Gas constant.

Q = Reaction quotient.

Q depends on the stoichiometry of chemical equation. Furthermore, since

$$\Delta G = -nF\Delta U \text{ and } \Delta G^o = -nF\Delta U^o \qquad (2.6)$$

where ΔU = Theoretical reversible potential.

ΔU^o = Theoretical reversible potential at standard conditions.

F = Faraday's constant with a value of 96,467 Coulombs/mole of electrons.

n = Number of electrons involved in the reaction.

by rearranging these two equations, we obtained an equation that relates the theoretical reversible potential to the concentrations of cell components. This equation is commonly referred to as Nernst equation:

$$\Delta U = \Delta U^o - \frac{RT}{nF} \ln(Q) \qquad (2.7)$$

However, in actual fuel cells application, normally, even under no current flowing conditions, the cell potential observed could be lower than the theoretical value. This can be attributed to the parasitic losses like leaking of gases, crossover of reactants, equipments not properly insulated and also due to the ineffectiveness of catalyst layer for chemisorptions of reactants.

9

2.1.3 Operating Principles of Fuel Cells

Principles of operation of fuel cells are similar to those of an electrochemical cell. Electron-transfer reactions occur at the surface of electrodes in contact with reactant gases. The reactions take place at the interface between electrodes and electrolyte. It is impossible for the electrons passing through the gas phase. If we have two separate electrode-gas interfaces, we will be able to measure the potential difference between them. Such an arrangement is called a galvanic cell.

Fuel cells involve the conversion of Gibbs free energy of two separated chemical species into electrical energy via redox reactions. The maximum electrical work, which happens to be the ideal voltage that can be obtained in a fuel cell at certain operating conditions, is given by Eqn. (2.6).

The negative sign on the right hand side of the Eqn. (2.6) indicates that a positive potential implies a negative free energy change, and thus the cell reaction is spontaneous.

Basically, fuel cells consist of individual cell units comprising an electrolyte (either in solid membrane, molten or liquid form), which is situated between anode and cathode. When the electrolyte is a membrane, the arrangement is termed 'Membrane-Electrode-Assembly', or in short form as MEA. The MEA separates two cell compartments; one is termed anode compartment, and the other as cathode compartment. The potential difference between anode and cathode is creating a driving force, which is termed the electromotive force (EMF). In the anode compartment, a reducing agent has a tendency to donate electrons and thereby become oxidized. These electrons will be transferred to the cathode side via external electrical circuit to combine with oxidizing agent. This transfer of electrons can be manipulated into useful electrical work.

To complete the electrical circuit, the non-electronic conducting membrane inserted in between these two compartments acts as a barrier to separate the reducing and oxidizing agents while at the same time possesses ionic conductivity, normally proton or oxide ions. The diagram in Figure 2-1 shows the schematic presentation of a general PEMFC cross-section.

10
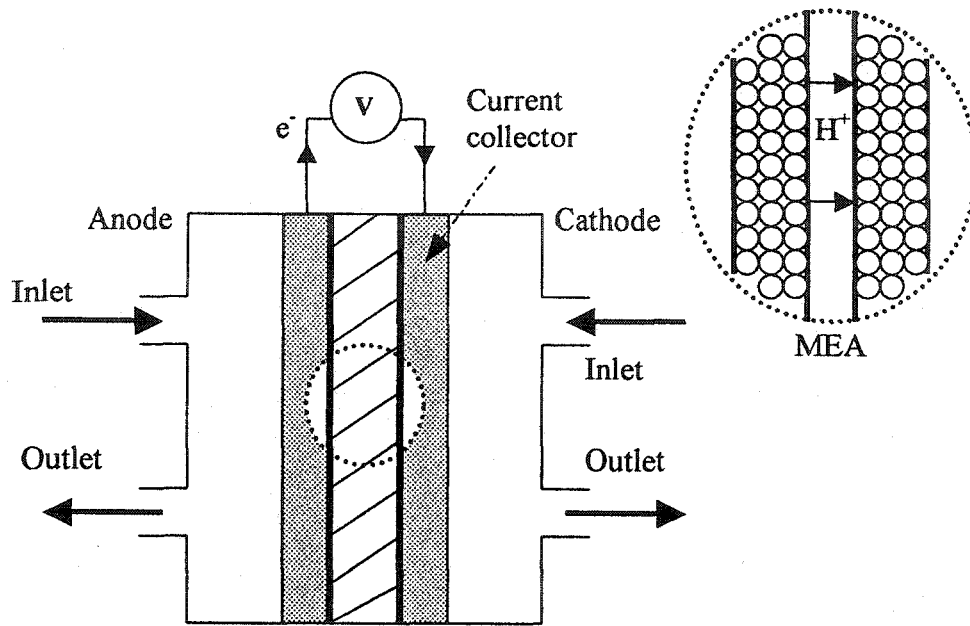
Figure 2-1 Schematic of a proton-conducting fuel cell.

An electrochemical cell like fuel cells offers a high degree of control for measurements of the cell reaction. If the external circuit is broken, the reaction stops. If we vary the resistance in the circuit, we will be able to control the rate of the cell reaction. Then, by measuring the amount of electric charge that passes through the external electrical circuit, we are able to calculate the number moles of reactants that get transformed into products during the cell reaction.

For PEMFC, which have been used within the scope of this work, a few alternative fuels have also been utilized as potential reducing agents. Among them are methanol [11], formic acid [12] and trimethoxymethane [13]. The choice of oxidizing agents has been limited so far to either pure O_2 or air, which contains diluted O_2. The complete reactions of reactants taking part in fuel cells must be of redox electrochemical reactions. A simple example is the following H_2-O_2 system:

$$\text{Anode}: \quad H_2 \rightarrow 2\,H^+ + 2\,e^- \qquad \Delta U_{ox} = 0.00 \text{ Volt} \qquad (2.8)$$

$$\text{Cathode}: \quad O_2 + 4\,e^- + 4\,H^+ \rightarrow 2\,H_2O \quad \Delta U_{red} = 1.23 \text{ Volt} \qquad (2.9)$$

Hydrogen is being oxidized at the anode compartment to form protons. This will release two electrons, which will then flow to the external electrical wire. At the same time, generated protons will be transported through the membrane to the cathode side. At

11

the cathode side, 1 mol of O_2 will dissociate into 2 mol of O^{2-} ions upon receiving 4 mol of electrons. These oxygen ions will recombine with protons to form water. Thus, the concept of clean energy source from fuel cells is achievable.

2.1.4 Cell Potential

Fuel cell applications involve electrode processes, also known as electrode reactions. These electrode processes are taking place at the surface of the electrode and create a slight unbalance in the electric charges between electrode and gas interface. The net result is an interfacial potential difference, which affects the rate and direction of the reaction. In the concept of electrochemistry, this net result is termed as individual half-cell potentials, which are not directly measurable at this time [3].

A measurement that can be performed is the voltage difference between two electrodes in the absence of any cell current. This voltage, known as the open cell potential, is the potential difference between the electrodes. It is the difference between the half-cell potentials of the anode and cathode sides:

$$E_{cell} = \Delta V = V_{anode} - V_{cathode} \qquad (2.10)$$

The individual half-cell potentials of two electrodes as shown in Eqn. (2.10) are not the absolute value of half-cell potentials. It is only possible to measure the value in relation to the potentials of other half-cells. The potential of a reference half-cell is arbitrarily set as zero, and potentials of other electrode systems are performed with reference to this electrode. The potentials so obtained are half-cell potentials on a scale that is relative to the specific reference electrode.

Cell potential is an important indicator for fuel cells operation because it reflects the tendency for the cell reaction to take place. A positive cell potential shows an electrochemical process which is deemed spontaneous and thus can be carried out. In addition, the more positive the cell potential, the greater the tendency for the electrochemistry reaction to proceed. If a cell potential shows a negative value, that means the specified reaction cannot be carried out spontaneously (galvanic cell), but requires an external force to drive it (electrolysis). The unit for cell potential is Volt (abbreviated V), which is defined as a work of 1 Joule per Coulomb of charge being

12

transported through an external wire. A spontaneous system always has a positive cell potential.

There are two ways to measure the cell potential. One way is by using a voltmeter, which works by drawing a small amount of current through a known resistance. The measured current is then related back to cell potential using the relationship between resistance, current and cell potential.

Another way is to use potentiostat instrument. Potentiostat instrument, which we used in our laboratory, basically operates by injecting current into the cell through an auxiliary electrode to control the voltage difference between anode and cathode compartment [14]. This voltage is adjusted until no current flows in the cell circuit. Under such condition, the cell potential will be determined.

2.1.5 Fuel Cells Performance

An ideal performance for fuel cells depends on types of fuels being utilized because different fuels will generate different electrochemical reactions. Ideal performance can only be obtained by operating fuel cells at open circuit potential where no losses will occur. This ideal performance is impossible to achieve because there are a few prominent losses, which contribute to the deviation of operating potential from ideal cell potential.

If ideal performance of fuel cells can be maintained, the performance graph shown in Figure 2-2 can be visualized.
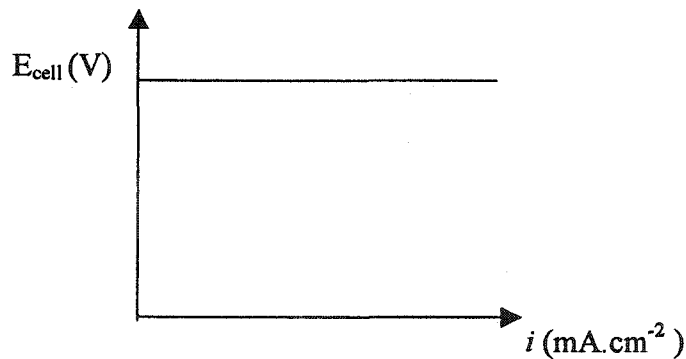
Figure 2-2 Ideal performance of fuel cells.

13

In practice, this performance is not achievable. Some losses, which we normally termed as 'overpotentials', could happen. The following graph shown in Figure 2-3 depicts a more realistic situation, which is likely to be obtained from fuel cells operations.

In general, losses in fuel cells operation can be grouped into:

(i)   Activation polarization

(ii)   Ohmic polarization

(iii)   Mass transport limitation

Figure 2-3 shows a typical cell potential of fuel cells versus its current density. It happens that cell potential is not ideal and decreases with increasing current density. Three distinct regions can be distinguished from this graph. Region I belongs to overpotentials, which is controlled mainly by activation polarization, region II by ohmic resistance while region III is mainly controlled by mass transport limitation.
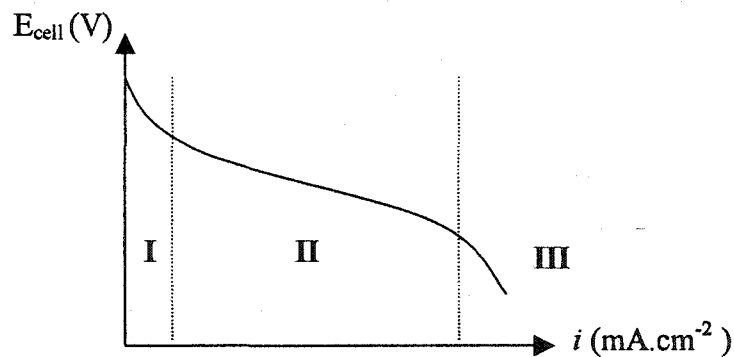
Figure 2-3 Actual performance of fuel cells.

2.1.5.1 Activation Polarization

Activation polarization happens because of finite rates of reactions at electrodes. Sluggish electrode kinetics contributes to the activation polarization. Activation polarization, η_{act}, can be described by the general form of Tafel equation [5]:

$$\eta_{act} = \frac{RT}{\alpha nF} \ln\left(\frac{i}{i_o}\right)$$

(2.11)

14

where α = Constant of electron transfer coefficient of reaction at the electrode.

i_o = Exchange current density (measurement of maximum current that can be obtained at negligible overpotentials [15]).

2.1.5.2 Ohmic Polarization

Ohmic resistance is mainly influenced by the ionic conductivity of membranes as well as resistance to the flow of electrons at the electrodes. Low ohmic resistance enables rapid transport of charge. Eqn. (2.12) relates ohmic losses in fuel cells to current density.

$$\eta_{ohmic} = i \times R \qquad (2.12)$$

where i = The flowing current density.

R = Total resistance of MEA which includes electronic resistance, ionic resistance and contact resistance.

2.1.5.3 Mass Transport Limitation

At high current density, operation of fuel cells consumes high amounts of reactants to generate high amounts of electricity. This will create a loss of potential due to the inability of the surrounding reactants to diffuse rapidly through the porous electrode to the catalyst site, where they then need to adsorb on the surface of catalyst before the subsequent electrochemical reactions take place. When this situation exists, the initial concentration of reactants in the surface fluids cannot be maintained and a concentration gradient exists between the reactants at the catalyst surface and bulk fluid. As a consequence, further reactions are mass transfer limited. In general, this overpotential can be expressed by:

$$\eta_{mass} = \frac{RT}{nF} \ln\left(1 - \frac{i}{i_L}\right) \qquad (2.13)$$

where i_L is the limiting current density. It indicates the maximum rate at which a reactant can be supplied to an electrode.

15

2.2 HYDROCARBON FUEL CELLS

2.2.1 Background of Low Temperature Hydrocarbon Fuel Cells

In U.S. Patents 5,747,185 and 3,718,506, details are made available for the design layout for hydrocarbon application in high temperature fuel cells, particularly in the range of 500 to 1200°C with the employment of internal or external steam reforming reactions [16, 17]. In another patent, Mazanec and Cable (1990) claimed that high temperature solid oxide fuel cells could be used in converting paraffin to olefins [18]. This particular patent is interesting because it mentioned the application of fuel cells as an alternative mean for converting hydrocarbons. Apart from functioning as electricity generator, fuel cells can also be used to produce value-added products.

Low temperature fuel cells normally involve indirect feeding of hydrocarbon, wherein the hydrocarbon is turned into a H_2-rich gas stream, followed by purification to eliminate CO, a catalyst poison, before feeding the gas stream into the fuel cells [19, 20]. Besides, there are also reports on direct utilization of hydrocarbons in electrochemical cells during the 1960s, especially after the discovery by Patterson and Kemball [21] that some partial oxidation reactions of hydrocarbons could happen and carbon dioxide and water were not necessarily the only two products being obtained. Anyway, at that time, due to the technological limitations, experiments were carried out in a strong acid bath, which functioned as electrolyte and moderated the temperature of reaction [22–24].

It has been proposed that oxidation processes in this acidic electrochemical cell involved adsorption of saturated light hydrocarbon on the electrocatalyst followed by the rapid formation of oxidized intermediates, which are then slowly oxidized into CO_2 [25]. According to studies conducted by Niedrach et al. [26], oxidation of paraffins C_nH_{2n+2} with $n \geq 2$ on platinum electrodes taken place in two different potential regions. This resulted in a conclusion being made that there is a distinction between two generically main-type species in the steady state adsorbate of the hydrocarbon. Brummer et al. [27] proposed that these types are the O type and the CH types adsorbates.

The O type is predominant in terms of coverage at all potentials and is the most highly oxidized of all the species and is the easiest to oxidize further to CO_2. CH types,

16

which are generalized as CH_α and CH_β are much less oxidized than the O type and are harder to oxidize at higher potentials and might represents polymeric material. Unlike O type, the composition of CH fragments changes with potential and probably with the hydrocarbon chain structure. CH_α was found at all potentials and normally was less reactive toward oxidation than the O type. CH_β was unreactive toward reduction and oxidation.

$$C_nC_nH_{2n+2} \rightarrow C_nH_{2n+2,\,ads}$$

O type

fast / \ slow

$$C_nH_{2n+2,\,ads} \rightarrow (fast) \rightarrow CH_\alpha \text{ (active) type} \rightarrow (fast) \rightarrow CO_2$$

fast \

$$CH_\beta$$
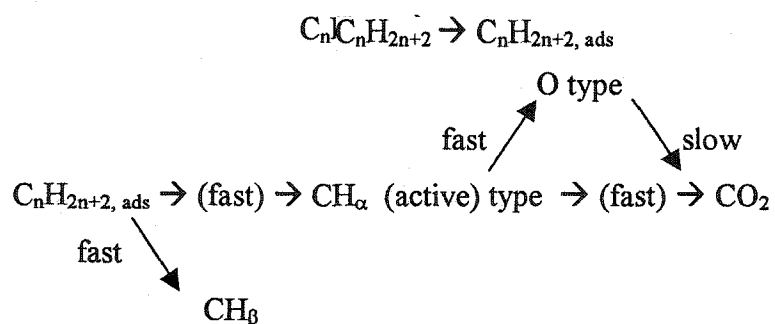
Figure 2-4 Proposed mechanistic of hydrocarbon oxidation in acidic electrochemical cell.

This view seems to be in agreement with Niedrach et al. who suggested that after the initial adsorption step, two important reaction paths are available. The highly desirable path involves cracking to form a partially oxygenated intermediate, which is oxidized further to CO_2 at low potential. The second path results in the accumulation of relatively refractory multiple carbon species on the surface. According to Cairns et al. [28], after initial adsorption step, the adsorbate is probably easily dehydrogenated further, resulting in bonding of alkenes-like intermediate species to more platinum sites. This additional bonding causes straining of C – C bonds leading to fracture of the molecules.

At the same time, Bockris et al. [29] proposed that the first step is the breaking of a C – H bond:

$$C_nH_{2n+2} \rightarrow C_nH_{2n+1,\,ads} + H_{ads}$$
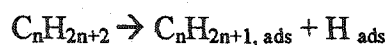
The second step is a chemical surface reaction, which cracks the C – C bonds rather than C – H bonds and is the rate determining step. This will produce carbon fragment on the surface of the noble metals.

$$C_nH_{2n+1\,ads} \rightarrow slow \rightarrow C_{1\,ads} + C_{2\,ads}$$
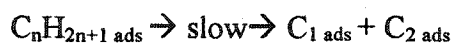
After 1960s era, no extensive research has been carried out at low temperature hydrocarbon fuel cells because applications before showed small current flow in acidic solution electrochemical cell. This is due to the complicated mechanism of oxidation of hydrocarbon at the anode side which resulted in unsatisfactory current densities, and hindered its commercial application.

According to Otsuka et al. [30], electrochemical cell reactions are possible for hydrocarbons under mild conditions (< 373 K) and at 1 atm pressure. This group used PAFC to carry out partial oxidation of hydrocarbons, for example, alkenes to aldehydes and organic acid. Although the partial oxidation of alkenes under mild condition has been successfully achieved, this is not the case for alkanes. They concluded that room temperature is not high enough to activate the breaking of C − H bonds. By applying H_2-O_2 fuel cells at room condition and further supplying light alkanes at the cathode side, some partial oxidations of alkanes could be observed.

As the fuel cell technology advanced, the introduction of highly conducting polymer like Nafion™, and better reactants separation, has once again sparked interest in low temperature hydrocarbon fuel cells application. In U. S. Patent 6,294,068 [31], authors had used low temperature PEMFC based on Nafion™ to carry out dimerization reactions of methane, ethane and methanol in electrochemistry mode to make higher hydrocarbons. The authors also used self-fabricated PBI membranes (PBI powder from Celanase) and operated the cell at high temperature (at least 200°C). But they have encountered some problems such as gas leakage and high internal resistance from MEA. These problems have resulted in very low yield of electrochemical products (< 1 ppm). They claimed to have successfully converting methane to C-2 and ethane to C-4 species. Nonetheless, the authors did not comment in their patent whether the final electrochemical products at the anode side might be influenced by the presence of O_2. There is no evidence presented to support their claim that the products produced were directly from observed current flow. These traces of higher chain hydrocarbon could have originated from thermocatalytic reactions.

Savadogo et al. [32] operated their fuel cells at 95°C and high humidification in Nafion™ using H_2SO_4-doped PBI membranes. H_2SO_4-doped PBI membranes, like Nafion™ membranes, need high humidification to maintain its ionic conductivity at a

18

satisfactory level. They bought the commercially available PBI membranes directly from Celanase. In their paper [32], Savadogo et al. reported the formation of CO_2 and not propylene as the final electrochemical product. No discussion was presented to explain the formation of CO_2 instead of C_3H_6 when PEMFC were employed.

2.2.2 Propane and Ethane as Fuels

Propane is a typical widespread fuel, which is often used for camping applications, because it can be stored in liquid form at relatively low pressure in tanks for mobile and portable use. Besides these advantages, propane is a relatively inexpensive fuel with high power density.

Unlike propane, it is more difficult to liquefy ethane. In addition, ethane has a much lower power density compared to propane. Nonetheless, these two light hydrocarbon fuels serve as an important starting material to produce olefins in chemical industry, and therefore it is desirable to develop a clean method for their efficient production.

Propane and ethane are two of the first three members of the paraffin hydrocarbon series having the chemical composition of C_nH_{2n+2}. Both are odorless and colorless gases under room conditions. Compared to propylene or ethylene, both propane and ethane are relatively unreactive because of the single bonds along the carbon chains. In the following tables, some important physical properties of propane, ethane, propylene and ethylene have been listed for comparison.

Table 2-1 Selected properties of ethane and propane.

Property	Ethane	Propane
CAS Registry No.	[74-84-0]	[74-98-6]
Molecular formula	C_2H_6	C_3H_8
Molecular weight	30.07	44.09
Melting point (K)	90.4	85.5
Boiling point (K)	185	231
Vapor Pressure at 273 K, MPa	2.379	0.475

Source: *Kirk-Othmer Encyclopedia of Chemical Technology*

19

Table 2-2 Selected properties of ethylene and propylene.

Property	Ethylene	Propylene
CAS Registry No.	[74-85-1]	[115-07-1]
Molecular formula	C_2H_4	C_3H_6
Molecular weight	28.0536	42.081
Melting point (K)	103.99	88
Boiling point (K)	169.29	225.3
Vapor Pressure at 273 K, MPa	4.10	1.41

Source: *Kirk-Othmer Encyclopedia of Chemical Technology*

Both Tables 2-1 and 2-2 show that ethane and propane exhibit higher boiling point than ethylene and propylene. This is expected since olefins have lower molecular weight compared to paraffins and therefore have weaker covalent bond. Although both gases are colorless, ethylene and propylene differ from ethane and propane in term of smell. Ethylene and propylene possess a slightly sweet odor.

2.3 POLYMER MEMBRANES

2.3.1 Applications of Membranes in Fuel Cells

Membranes are vital hardware in fuel cells system because they act as a barrier to separate both oxidizing and reducing agents from each other. At the same time, membranes must permit ionic movement, in our case, protons, transferring to cathode compartment from anode compartment. A good membrane has the following criteria:

- Must be chemically and electrochemically stable under oxidizing and reducing environments.
- Has the mechanical strength to withstand operating conditions, for example, pressure difference between two compartments.
- Good ionic conductivity, preferably at least 10^{-2} S.cm^{-1} to minimize ohmic losses.
- Must be electronically insulating to prevent any electrical losses to surrounding.

- Low gas permeability to reduce reactant crossover. Crossover of reactants, either from the anode compartment to cathode compartment or vice-versa, will contribute to performance losses.

- Low cost so that it can be commercialized.

2.3.2 Nafion™ Membranes

Nafion™ membrane is the first commercially available membrane that was introduced in 1966 as a product of E.I. DuPont de Nemours & Co. It has been tipped as the most promising membranes for low temperature fuel cells application. The Nafion™ membranes produced by DuPont have the following chemical schematic structure [33]:

$$[(CF_2CF_2)_x \quad - \quad (CF\!\!-\!\!CF_2)_y]$$
$$|$$
$$(OCF_2CF)_z \quad - \quad OCF_2CF_2SO_3^- \bullet H^+$$
$$|$$
$$CF_3$$
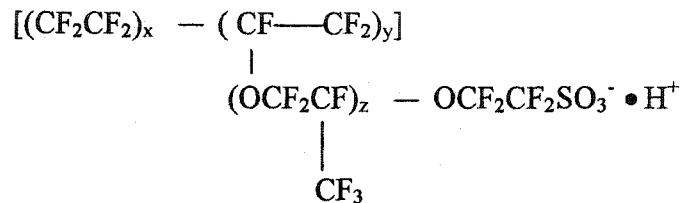
Figure 2-5 Molecular structure of Nafion™ membranes.

In Figure 2-5, the values of x, y and z can be varied to create materials with different equivalent weights (E.W.). E.W. here refers to the number of grams of polymer per mole of fixed sulfonic acid (SO_3H) sites. The structure of Nafion™ consists of three distinct regions:

- The hydrophobic PTFE structure, which serves as polymer backbone. Basically, this structure is chemically inert.

- The hydrophilic ionic species, which is introduced by the SO_3H group in the form of ionic clusters. This region is quite hydrophilic, absorbs water the most, and counter-ions exist in this region.

- An intermediate region.

There are two most commonly used materials of Nafion™ [33]. One is Nafion™ 120, which means 1200 E.W. and is 10 mils in thickness and the other is Nafion™ 117, which has 1100 E.W. and is 7 mils thick. Higher E.W. will only reduce the power density because it has lower concentration of SO_3H, which are important for proton conduction.

21

So far, for fuel cells operating at temperature of 85 to 105°C, perfluorocarbon sulfonic acid membrane shows promising potential as future energy converter since it is chemically and thermally stable. It also has the highest ionic conductivity, which reaches 0.1 S.cm^{-1} at room temperature with 100% relative humidity (R.H.) [34].

2.3.3 Water Management in Nafion™ Membranes

The proton conductivity of Nafion™ is dependant on its degree of hydration. In the dry state, Nafion™ is a poor ion conductor, but its ionic conductivity increases sharply with water content [35]. The water profile inside Nafion™ membranes can vary according to water transportation in the membranes and also on current flow. Sources of water and various flux components, which has the effect of redistributing the water in operating fuel cells, are shown schematically in Figure 2-6.

The illustration in Figure 2-6 shows the water balance inside Nafion™ membranes under normal operating conditions. Water is being produced at the cathode compartment by the electrochemical reactions taking place, which involve protons and oxygen. At the same time, water also enters the cell via humidified reactant gases. Inside Nafion™ membranes, water is being transported through the membranes from anode to cathode by a process call electro-osmotic drag [34].
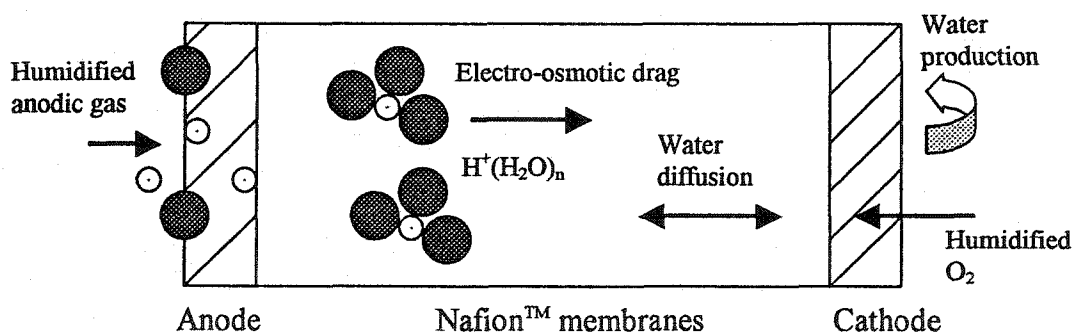
Figure 2-6 Water balance in Nafion™ membranes.

Electro-osmotic drag of water from the anode compartment to cathode will tend to dry the membranes at the anode side under current flow and, at the same time, flood the cathode side because this amount of water will be added to the amount of water being produced initially at the cathode side. So, buildup of water occurs at the cathode side.

22

Nonetheless, part of this problem is relieved by back diffusion of water from cathode to anode due to the concentration gradient and by the hydraulic permeation of water (e.g. by maintaining pressure at cathode higher than pressure at the anode side). Careful manipulation of above factors ensures that no dehydration of membranes happens at the anode side while at the same time preventing the cathode side from flooding.

2.3.4 Proton Conductivity Mechanism in Nafion™ Membranes

The proton conductance mechanism in Nafion™ membranes is based on movement of hydroxonium ions between immobile SO_3^- sites on the Nafion™ backbone [36]. SO_3H are chemically bonded to the polymer backbone. Therefore, these sulfonic groups have no ability to move freely.

The presence of water is primarily important because it assists the proton conduction in two meaningful ways. According to Zawodzinski et al. [36], at membranes hydration, λ (=$N(H_2O)/N(SO_3H)$) of two to three, hydroxonium ions have quite a limited motion via vehicle mechanism. But at fully hydrated condition, separation of hydrophobic and hydrophilic region occurs and acidic functional groups are rearranged into well-connected hydrophilic network domains. As a result, water and protons can move more freely compared to low membranes hydration.

The second contribution of water is it can increase the hydrogen bond breaking and forming which is important for proton movement due to its good proton acceptor and donor behavior [37].
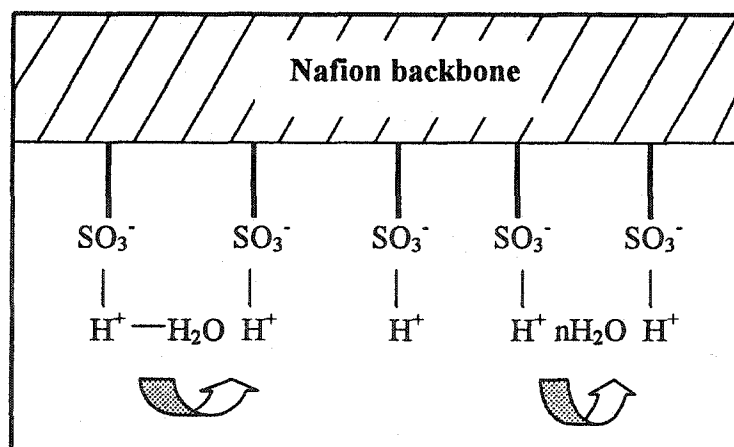
Figure 2-7 Protonic conduction mechanisms in Nafion™ membranes.

Figure 2-7 shows a schematic of the proton conduction mechanism occuring inside the Nafion™ membranes. Protons which are generated from electrochemical reaction at the anode compartment will be coupled to water to form $H\text{-}(H_2O)_n^+$ (n is between 0.9 to 2.5, depends on the hydration state of membrane) before being transported [38]. These ions will then "jump" to its neighboring SO_3H sites. In this way, hydroxonium ion transport effects proton conduction from anode to cathode.

2.3.5 Limitations of Nafion™ Membranes

Perfluorosulfonated polymer membranes like Nafion™ membranes are stable to oxygen and hydrocarbons, and have found wide application in electrochemical processes and fuel cells. Unlike hydrocarbon polymer chains, perfluorosulfonated membranes are also less susceptible to thermal degradation and thermal oxidation processes [39].

However, it has several limitations. One of them is high manufacturing cost reaching 780 US\$/m^2 [40]. Another problem is related to low operating temperature. Samms et al. reported that Nafion™ polymer membrane is only stable up to 280°C, after which it began to decompose by losing of SO_3H [41]. Furthermore it only has a glass transition (T_g) point around 103°C [42].

A further limitation on the use of Nafion™ membranes arises from the conductivity behavior, which depends on the level of humidification of the polymer. Zawodzinski et al. [38] has reported water sorption data for Nafion™ membranes from liquid water and also from different water vapor activity. In the liquid phase, 1 mol of SO_3H can absorb around 22 mol of water while at nearly water vapor activity of one, about 10 mol H_2O/ SO_3H were obtained at 80°C and nearly 14 mol H_2O/SO_3H at 30°C. The specific conductivity of fully hydrated Nafion™ membranes immersed in liquid is about 0.1 $S.cm^{-1}$ at room temperature, and about 0.15 $S.cm^{-1}$ at a cell operating temperature of 80°C [43]. Litt [44] reported that, at room temperature, the conductivity of Nafion™ membrane was about 10^{-1} $S.cm^{-1}$ at 100% R.H., but the performance dropped to only 10^{-5} $S.cm^{-1}$ at approximately 15% R.H. Suzuki et al. [45] further claimed that the conductivity of Nafion™ membranes was of the order of 10^{-4} $S.cm^{-1}$ levels under dry conditions from 25 to 130°C. Hence, it is clear that applications of Nafion™ membranes require operation under conditions of high humidification, preferably 100% R.H., in order to keep the

24

membranes hydrated. Hydration of Nafion^{TM} membranes is required for maintaining high ionic conductivity (10^{-1} S.cm^{-1}). As a result, operation by using Nafion^{TM} based polymer fuel cells above 100°C requires operation at elevated pressures in order to prevent loss of moisture from membranes.

On the other hand, dehydrogenation of light paraffins is thermodynamically favorable at high temperatures and low pressures; with 1 atm is the most practical pressure. By using Nafion^{TM} membranes, fuel cells operation only can be carried out at low temperature (< 100°C). Above this temperature, high pressure is needed. This does not provide an ideal condition for dehydrogenation process. Higher temperatures also avoid the poisoning of platinum catalyst. Concentration of CO above 10 ppm in fuel will cause a detrimental effect on the catalyst performance [46]. But, at temperatures above 150°C, platinum catalyst will not retain CO [47]. Therefore, PBI polymer membranes were developed to conduct protons under minimal influence from water vapor activity at temperatures greater than 200°C. This is in order to eradicate the limitations imposed by Nafion^{TM} membranes for the operation of hydrocarbon conversion fuel cells.

2.3.6 PBI Polymer

In 1995, a landmark discovery was described by researchers at Case Western Reserve University (CWRU), when they introduced PBI, or poly-(2,2'-(m-phenylene)-5,5'-bibenzimidazole, as a promising polymer electrolyte for fuel cell applications, upon doping with strong acids [48, 49]. Since then, acid treated PBI membranes have been applied extensively in hydrogen fuel cells and DMFC [50–53]. The properties of acid-treated PBI membranes have been systematically studied by numerous researchers, culminating in the production of MEAs based on phosphoric acid-doped PBI by Celanese Ventures.

PBI is a basic polymer with a pK$_a$ value of 5.5 [51]. This aromatic PBI is highly thermostable, with melting point over 600°C [54]. At ambient conditions, PBI can absorb approximately 15 to 18 wt% of its own weight of liquid water at equilibrium [55]. This represents approximately 2.56 mol of water absorbed for every repeat monomer unit of PBI for 15 wt% of water. PBI readily absorbs water by forming intermolecular hydrogen bonding between water and the N atoms and N-H groups of PBI [55].

25

The ionic conductivity of undoped PBI is about 10^{-12} S.cm^{-1} [56]. Undoped PBI contains three benzene rings that are coupled to two imidazole groups (Figure 2-8). In each imidazole group, there are proton donor and acceptor groups that enable conduction, thus making PBI an amphoteric material. This molecular structure provides PBI with superior mechanical and thermal stability as well as its rigidity.
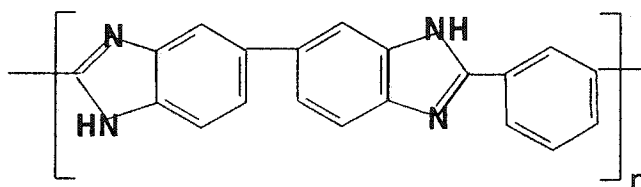
Figure 2-8 Molecular structure for a repeat unit of PBI.

Listed below are some important facts about the superiority characteristics of PBI:

- It is an amorphous thermoplastic polymer with T_g up to 430°C [57].

- Production cost is 150 to 220 US$/kg [33]. 1 kg of PBI powder can be cast into approximately 12 m^2 of 100 µm thick PBI membranes, translating to about 12.5 to 18 US$/m^2. This is far cheaper than Nafion™ membranes with manufacturing cost reaching 780 US$/m^2 [40].

- PBI has an almost zero electro-osmotic drag number, meaning that every proton transported through PBI membranes carries no water with it [50]. On the other hand, Nafion™ has a drag number in the range 0.6 to 2.0 [38, 58].

- PBI film does not undergo thermal degradation below 550°C under nitrogen atmosphere [48]. By doping PBI with strong acid, the thermal degradation point increased to 600°C. This increase in thermal stability was attributed to the formation of benzimidazonium cations [54].

- PBI treated with phosphoric acid has been found to be stable in nitrogen atmosphere, reducing environment (5% hydrogen) or even in the presence of air. In all cases, weight loss below 400°C was attributed to the loss of water [59].

- PBI is sensitive to aging (> 200 hours) at temperatures above 260°C. By protonation of the imidazole rings by acid, a phosphate layer is formed around the membranes and the thermal properties of PBI are improved [55].

26

It is well known that polymers containing basic groups like PBI can form complexes with stable acids, or other polymers containing acidic groups, in a process called polymer blending [60–62]. To better understand formation of these complexes, two simple illustrations have been provided here. They were drawn using Bio-Rad ChemWindows 6.0 software. The interaction between PBI and strong acids (e.g. H_2SO_4 and H_3PO_4) will give complexes shown in Figure 2-9.
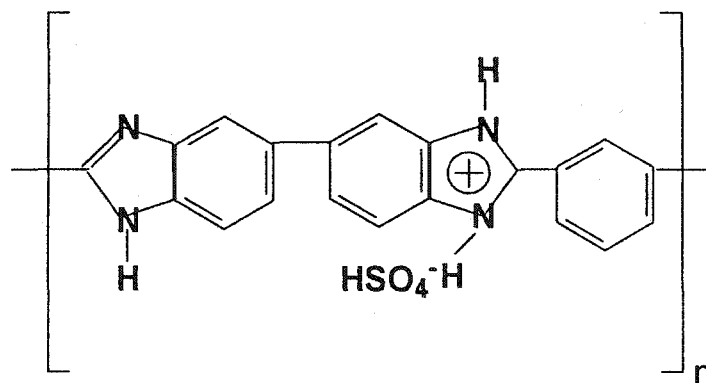
(a) Complex formation after treatment with H_2SO_4.
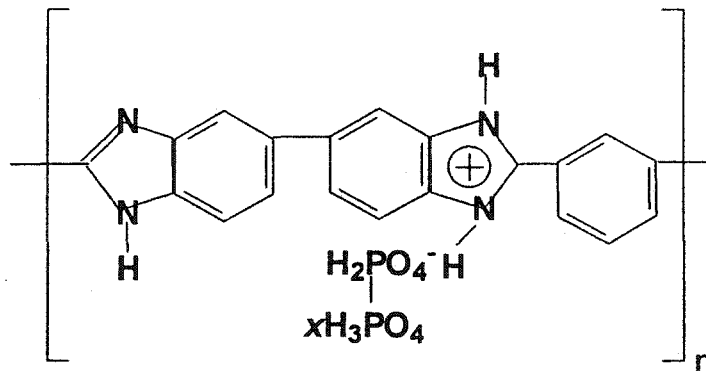
(b) Complex formation after treatment with H_3PO_4.

Figure 2-9 Complex formations by PBI on treatment with acids.

The imidazole group, like water, acts as a solvating agent for the proton [63]. It donates free electrons to the proton (from strong acids) to form stable complex. Bouchet and Siebert [64] using infrared spectroscopy showed that the interaction between PBI and

27

strong acids involved protonation and not hydrogen bonding. This strong interaction ensures the stability of acid-doped PBI membranes.

Glipa et al. discovered that PBI has a remarkable ability to absorb and concentrate H_3PO_4 in the polymer itself [65]. For example, in a H_3PO_4 solution of 3 M, the concentration of acid inside the PBI matrix was about 14.5 M, an increment of nearly five-fold.

2.3.7 Dissolution of PBI Powder

The dissolution capability of PBI depends on its molecular weight (M.W.). In the case of M.W. exceeding 100,000, solubility of the polymers in solvents decreases unfavorably, thus, preventing PBI from forming membranes. There are several solvents capable of dissolving typical unsubstituted PBI polymers. These include N,N-dimethylacetamide (DMAc), N,N-dimethylformamide, dimethylsulfoxide (DMSO) and N-methyl-2-pyrrolidone. Other solvents include formic acid, acetic acid, trifluoroacetic acid, and sulfuric acid [66].

Although there are varieties of solvents that can be used to dissolve the PBI polymer, particular attention must always focus on the difficulty of solvent removal during membranes film formation. Thus, strong acids like H_2SO_4 are obviously not a preferred choice since it has a high boiling point and is difficult to eliminate. Besides, solvents that have low boiling point can vaporize easily so, for example, trifluoroacetic acid is not a good choice because its rapid evaporation rate will make the formation of film difficult.

2.3.8 PBI Membrane Preparation

To date, there are numerous scientific reports available on different techniques that can be applied in preparing proton-conducting PBI membranes. Although these methods differ from one another, there is one common characteristic for all the methods: the basicity of undoped PBI is used to form complexes with strong acids such as sulfuric or phosphoric acid. These different methods are briefly summarized here as:

(i)   Solution casting method

(ii)   Phase inversion method

(iii)   Solution blend method

(iv)   Chemical grafting method

(v)   Polymer blending method

(i) Solution casting method

In this method, PBI powder is first dissolved in suitable solvents, followed by casting of the membranes via heat treatment. After that, protonic behavior is introduced into the membranes by immersing PBI membranes into the acid solution. Normally, DMAc [48, 50, 53, 67] or DMSO [65] is preferentially used. DMAc has a boiling point of about 166°C [68] while DMSO has a boiling point of 189°C [69].

Since the dissolution of PBI powder is quite a difficult task, especially at low temperature, elevated pressure and temperature typically are chosen to increase the dissolution rate while ensuring slow solvent evaporation. One suitable condition uses mixing of the mixtures (ranging from 5 to 30 wt% of PBI powder) at a temperature above the normal boiling point of the solvent, for example, about 25°C to 120°C above the normal boiling point, and at a pressure of 2 to 15 atm for a period of 1 to 5 h under constant stirring [66]. Because high pressure is used, this dissolution technique requires use of a stainless steel bomb reactor.

After dissolving the powder, the solution is filtered and cast onto a glass plate using the *doctor blade* technique. Then, the solution is heat treated to eliminate solvents. After elimination of solvent, the membranes can be detached from the glass plate by immersion into a water bath. The self-supported membranes are later immersed into acid solution to introduce proton-conducting behavior.

No reports describe degassing of the solution after the powder dissolution stage. Stirring may introduce air bubbles into the polymer solution during the dissolution process. If these air bubbles entrapped inside the solution are not eliminated prior to membrane casting, the resulting membranes may have increased porosity.

The *doctor blade* technique is commonly used in shape forming of polymer solution from slurry through its shearing action. When the PBI is in slurry form, it increases the

29

handling difficulty. The job of filtering the slurry from powder traces will be more difficult compared to use of PBI in solution form. In addition, this technique also requires careful control in order to get uniform thickness of membranes. For example, if the spreading rate of slurry is not rapid enough, as a result of high viscosity of slurry, spread slurry will be 'pulled away' by the moving blade, causing non-uniformity in membrane formation.

There are different heating treatments reported to prepare self-supported PBI membranes using solution casting method. Savinell et al. [48] dissolved the PBI powder (20 wt%) by using DMAc and prepared the PBI film by heating the film at 140°C in air for 15 min. and later on in a vacuum oven for overnight at 90°C to dry the film. The average M.W. of PBI that they used was about 25,000. Glipa et al. [65, 70] vacuumed dried the cast solution at 120°C for 5 to 6 h. The authors also mentioned in their articles about dissolving the PBI powder under reflux for 2 h, but without giving any specific temperature condition. Li et al. (2001) [53] dissolved the powder in a closed stainless steel bomb reactor at 250°C for 3 h. They further reported that majority of the solvent was evaporated in a ventilated oven from 80 to 120°C without indicating the effect of these different heating temperatures towards PBI film formation and morphology. Bouchet et al. [64] on the other hand prepared the membranes by heating the PBI at 100°C for the first 5 h followed by treatment at 200°C for another 2 h. The authors didn't mention the method they used to dissolve PBI powder.

During doping with acid, few parameters determine the amount of H_3PO_4 solution absorbed into PBI film [51, 62, 65, 70, 71]. These parameters include concentration of H_3PO_4 dopant and doping time. Glipa et al. [65] only investigated the acid concentration and ionic conductivity of H_3PO_4 and H_2SO_4 in PBI membranes after 1 h and 16 h at room temperature, but did not investigate the variation of acid uptake with time and temperature. Li et al. [53] only studied the H_3PO_4 uptake with concentration of H_3PO_4 dopant at room temperature for 4 to 5 days. No effort was done to determine exactly when the concentration equilibrium would be established.

On the other hand, Xing et al. [71] investigate the variation of ionic conductivity as a function of doping time (after 250 min. and after 10 days) in different acids with dissimilar concentration at room temperature, but no determination of acid doping uptake

30

with time was done. Savinell et al. [51] mentioning of doping in 11 M H_3PO_4 for at least 24 h to get 5 mol H_3PO_4 per repeat unit. At the same time, Hasiotis et al. [62] have studied the H_3PO_4 uptake in their polymer blending of sulfonated polysulfone and PBI (~25,000 M.W. from Celanase) in room temperature and temperatures higher than 80°C.

(ii) Phase inversion method

In this method, PBI solution is coagulated at an interface between the PBI solution itself and non-solvent (present in excess). This non-solvent contains strong acids like H_3PO_4. One typical example is 50 wt% H_3PO_4 in alcohol solution. Normally, the PBI slurry is cast first, then it is directly immersed into the non-solvent where doping and coagulation of PBI into solid film happens concurrently. The doping amount and elimination of solvent are determined by immersion time [72].

This method produces a completely different morphology from the solution casting method, because the interaction between non-solvent molecules and PBI slurry leads to the formation of porous membranes. These pores at the same time became filled with the acid solution. Removal of the residual non-solvent during the drying step collapses the porous structure, entrapping the acid and forming dense film. Nonetheless, no attempts have been done to ascertain the density, especially after heat treatment.

(iii) Solution blend method

In this method, blending of a fixed amount of strong acid and PBI are done in the same solvent. The solvent used is required to dissolve not only the imidazole ring-containing polymer and the dopant, but also the acid doped polymer produced. Thus, solvents such as DMAc, DMSO and N-methyl-2-pyrrolidone cannot be used because they produced acid doped polymer with low solubility. The preferred choice is trifluoroacetic acid solvent [73], which has a normal boiling point of 72°C [74]. A doped polymer having a slightly higher conductivity is obtained from this method, compared to the solution casting method, even though the conductivity of membranes still originated from doping with H_3PO_4. The cast film was heated at 140°C in air for 15 minutes to get self-supported membranes. Attempts to repeat this procedure at the reported temperatures

produced cracked membranes. This is because trifluoroacetic acid has a high vapor pressure.

(iv) Chemical grafting method

In this method, an unsubstituted PBI is first reacted with lithium hydride to produce PBI anions. Then, the anions are reacted with a substituted or an unsubstituted alkyl, aryl or alkenyl methyl halide to produce N-substituted alkyl, aryl or alkenyl PBI polymer [75]. The ionic conductivity of the substituted polymer depends on the SO_3H that are attached to the alkyl, aryl or alkenyl groups. The control of sulfonation is therefore, in principle, possible at two stages: by the extent of activation of the polymer (number of N–H groups ionized), and by the degree of chemical substitution of the activate sites [76].

By chemical grafting of sodium (4-bromo-methyl)-benzenesulfonate onto the anions form of PBI, Glipa et al. reported conductivity of 10^{-2} S.cm^{-1} at room temperature and 100% humidification for highly sulfonated samples [70]. In air, they rapidly and irreversibly shrank, and this change in size was accompanied by partial loss of conductivity to 10^{-4} S.cm^{-1}.

The drawback of this method is it involves too many reaction steps in producing proton-conducting PBI membranes. Furthermore, those steps are too time consuming. For example, the dissolution of PBI powder with lithium hydride was normally carried out in DMAc solution for at least 12 hours at 70°C [66]. Then, the reaction with grafting agents was completed in another 24 to 48 hours. After the reaction, the solution was precipitated and purified further. Then, the obtained solids was dissolved again and cast to form protonic conducting PBI membranes.

(v) Polymer blending method

In the polymer blending method, undoped PBI was coupled with other polymers through chemical grafting. Normally, a mixture of polymers cannot be established without specific interactions between polymers. In this method, the basic characteristics of PBI are changed by interacting it with acidic polymers. Upon mixing of an acidic polymer solution with basic PBI polymer in a suitable solvent (e.g. DMAc), the interactions between the two polymers occur by formation of hydrogen bonds and by

32

proton transfer from the acidic polymer to the basic polymer. Examples of acidic polymers include sulfonated poly-(2,6-dimethyl-1, 4-phenylene oxide) and sulfonated polysulfones [61, 62].

Although this is a completely different method from the previous case, the ionic conductivity is still dependant not on the degree of sulfonation, but mainly on the doping level of strong acids after immersion of the blended membranes into an acid bath. Furthermore, no significant improvement in tensile strength of blended PBI was found at 25°C; however, at 150°C a slight improvement was observed [77].

2.4 PHOSPHORIC ACID AS DOPANT FOR PBI

2.4.1 Introduction

Phosphoric acid, also known as orthophosphoric acid, H_3PO_4 is the building block for other phosphate derivatives. One of these derivatives is polyphosphate and another is pyrophosphate. Both occur through a condensation process, (thus they are called condensed phosphates) in which oxygen atoms shared between PO_4 tetrahedral lead to the formation of a covalent backbone of $P - O - P$ linkages [78].

H_3PO_4 is a tri-basic acid, in which the first hydrogen ion is strongly ionizing, the second one moderately weak and the third one extremely weak for ionizing. The dissociation constant for each step is $K_1 = 7.1 \times 10^{-3}$, $K_2 = 6.3 \times 10^{-8}$, and $K_3 = 4.4 \times 10^{-13}$ [78].

2.4.2 Conductivity Mechanism of Phosphoric Acid

H_3PO_4 has a high ionic conductivity. This is reflected by its remarkably high electrical conductivity, which is 0.04596 S.cm^{-1} at 25°C. Owing to the high viscosity of molten H_3PO_4, which is about 178 cP at 25°C [79], ordinary Stokesian migration of ions cannot explain this phenomenon, even if the compound is considered to be completely ionized. Greenwood and Thompson [80] attribute the high conductivity to the existence of a protonic chain conduction mechanism, which utilizes the movement of self-ionized ions such as $H_4PO_4^+$ or $H_2PO_4^-$ ions through the highly hydrogen-bonded structure. The self-dissociation of H_3PO_4 can be represented by two equilibrium reactions.

33

The first reaction is the rapid autoprotolysis equilibrium while the second reaction is ionic self-dehydration, which is slower compared to the first reaction [79]:

$$2 \text{ H}_3\text{PO}_4 \Leftrightarrow \text{H}_4\text{PO}_4^+ + \text{H}_2\text{PO}_4^- \qquad (2.14)$$

$$2 \text{ H}_3\text{PO}_4 \Leftrightarrow \text{H}_3\text{O}^+ + \text{H}_3\text{P}_2\text{O}_7^- \qquad (2.15)$$

Extensive hydrogen bonding has been found to take place in concentrated H_3PO_4, for example 90 wt%. In the crystal structure of the anhydrous acid, the tetrahedral H_3PO_4 groups are linked together by hydrogen bonding. At lower concentrations (75 wt% H_3PO_4), the tetrahedral are hydrogen-bonded to the water lattice [78]. In a dilute H_3PO_4 solution, the major contribution to conductance comes from the Stokesian ion transport, which accounts for nearly 0.002 $S.cm^{-1}$.

The introduction of an ionizing solute other than water into H_3PO_4 would decrease the conductivity of the H_3PO_4. This is because the addition of alien ions breaks the hydrogen-bonded structure of the H_3PO_4, which results in inhibition of the protonic chain structure formation that is necessary for proton hopping [79].

2.4.3 Conductivity of Phosphoric Acid Doped PBI Membranes

Although phosphoric acid doped PBI membranes have been used extensively in fuel cells, the reported conductivity data were quite scattered. Wainright et al. [49] reported a conductivity value of 2.5×10^{-3} $S.cm^{-1}$ at 130°C in a dry atmosphere for a PBI membrane doped with 338 mol% H_3PO_4. Fontanella et al. [81] obtained a conductivity of 4.5×10^{-5} $S.cm^{-1}$ for dry PBI doped with 600 mol% H_3PO_4 at 25°C while Bouchet et al. [64] reported an anhydrous conductivity of 7×10^{-6} $S.cm^{-1}$ at temperature of 30°C and doping level of 305 mol% H_3PO_4. At the same time, Kawahara et al. [82] obtained ionic conductivities of different doping levels, from 1.4 up to 2.9 mol H_3PO_4 and reported conductivity values of reaching 10^{-5} $S.cm^{-1}$ at 160°C for the highest doping level and Li et al. [53] reported conductivity of 4.5×10^{-3} $S.cm^{-1}$ at 25°C and 4.6×10^{-2} $S.cm^{-1}$ at 165°C for 450 mol% doping at R.H. of 80 – 85%. Savinell et al. reported that conductivity for 501 mol% H_3PO_4 was in the range of 0.01 $S.cm^{-1}$ to 0.04 $S.cm^{-1}$ for temperature from 130°C to 190°C and water vapor partial pressures up to 1 atm [73].

REFERENCES

[1]   Stambouli, A.B., and E. Traversa, "Fuel cells, an alternative to standard sources of energy", Renewable and Sustainable Energy Reviews, 6, 297 – 306 (2002).

[2]   Acres, G.J.K., "Recent advances in fuel cells technology and its applications", J. Power Sources, 100, 60 – 66 (2001).

[3]   Lower, S.K., "Chemistry and electricity" in "Electrochemistry", Retrieved January 15, 2004, from Chem1 Supplement Test, Simon Fraser University website: http://www.chem1.com/acad/pdf/c1xElchem.pdf

[4]   Carrette, L., K.S. Friedrich and U. Stimming, "Fuel cells - Fundamentals and applications", Fuel Cells, 1, 5 – 39 (2001).

[5]   Hirschenhofer, J.H., D.B. Stauffer, R.R. Engleman and M.G. Klett, "Fuel cells Handbook", 4th Ed., DOE/ FETC, (1998) pp. 2 – 20.

[6]   Liu, M., "H$_2$S powered fuel cells", PhD Thesis University of Alberta, p. 55 (2004).

[7]   Yates, C., and J. Winnick, "Anode materials for a hydrogen sulfide solid oxide fuel cell", J. Electrochem. Soc., 146, 2841 – 2844 (1999).

[8]   Williams, M.C., "Fuel cell", U. S. Department of Energy, 178 – 186.

[9]   Smith, J. M., H.C. van Ness and M.M. Abbott, "Introduction to Chemical Engineering Thermodynamic", 5th Edition, McGraw-Hill International Editions, Singapore (1996), pp. 18 – 171.

[10]   Retrieved November 20, 2003 from the website: http://www.tannerm.com/cellpot.htm

[11]   Wang, J.-T., J.S. Wainright, R.F. Savinell and M. Litt, "A direct methanol fuel cell using acid-doped polybenzimidazole as polymer electrolytes", J. Appl. Electrochem., 26, 751 – 756 (1996).

[12]   Weber, M., J.-T. Wang, S. Wasmus and R.F. Savinell, "Formic acid oxidation in a polymer electrolyte fuel cells. A real-time mass-spectrometry study", J. Electrochem. Soc., 143 (7), L158 – L160 (1996).

[13] Wang, J.-T., W.F. Lin, M. Weber, S. Wasmus and R.F. Savinell, "Trimethoxymethane as an alternative fuel for a direct oxidation PBI polymer electrolyte fuel cells", Electrochim. Acta, **43 (24)**, 3821 – 3828 (1998).

[14] Retrieved June 02, 2003 from the Gamry Instrument website at: http://www.gamry.com/App_Notes/EIS_Primer/EIS_Primer.pdf

[15] Appleby, A.J. and F.R. Foulkes, "Fuel cells Handbook," Van Nostrand Reinhold, New York, (1996).

[16] Hsu, M.S., "High temperature electrochemical converter for hydrocarbon", U. S. Patent #5,747,185 (1998).

[17] Fischer, W., "Fuel cells system for reacting hydrocarbon", U. S. Patent #3,718,506 (1973).

[18] Mazanec, T.J., and T.L. Cable, "Electrocatalytic oxidative dehydrogenation of saturated hydrocarbon to unsaturated hydrocarbon", U. S. Patent #4,933,054 (1990).

[19] Ahmed, S., J. Kopasz, R. Kumar and M. Krumplet, "Water balance in a polymer electrolyte fuel cells system", J. Power Sources, **112**, 519 – 530 (2002).

[20] Buswell, R.F., J.V. Clausi, R. Cohen, C. Louie and D.S. Watkins, "Hydrocarbon fueled solid polymer fuel cells electric power generation", U. S. Patent #5,360,679 (1994).

[21] Patterson, W.R., and C. Kemball, "The catalytic oxidation of olefins on metal films", J. Catal., **2**, 465 – 478 (1963).

[22] Oswin, H.G., A.J. Hartner and F. Malaspina, "A direct hydrocarbon/air fuel cell", Nature, **200**, 256 – 257 (1963).

[23] Cairns, E.J., "High-performance hydrocarbon fuel cells with fluoride electrolytes", Nature, **210**, 161 – 162 (1966).

[24] Niedrach, L.W., "The performance of hydrocarbon in ion exchange membranes fuel cells", J. Electrochem. Soc., **109**, 1092 – 1096 (1962).

[25] Brummer, S.B., and M.J. Turner, "The adsorption and oxidation of hydrocarbon on Noble Metal", J. Phys. Chem., **71**, 3902 – 3906 (1967).

[26]   Niedrach, L.W., and M. Tochner, "Behavior of saturated hydrocarbon on conducting porous teflon electrodes with a phosphoric acid electrolyte", J. Electrochem. Soc., **114**, 17 – 22 (1967).

[27]   Brummer, S.B., and M.J. Turner, "Oxidation and adsorption of hydrocarbon on noble metal electrodes. CH-type and O-type intermediates during the oxidative", J. Phys. Chem., 71, 2825 – 2837 (1967).

[28]   Cairns, E.J., and A.M. Breitenstein, "The kinetics of propane adsorption on platinum in hydrofluoric acid", J. Electrochem. Soc., **114**, 764 – 772 (1967).

[29]   Bockris, J.O.M., E. Gileadi and G.E. Stoner, "The anodic oxidation of saturated hydrocarbon. A mechanistic study", J. Phys. Chem., **73**, 427 – 434 (1969).

[30]   Otsuka, K., and I. Yamanaka, "Electrochemical cells as reactors for selective oxygenation of hydrocarbon at low temperature", Catal. Today, **41**, 311 – 325 (1998).

[31]   Petrovic, S., J.C. Donini, S.S. Thind, S. Tong and A.R. Sanger, "Electrochemical conversion of hydrocarbon", U. S. Patent #6,294,068 (2001).

[32]   Savadogo, O., and F.J.R. Varela, "Low-temperature direct propane polymer electrolyte membranes fuel cells (DPFC)", J. New Mat. Electrochem. Systems, **4**, 93 – 97 (2000).

[33]   Savadogo, O., "Emerging membranes for electrochemical systems: (I) solid polymer electrolyte membranes for fuel cells systems", J. New Mat. Electrochem. Systems, **1**, 47 – 66 (1998).

[34]   Gottesfeld, S., and T. Zawodzinski, "Polymer electrolyte fuel cells" in "Advances in electrochemical science and engineering", 5th Ed., R.C. Alkire, H. Gerischer, D.M. Kolb and C.W. Tobias, Eds., Wiley-VCH:Weinheim, New York (1997), pp. 260.

[35]   Anantaraman, A.V., and C.L. Gardner, "Studies on ion-exchange membranes. Part 1. Effect of humidity on the conductivity of Nafion[®]", J. Electroanalytical Chem., **414 (2)**, 115 – 120 (1996).

[36]   Retrieved   April   2,   2004   from   the   following   website: http://www.fuelcellseminar.com/pdf/2002/Zawodzinski.pdf

37

[37] Kreuer, K.D., "On the complexity of proton conduction phenomena", Solid State Ionics, **136 – 137**, 149 – 160 (2000).

[38] Zawodzinski Jr., T.A, T.E. Springer, J. Davey, R. Jestel, C. Lopez, J. Valerio and S. Gottesfeld, "A comparative study of water uptake by and transport through ionomeric fuel cell membranes", J. Electrochem. Soc., **140**, 1981 – 1985 (1993).

[39] Roziere, J., and D.J. Jones, "Non-perfluorinated polymer materials for proton exchange membranes fuel cells", Annu. Rev. Mater. Res., **33**, 505 – 555 (2003).

[40] Barbir F., and Gomez T., "Efficiency and economics of proton exchange membranes (PEM) fuel cells", Int. J. Hydrogen Energy, **21 (10)**, 891 – 901 (1996).

[41] Samms, S.R., S. Wasmus and R.F. Savinell, "Thermal stability of Nafion in simulated fuel cell environments", J. Electrochem. Soc., **143**, 1498 – 1504 (1996).

[42] Reichert, D., DuPont Fuel Cells. Contact: David.L.Reichert@usa.dupont.com

[43] University of Bremen (2004). Retrieved February 16, 2004 from: http://www.ceramics.uni-bremen.de/kwb/mitarbeiter/mark/FCFLecture_F.ppt

[44] Litt, M., "New polymer electrolytes", Case Western Reserve University (2001). Retrieved October 20, 2003 from the following website: http://electrochem.cwru.edu/NSF/posters/NSF-Litt-Poster.pdf

[45] Suzuki, H., Y. Yoshida, M.A Mehta, M. Watanabe and T. Fujinami, "Proton conducting borosiloxane solid electrolytes and their composites with Nafion[®]", Fuel Cells, **2 (1)**, 46 – 51 (2002).

[46] Gorer, A., "Platinum-ruthenium-palladium alloys for use as a fuel cells catalyst", U. S. Patent #6,498,121 (2002).

[47] Asensio, J.A., S. Borros and P.G. Romero, " Polymer electrolyte fuel cells based on phosphoric acid impregnated poly (2, 5-benzimidazole) membranes", J. Electrochem. Soc., **151 (2)**, A304 – A310 (2004).

[48] Savinell, R.F., and M.H. Litt, "Proton conducting polymers used as membranes", U.S. Patent #5,525,436 (1996).

[49] Wainright, J.S., J.-T. Wang, D. Weng, R.F. Savinell and M. Litt, "Acid-doped polybenzimidazoles: A new polymer electrolyte", J. Electrochem. Soc., **142**, L121 – L123 (1995).

[50] Wainright, J.S., R.F. Savinell and M.H. Litt, "Acid doped polybenzimidazole as a polymer electrolyte for methanol fuel cells" in "Proceedings of the 2nd International Symposium on New Materials for Fuel cells and Modern Battery Systems", Eds. O. Savadogo and P.R. Roberge, Montrèal, Canada, July 6 – 10, 1997, pp. 808 – 817.

[51] Wang, J.-T., R.F. Savinell, J. Wainright, M. Litt and H. Yu, "A H_2/O_2 fuel cell using acid doped polybenzimidazole as polymer electrolyte", Electrochim. Acta, **41 (2)**, 193 – 197 (1996).

[52] Savadogo, O., B. Xing, "Hydrogen/oxygen polymer electrolyte membranes fuel cell (PEMFC) based on acid-doped polybenzimidazole (PBI)", J. New Mat. Electrochem. Systems, **3**, 343 – 347 (2000).

[53] Li, Q., H.A. Hjuler and N.J. Bjerrum, "Phosphoric acid doped polybenzimidazole membranes: Physiochemical characterization and fuel cells applications", J. Appl. Electrochem., **31**, 773 – 779 (2001).

[54] Powers, E.J., and G.A. Serad, "High performance polymers: Their origin and development, Eds. R.B. Seymour, G.S. Kirschenbaum", New York: Elsevier, 355–373 (1986).

[55] Chung, T.S., "A critical review of polybenzimidazoles: Historical development and future R & D", 277 – 298 (1997).

[56] Aharoni, S.M., and A.J. Signorelli, "Electrical resistivity and ESCA studies on neutral poly (alkylbenzimidazoles), their salts, and complexes", J. Appl. Polym. Sci., **23 (9)**, 2653 – 2660 (1979).

[57] Singleton, R.W., H.D. Noether and J.F. Tracy, "The effects of structural modifications on the critical properties of PBI fiber", J. Polym. Sci.: Part C Polym. Symp., **19**, 65 – 76 (1967).

[58] Fuller, T.F., and J. Newman, "Experimental determination of the transport number of water in Nafion 117 membranes", J. Electrochem. Soc., **139**, 1332 – 1337 (1992).

[59] Samms, S.R., S. Wasmus and R.F. Savinell, "Thermal stability of proton conducting acid doped polybenzimidazole in simulated fuel cells environments", J. Electrochem. Soc., **143**, 1225 – 1232 (1996).

39

[60]   Asensio, J.A., S. Borros and P.G. Romero, "Proton-conducting polymers based on benzimidazoles and sulfonated benzimidazole", J. Polym. Sci.: Part A, **40**, 3703 – 3710 (2002).

[61]   Kosmala, B., and J. Schauer, "Ion-exchange membranes prepared by blending sulfonated poly (2,6-dimethyl-1, 4-phenylene oxide) with polybenzimidazole", J. Appl. Polym. Sc., **85**, 1118 – 1127 (2002).

[62]   Hasiotis, C., V. Deimede and C. Kontoyannis, "New polymer electrolytes based on blends of sulfonated polysulfones with polybenzimidazole", Electrochim. Acta, **46**, 2401 – 2406 (2001).

[63]   Kreuer, K.D., A. Fuchs, M. Ise, M. Spaeth and J. Maier, "Imidazole and pyrazole-based proton conducting polymers and liquids", Electrochim. Acta, **43**, 1281 – 1288 (1998).

[64]   Bouchet, R., and E. Siebert, "Proton conduction in acid doped polybenzimidazole", Solid State Ionics, **118**, 287 – 299 (1999).

[65]   Glipa, X., B. Bonnet, B. Mula, D.J. Jones and J. Roziere, "Investigation of the conduction properties of phosphoric acid and sulfuric acid doped polybenzimidazole", J. Mater. Chem., **9**, 3045 – 3049 (1999).

[66]   Sansone, M.J., F.J. Onorato and N. Ogata, "Acid-modified polybenzimidazole fuel cells elements", U. S. Patent #5,599,639 (1997).

[67]   Pu, H., W.H. Meyer and G. Wegner, "Proton transport in polybenzimidazole blended with H_3PO_4 or H_2SO_4", J. Polym. Sc.: Part B: Polym. Phys., **40**, 663 – 669 (2002).

[68]   Retrieved   March   18,   2004   from   the   website: http://ptcl.chem.ox.ac.uk/MSDS/DI/dimethyl_acetamide.html

[69]   Retrieved   March   18,   2004   from   the   website: http://ptcl.chem.ox.ac.uk/MSDS/ME/methyl_sulfoxide.html

[70]   Glipa, X., M.E. Haddad, D.J. Jones and J. Roziere, "Synthesis and characterization of sulfonated polybenzimidazole: A highly conducting proton exchange polymer", Solid State Ionics, **97**, 323 – 331 (1997).

[71]   Xing, B., and O. Savadogo, "The effect of acid doping on the conductivity of polybenzimidazole (PBI)", J. New Mat. Electrochem. Systems, **2**, 95–101 (1999).

40

[72] Sansone, M.J., F.J. Onorato, S.M. French, F. Marikar, "Process for producing polymeric films for use as fuel cells" U. S. Patent #6,187,231 B1 (2001).

[73] Savinell, R., and M.H. Litt, "Proton conducting polymers prepared by direct acid casting", U. S. Patent #5,716,727 (1998).

[74] Retrieved March 18, 2004 from the website: http://physchem.ox.ac.uk/MSDS/TR/trifluoroacetic_acid.html

[75] Sansone, M.J., "N-substituted polybenzimidazole polymer", U. S. Patent #4,898,917 (1990).

[76] Gieselman, M.B. and J.R. Reynolds, "Water-soluble polybenzimidazole-based polyelectrolytes", Macromol., 25, 4832 – 4834 (1992).

[77] Hasiotis, C., Q. Li, V. Deimede, J.K. Kallitsis, C.G. Kontoyannis and N.J. Bjerrum, "Development and characterization of acid-doped polybenzimidazole/ sulfonated polysulfone blend polymer electrolytes for fuel cells", J. Electrochem. Soc., 148, A513 – A519 (2001).

[78] Gard, D.R., (1996) "Phosphoric acids and phosphates", Kirk-Othmer Encyclopedia of Chemical Technology. Retrieved November 04, 2003 from the University of Alberta Library Website:

http://www.mrw.interscience.wiley.com/kirk/articles/phosgard.a01/sect1_1.html

[79] Ronald, A.M., and E.L. Michael, "The influence of ionic solutes upon the conductivity of molten phosphoric acid", J. Phys. Chem., 71, 3245 – 3248 (1967).

[80] Greenwood, N.N., and A. Thompson, "The mechanism of electrical conductivity in fused phosphoric and trideuterophosphoric acids", J. Chem. Soc., 3485 – 3492 (1959).

[81] Fontanella, J.J., M.C. Wintersgill, J.S. Wainright, R.F. Savinell and M. Litt, "High pressure electrical conductivity studies of acid doped polybenzimidazole", Electrochim. Acta, 43, 1289 – 1294 (1998).

[82] Kawahara, M., J. Morita, M. Rikukawa, K. Sanui and N. Ogata, "Synthesis and proton conductivity of thermally stable polymer electrolyte: Poly (benzimidazole) complexes with strong acid molecules", Electrochim. Acta, 45, 1395 – 1398 (2000).

41

CHAPTER 3

PBI POLYMER MEMBRANES

3.1 INTRODUCTION

In this chapter, details on the PBI membranes preparation method for the fuel cells application in our laboratory will be provided followed by some characterizations of the prepared membranes. PBI used was of high M.W. with an average value of 75,000, in contrast to PBI membranes prepared by other researchers. Consequently, it was not known whether this high M.W. PBI could be dissolved to make solutions from which defect-free film could be formed. The capability of high M.W. PBI to absorb strong acid has also been investigated.

To prepare PBI membranes, there are several aspects and limitations that need to be considered. For the purpose of preparing dense membranes for fuel cells application, the solution casting method was chosen because of its preparation simplicity. This method does not require utilization of highly sophisticated equipments, is not too time consuming and can produce membranes with controlled thickness and uniformity. Preparation parameters that had to be carefully controlled including temperature and duration of treatment.

The characterization of prepared PBI membranes included morphology studies on undoped and doped PBI membranes, the relationship of protonic conductivity behavior of H_3PO_4 doped PBI membranes to temperature under anhydrous conditions, and its stability over extended operating times, the thermal stability of H_3PO_4 doped PBI membranes in severe oxidizing and reducing environments, and its permeability to H_2 and O_2 gases.

3.2 EXPERIMENTAL PROCEDURE

3.2.1 PBI Membrane Preparation Procedure

Although solution casting was a method that has often been used in preparing PBI polymer membranes, the steps and treatments commonly used in earlier reports have been adapted to accommodate the equipment limitations existing in our laboratory. The first step in PBI membranes preparation is dissolution of PBI powder in DMAc. PBI powder used is the product of Aldrich with M.W. of ~75,000. Since one repeat unit of PBI has a mass of 308 a.u., this PBI powder has an average of 243 repeat units of PBI in one complete chain. This high M.W. PBI differed from those used by Savinell et al. (~25,000) [1], Bouchet et al. (~50,000) [2] and Asensio et al. (~27,200) [3], which had an average of 81, 162 and 88 repeat units respectively. It was anticipated that it would be more difficult to dissolve higher M.W. of PBI, because higher M.W. implies a longer molecular chain length. Therefore, a suitable weight ratio between PBI powder and solvent for dissolution had to be determined first.

In the first step, PBI powder was dissolved using DMAc (Aldrich) as solvent at 150°C for about 3 h in a closed Pyrex glass vessel. The main purpose to close the vessel was to avoid rapid evaporation of the DMAc solvent, as DMAc has a boiling point of 166°C at 1 atm. It was discovered that a weight ratio of 1:9 of PBI:DMAc effectively dissolved the PBI powder. The resulting solution was easily handled and readily filtered to provide a solution from which more uniform PBI membranes formation could be made, when compared to use PBI in slurry form.

Traces of PBI powder were removed from the PBI solution by filtration using glass microfiber filters with a nominal pore diameter of 1.5 µm (Whatman®). The solution so obtained was then degassed at room conditions to eliminate dissolved air bubbles and thereby prevent them causing defects in PBI film during PBI film formation. To date, there are no reports including this advantageous step in the PBI membrane preparation procedures. Thus there exists a high probability that earlier membrane morphology was not as dense as those in the present study.

43

The thickness of PBI membranes was controlled by varying the concentration of PBI solution, volume of PBI solution, or diameter of casting mold, which was a glass petri dish. Teflon was not used because it had poor wettability towards PBI solution. Since the PBI/DMAc was in solution form, the *doctor blade* technique was not used to regulate membrane thickness. The drawback of using the *doctor blade* technique was discussed in the previous chapter (Section 2.3.8).

Normally, the thickness of PBI membranes was in the range of 87.5 to 100 microns before doping. This was thicker than PBI membranes that were used by Xing and Savadogo in their H_2-O_2 fuel cells [4], who purchased PBI film from Hoechst Celanase with thickness of 40 μm before doping. Researchers from CWRU used PBI membranes with a typical thickness about 80 μm after doping [1].

The first step in preparation of self-supporting membranes was mild heat treatment. For this purpose, the solutions were warmed to dryness in an oven at 80°C for 5 h. After 5 h, the PBI film was immersed into water solution until the self-supporting membrane could be detached readily from the glass surface. The PBI film then was subjected to heat treatment at 195°C for more than 12 h to eliminate residual traces of DMAc solvent.

The last step was doping PBI membranes in acid solution, to ensure protonic conductivity. In the present case, since an objective was preparation of protonic conducting polymer membranes that can be used under substantially anhydrous condition, H_3PO_4 was preferred over other strong acids like H_2SO_4. This is because H_3PO_4 can ionically self-dissociate even in the absence of water. Movement of ions is essential for conductivity. Doping was done in 85 wt% H_3PO_4 solution (Aldrich) at selected temperatures and doping times. The optimum doping temperature, concentration of H_3PO_4 dopant solution and doping time were systematically varied, and the amount of acid doped into the PBI matrix was determined.

After doping, excess acid was removed from the PBI film surface using soft and dry tissue. This procedure was repeated until a constant mass was obtained. To determine the doping level, this film was dried at 130°C overnight to eliminate structural and hydration water from the PBI film.

The doping level was defined according to the following formula:

$$\text{Doping Level} \left(\frac{mol\% \ H_3PO_4}{repeat \ unit} \right) = \frac{(Weight_{130^\circ C} - Weight_{initial})}{Weight_{initial} \times 98} \times 308 \times 100\% \quad (3.1)$$

where $Weight_{130^\circ C}$ = Weight of acid doped PBI after stabilization at 130°C overnight.

$Weight_{initial}$ = Initial weight of undoped PBI polymer before doping.

Molecular weight of H_3PO_4 = 98 g.mol^{-1}.

The elimination of structural and hydration water was performed at 130°C because DSC analysis on fresh PBI membranes after doping showed an endothermic heat flow at 110 to 120°C. By heat-treating the membranes film at this temperature, it was discovered that the PBI membranes became less susceptible to cracking during fuel cell operation, especially during the temperature elevation from room temperature to over 100°C. The elimination of structural water from PBI matrix appeared to be followed by dimensional changes in the PBI film. It is suspected that there was movement of the polymer chain during this temperature elevation. Consequently, it was essential for the PBI film to be stabilized at 130°C overnight before determination of the required doping level. Complete DSC analysis on PBI membranes is presented in Section 3.3.5.

3.2.2 Protonic Conductivity Measurements

The protonic conductivity of acid treated PBI membranes was measured in a specially designed homemade cell during fuel cell operation. The apparatus for fuel cell applications will be described in detail in Chapter 4.

The protonic conductivity of PBI membranes was measured using electrochemical impedance spectroscopy (EIS) from Gamry Electrochemistry instrument, Version 3.20 © 2000. A 10 mV alternating potential signal was used with frequency ranging from 0.2 Hz to 100 kHz across the cell, to measure the alternate current response.

A complex impedance $Z(\omega)$ was determined and translated into a Nyquist plot, which is a plot of imaginary impedance (Y-axis) against the real impedance (X-axis) in a

complex plane at different frequencies. The resistance of cell was determined from the intercept with the X-axis of the Nyquist plot.

To measure the protonic conductivity of PBI membranes alone, all external factors that could contribute towards the overall measured resistance were eliminated.

$$R_{measured} = R_{PBI} + R_{external} \qquad (3.2)$$

The external resistance, $R_{external}$, includes the resistance from external electrical wires, resistance caused by bipolar plates, mesh and carbon cloth used as electrodes.

$$R_{external} = R_{wires} + R_{bipolar\ plates} + R_{mesh} + R_{carbon\ cloth} \qquad (3.3)$$

A blank test, without treated PBI membranes, was first carried out under the same conditions as the one with treated PBI membranes to measure the external resistance. The bulk resistance of PBI membranes was related to the ionic conductivity using the following equation:

$$\sigma_{PBI} = \frac{l}{R_{PBI}A} \qquad (3.4)$$

where σ_{PBI} = Ionic conductivity of membranes.

l = Thickness of membranes.

R_{PBI} = Resistance of PBI membranes.

A   = Area of tested membranes (corresponding to the area of electrode).

3.2.3 Differential Scanning Calorimetry (DSC)

DSC is an experimental technique for measuring the energy required to maintain a nearly-zero temperature difference between a specimen, sample S, and an inert reference material R, while both samples are subjected to an identical temperature programme [5].

Referring to Figure 3-1, S and R were enclosed in the same furnace together with a metallic block with high thermal conductivity that ensured a good heat-flow path between S and R. The enthalpy or heat capacity changes in the specimen S led to a temperature gradient relative to R. As a result, heat flow occurred between S and R. The temperature

46

difference, ΔT, between S and R was then recorded and further related to the enthalpy change in the specimen after calibration.

Heat-flux plate   Heating coil

Sample (S)   Reference R

T_{SP} T_{RP}

ΔT
Thermocouple

Inert gas
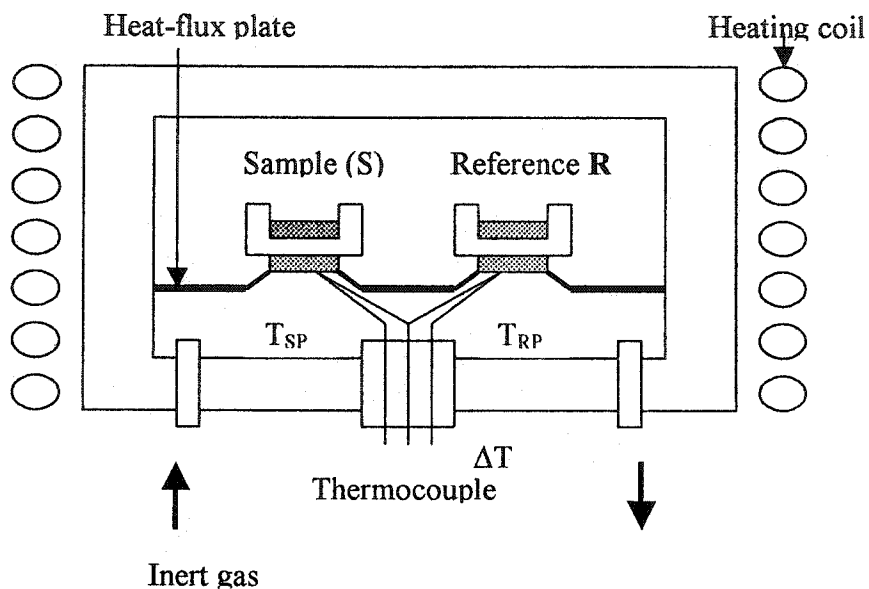
Figure 3-1 Illustration of DSC analyzing method (Nicula, 2000).

In a heat flux DSC instrument, the difference in energy required to maintain both S and R at the same temperature is a measure of the energy changes in the test specimen S relative to the inert reference R. The temperature difference ΔT that developed between S and R was proportional to the heat flow between the two [6]. In order to detect such a small temperature differences, it was essential to ensure that both S and R were exposed to the same temperature programme.

DSC was used to evaluate the thermal endurance of PBI membranes. It measured the amount of energy absorbed (endothermic heat flow) or released (exothermic heat flow) by undoped and doped PBI membranes during a controlled program of increasing temperatures. Any physical or chemical changes to PBI were shown by this analysis.

47

3.2.4 Gas Permeation Test

Permeation tests for H_3PO_4 doped PBI membranes as well as dry and untreated Nafion™ membranes were carried out using a homemade permeation test system, for both hydrogen and oxygen gases. Permeability of membranes refers to the dependence of flux towards the differential of pressure between feed side and permeate side. It has the unit of $mol.s^{-1}.m^{-1}.Pa^{-1}$.

$$\text{Permeability} = \frac{\dot{M} \times l}{A \times \Delta P} \qquad (3.5)$$

where $\dot{M}$ = Molar flowrate of permeating gas $(mol.s^{-1})$.

ΔP = Pressure difference (Pa).

Silicon black, which can withstand temperatures up to 200°C, was used as sealant in all tests. The test system consisted of two separate cylindrical stainless steel tubes, which had coaxial streams for both gas inlet and outlet. One of these tubes was reserved for the feed, where hydrogen or oxygen gases entered, while the tube attached to the opposite face of the membrane was for helium gas, which acted as sweeping gas. Specimens, either PBI or Nafion™ membranes, were inserted between these two tubes and sealed so that no leaking occurred.

To ensure no gas leak, before every permeation test the gas pressure at the feed side was increased to about 5 psig or higher and maintained at that value for several minutes, typically about 5 min. If, after 5 min., the pressure had not changed, then, no gas leak had happened.

Thus, any hydrogen or oxygen gas detected in the permeation side during the permeation tests using G.C. had resulted from permeation of the feed gases through the membranes. Figure 3-2 shows the gas permeability apparatus.

48
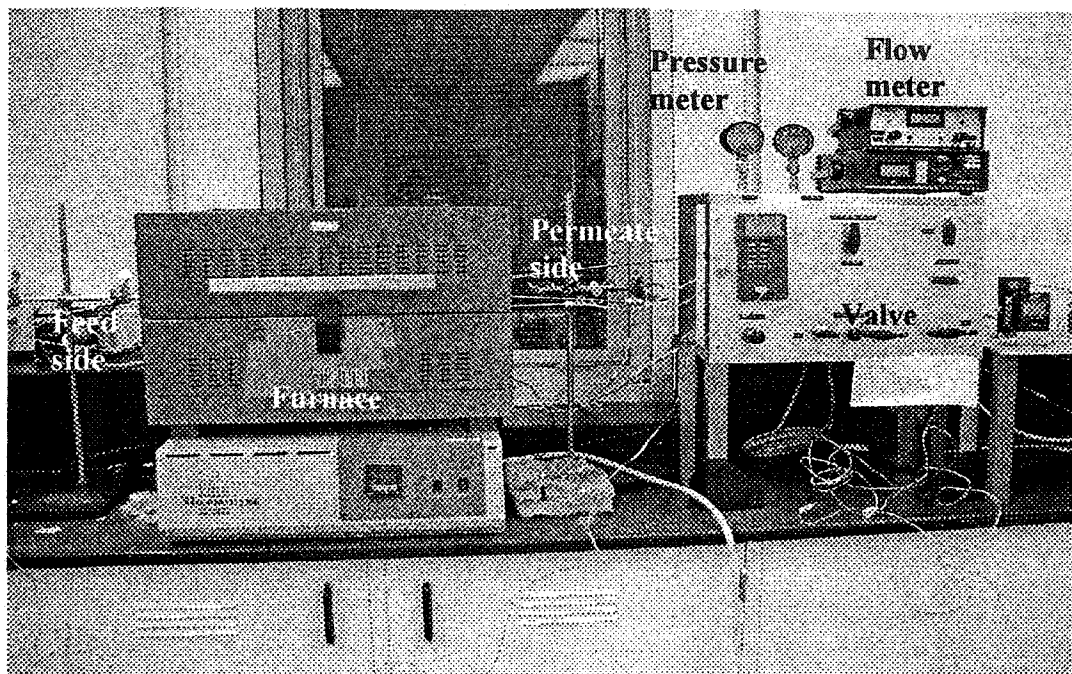
Figure 3-2 Experimental setup for gas permeability measurements.

3.3 RESULTS AND DISCUSSION

3.3.1 PBI Membranes Formation

3.3.1.1 Effect of PBI Solution Concentration on Membrane Formation

DMAc was utilized as solvent in casting PBI membranes from solution. A ratio of 9:1 by weight of DMAc to PBI powder was adopted because of the following effects:

i) A combination of 1 atm pressure and heating temperature of about 150°C can easily dissolve PBI powder. It took less than 2 h to completely dissolve PBI powder into solution, even though dissolving high M.W. PBI powder was not an easy task. Previous attempts to dissolve the PBI powder at a temperature of 60°C for more than 5 days did not effect the dissolution of PBI powder.

ii) This ratio enabled easier handling of PBI solution. Since it was in solution form and not too viscous, it was not necessary to regulate the thickness using the *doctor blade* technique. As mentioned before, the *doctor-blade* technique could cause inhomogeneous thickness if the spreading of PBI slurry was not

49

done properly. Instead, in solution form, it was only necessary to make sure that the floor of oven compartment was leveled before drying the solution.

iii)   A lower weight ratio of DMAc:PBI powder would have increased the powder dissolution difficulty. DMAc can dissolve PBI powder up to approximately 25 wt% PBI powder in 75 wt% DMAc solution, but the resulting mixture would be in slurry form and very viscous due to the high concentration.

iv)   A lower ratio also increased the handling difficulty, especially during casting. It became increasingly difficult to filter away remaining PBI powder traces from PBI solution before casting due to the high viscosity. High viscosity also increased the difficulty of elimination of air bubbles from PBI solution, which were induced during PBI dissolution as an effect from stirring. If the air bubbles were not eliminated, it affected the membrane's morphology.

v)   A higher ratio was not economic, because of use and then evaporation of excess solvent.

3.3.1.2 Effect of Temperature on Membranes Formation

DMAc has a boiling point of 166°C at 1 atm. To ensure that PBI film formed was free from DMAc solvent, a suitable heat treatment program was used. The heating temperature was high enough to evaporate DMAc, while maintaining film integrity. The membrane morphology must be dense and impermeable to gases. In fuel cell applications, it is essential to have an effective separation between gases in the anode and cathode compartments.

By applying an initial heating temperature of 80°C for 5 h after raising the temperature at 1.5°C.min^{-1} from room temperature, a dense, self-supporting homogenous film with a superior morphology was formed. The density was proven using gas permeability tests, which will be presented later (Section 3.3.6). Further investigation revealed that at 80°C, after continuous heating for 5 h, the majority of the solvent had evaporated, as shown in Figure 3-3. After this period, continuous heating at 80°C did not remove residual traces of DMAc solvent. So, in order to eliminate the solvent residual traces, a higher temperature than the boiling point of DMAc solvent was used.

50
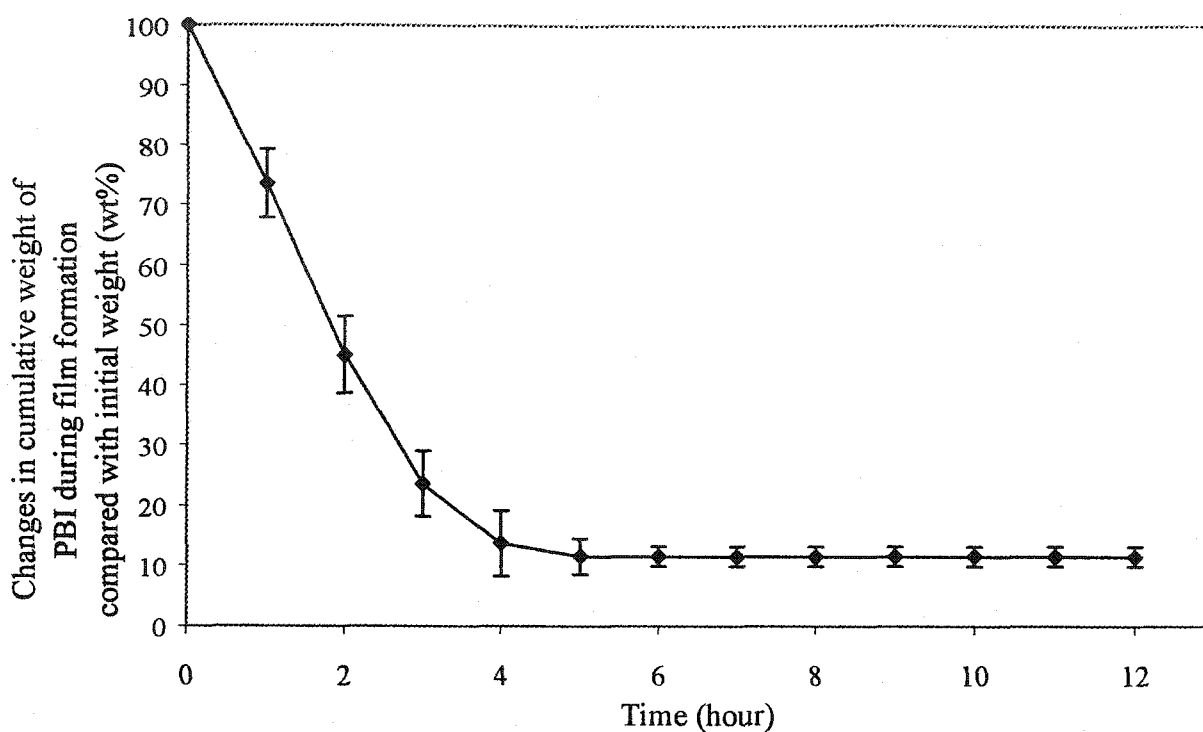
Figure 3-3 Variation of cumulative changes in PBI solution weight (wt%) as a function of time at 80°C.

A temperature of 195°C and continuous heating for overnight has been used to eliminate the final traces of DMAc solvent. Since DMAc has good solubility in water, it was expected that, during doping with acid solution, any DMAc solvent still present in small amounts would be eliminated entirely from the PBI film [7].

It was also undesirable to subject the PBI solution directly to a drying temperature of 100°C or higher, as had been done by other investigators. It was found that films produced using high heating temperature were inhomogeneous, visible to the naked eyes as different colors at different parts of the membranes. Inhomogeneous membranes had different thickness in different parts of the membranes. Normally, the membrane's center was thicker than the membrane's side. As the side of membranes was thinner, it had lower mechanical strength. The rapid heating rate also increased the solvent evaporation rate. Theoretically, the membrane should have been more porous than when using slower solvent evaporation rates. A slow evaporation rate ensured uniform solvent evaporation from the surface of PBI solution.

51

3.3.2 Effect of H$_3$PO$_4$ Doping on PBI Membranes

The undoped PBI membranes had typical thickness of 87.5 to 100 microns. These PBI membranes had very good mechanical properties in hydrated form. However, in the dry state, undoped PBI membranes became brittle and inflexible, making these membranes vulnerable to cracking.

Before doping, PBI membranes had insignificant ionic conductivity. Therefore, to convert undoped PBI into protonic conducting polymer membranes, they were doped with strong acid. H$_3$PO$_4$ was chosen because it is the only widely recognized low vapor pressure proton conductor in the 100 - 200°C range with high conductivity. Another advantage of doping PBI with H$_3$PO$_4$ was the improvement in mechanical properties. This was because under anhydrous conditions where undoped PBI normally dried up and became brittle, acid doped PBI remained flexible.

After doping with H$_3$PO$_4$, the excess acid was removed by adsorbtion into soft, dry tissues. It was very important not to remove excess acid from PBI surface with water or polar solvents like alcohols after doping. The dimensions of the membranes contracted greatly on drying, especially when alcohols were used to clean the PBI membranes surface. Furthermore, during heating at 130°C to determine the doping level, these PBI membranes became brittle and cracked easily. As the dimension of PBI membranes changed easily, this showed that H$_3$PO$_4$ doped PBI membranes were still amorphous polymer and no cross-linking between chains had occurred. By removing the excess acid using these polar solvents, the free H$_3$PO$_4$ molecules were pulled from PBI matrix. As a result, PBI membranes contracted.

Normally, the thickness of PBI membranes increased to about 100 to 125 microns after doping and the membranes were very flexible compared to their brittle nature before doping. Only flexible membranes were used in fuel cells, to avoid cracking of membranes during fuel cells operation.

In this study, I determined whether the PBI membranes, with an average M.W. of 75,000 had the same H$_3$PO$_4$ uptake capability as that reported by previous authors. This was important since H$_3$PO$_4$ was responsible for protonic conductivity. If the PBI

membranes with ~75,000 M.W. had not been able to absorb acid well, then the membranes could not be used in fuel cells.

Figure 3-4 shows the variation of H_3PO_4/PBI doping level with the concentration in H_3PO_4 dopant solution. The data were obtained after an immersion period of at least 3 days under ambient conditions. The amount of H_3PO_4 absorbed into the polymer matrix increased with concentration of H_3PO_4 dopant solution. Acid absorption was rather low at low concentration of H_3PO_4. This result is in good agreement with results reported by Li et al. by using low M.W. PBI [8]. Thus, it was shown that the molecular chain length played a relatively minor role in determining the acid uptake ability of PBI membranes.
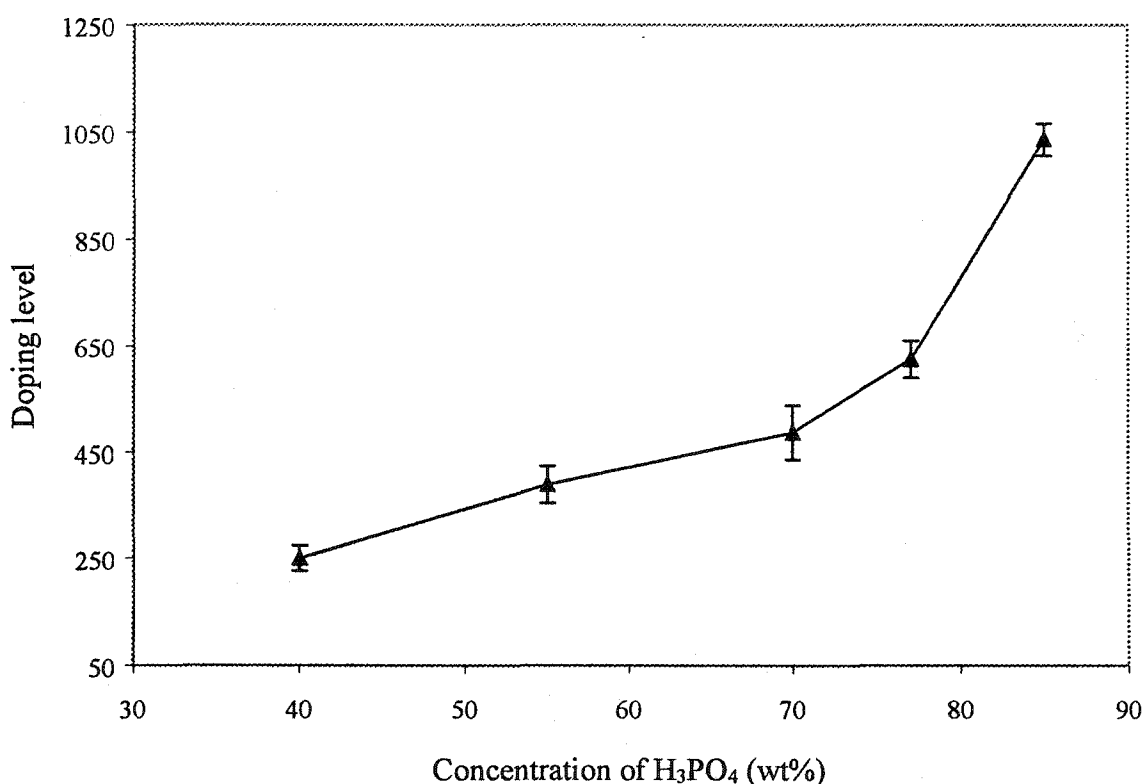
Figure 3-4 Variation in amount of H_3PO_4 doping level with concentration of H_3PO_4 dopant solution.

Referring to Figure 3-4, a doping level of about 470 mol% of H_3PO_4 per repeat unit was obtained using 70 wt% concentration of H_3PO_4 dopant. At higher concentrations, there was a sudden increase in the amount of H_3PO_4 absorbed. In the 85 wt% H_3PO_4 dopant solution, a doping level of 1050 mol% of H_3PO_4 per repeat unit was achieved. The

increase of concentration in acid dopant that resulted in greater acid absorption provided a larger driving force for diffusion of H_3PO_4 into the PBI matrix.

By fixing the H_3PO_4 dopant at certain concentration levels, the effect of doping time and temperature on the total amount of acid solution absorbed into the PBI film was able to be determined. After a sufficient doping time, a dynamic equilibrium was established between the H_3PO_4 acid inside the PBI film and the solution of H_3PO_4 dopant.

Referring to the graphs depicted in Figure 3-5, the doping time had a close correlation with temperature of H_3PO_4 solution dopant. As shown in Figure 3-5 (a), at ambient conditions, more than 20 h were needed for PBI film to reach doping equilibrium with 85 wt% H_3PO_4 solutions. Researchers from CWRU doped their PBI film by immersion into 11 M H_3PO_4 (~75 wt%) for at least 24 h to produce an equilibrated PBI membrane, consistent with the present results obtained for 85 wt% concentration.

Figure 3-5 (a) also shows that different acid uptakes could be obtained at different PBI membranes doping times. After nearly 6 h of doping, a doping level of 400 mol% H_3PO_4 per repeat unit of PBI was obtained.

Prolonged immersion of PBI membranes in the dopant solution increased the amount of H_3PO_4 absorbed into the PBI. After 10 h, a doping level of 600 mol% of H_3PO_4 per repeat unit of PBI was obtained. The doping level kept increasing until it reached above 1000 mol% after nearly 20 h. Then, further doping time did not increase significantly the doping level, as at this point equilibrium had been established. After 21 - 22 h, further doping did not result in higher doping levels. So, further doping at room temperature was not necessary.
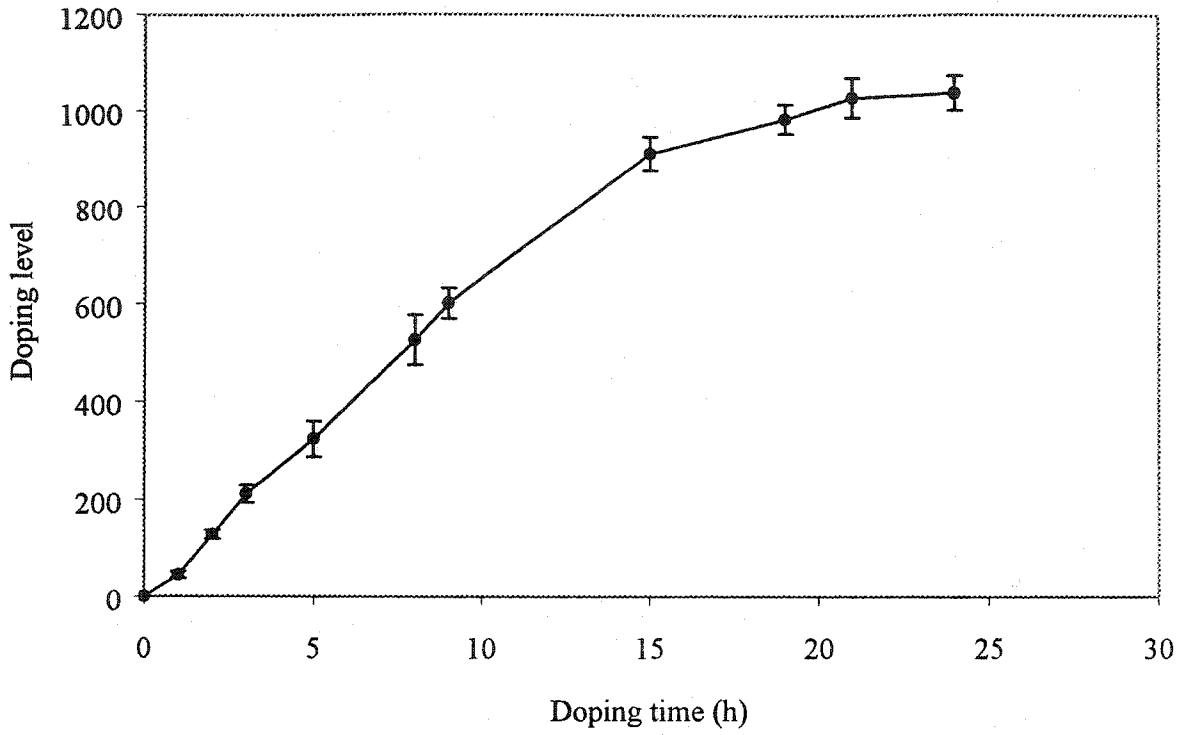
(a) H_3PO_4 doping in 85 wt% H_3PO_4 dopant at room condition.
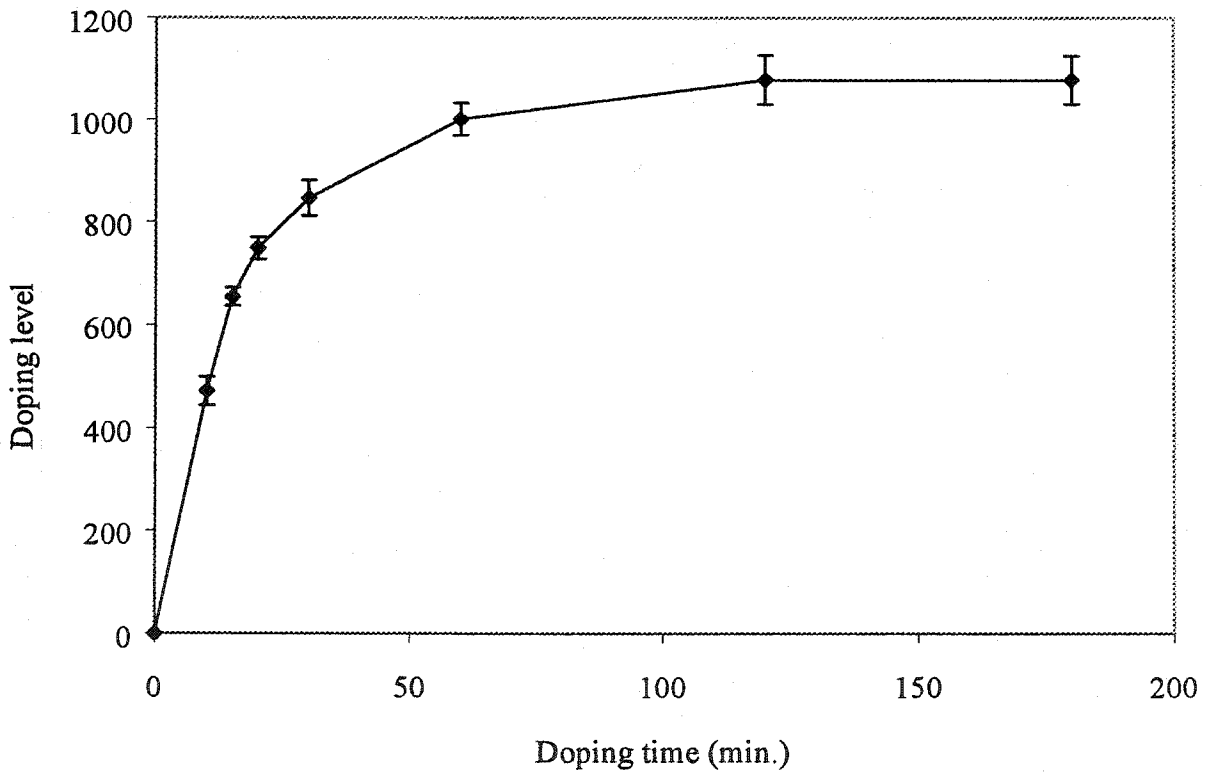
(b) H_3PO_4 doping in 85 wt% H_3PO_4 dopant at 60°C.

Figure 3-5 Effect of doping time and doping temperature on doping level.

55

Hasiotis et al. [9] described doping their blended PBI by immersion into H_3PO_4 solution (85 wt%) sequentially at temperatures of 80°C and 130°C. I found that incrementation of doping temperatures above 60°C was unfavorable since, at high H_3PO_4 concentration (85 wt%), a higher solution temperature caused dissolution of some of the PBI into the acid solution. Consequently, it is possible that the membranes that they developed were partly dissolved during doping at high temperature. Nevertheless, doping at higher temperature increased the doping rate, as reported by Hasiotis et al. for their blended PBI membranes. When I carried out doping at 60°C, the doping time was reduced greatly compared to doping at room temperature, as shown in Figure 3-5 (b). Equilibrium was established after about 1 h instead of 24 h. So, higher temperatures had enhanced the doping rate.

The optimum conditions for preparing protonic conducting PBI membranes were determined by carefully manipulating doping time with fixing both acid solution concentration at 85 wt% and doping temperature at 60°C. Savadogo et al. [10] reported doping times of up to 10 days at room temperature for PBI membranes used for H_2-O_2 fuel cells. In contrast, we were able to control doping levels by treating PBI film at 60°C within 1 h, thus saving preparation time.

Although a higher doping level was desirable for enhancement of ionic conductivity, the mechanical property of PBI film deteriorated if the doping level was too high. Typically, 500 mol% to 600 mol% doping levels did not cause adverse effects on PBI film's mechanical strength. Whenever very high doping levels of PBI membranes were used (> 1000 mol% per repeat units of PBI), the mechanical properties of the PBI membranes deteriorated. The film obtained was soft, even at room temperature, although it remained in the solid state. During fuel cell operation, the heavily doped membranes suffered cracking, especially at elevated temperatures, as the membranes became even softer.

56

3.3.3 Morphology of PBI Membranes

The morphology of PBI membranes has been studied using optical microscope (Olympus PME 3). The objective of this study was to have a better understanding of the type of PBI membranes morphology that were produced through the solution casting method. Savinell et al. [11] reported the formation of single-phase PBI membranes after doping, but this was expected since concentrated H_3PO_4 is itself a solvent for PBI.

There were no published PBI morphology studies. Furthermore, different heating temperatures and casting methods were used to prepare PBI membranes. Hence, it was particularly interesting to investigate whether the solution casting method produced membranes that were homogenous at microscopic level, and the effects of acid doping on membrane morphology. The suitability of the temperature treatment used during casting was dictated by the need for dense morphology and no visible macropores, normally termed as pinholes. Several figures depicting membrane morphology of untreated PBI membranes and doped membranes after treatment with H_3PO_4 are presented in this section. Figure 3-6 shows the morphology of PBI membranes at two different locations, before treatment with H_3PO_4. Both show dense microstructure with some visible micropores. No pinholes were observed on membranes prepared at the heating temperature that I used.
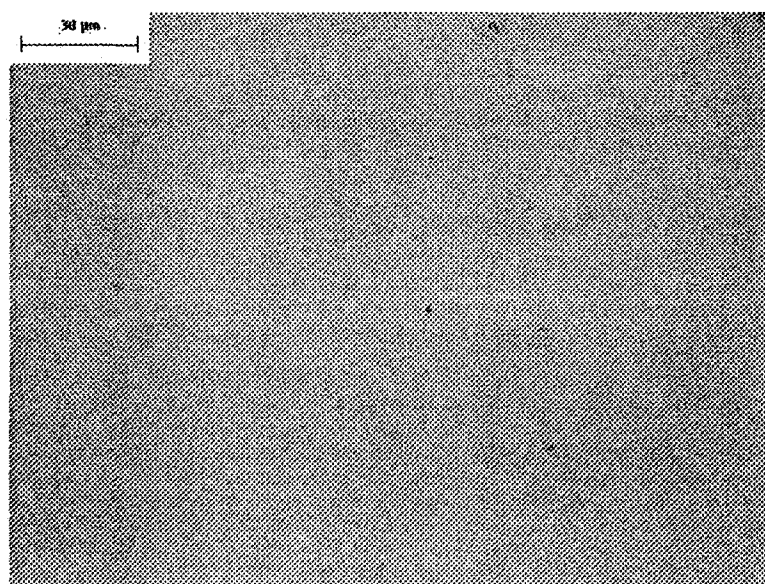
(a) Morphology of undoped PBI membrane.

57
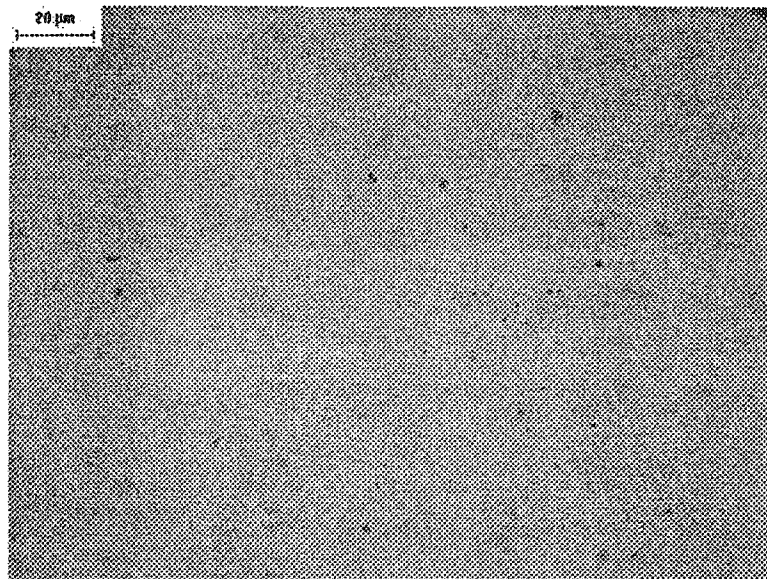
(b) Morphology of undoped PBI membrane at different locations.

Figure 3-6 Magnified undoped PBI membranes morphology by optical microscope at two different locations (200X).

At greater magnification, the most visible pores that were detected by optical microscope, with 500X resolution, were about 1.2 µm in diameter (Figure 3-7).

From optical microscope analysis, the membranes produced from this casting method were shown to be homogeneous with identical microstructures, based on observations done at several different locations. Although membrane surface morphology was not able to be ascertained fully using optical microscope analysis, it was expected that membrane morphology on the surface facing the base of the petri dish would be denser compared to the top surface. This was because the solvent evaporation rate was faster at the top surface, which was exposed to the heated surrounding atmosphere, resulting in more micropore formation.

The PBI membranes that were cast using the solution casting method were found to have morphology comparable to that of commercial Nafion™ polymer membranes. Figure 3-8 shows the morphology of Nafion™ membranes under a magnification of 100X. Referring to this figure, it is obvious that commercialized Nafion™ membranes has

58

a structure which is quite coarse and not smooth like the present PBI membranes. It also exhibits a significant number of tiny micropores.
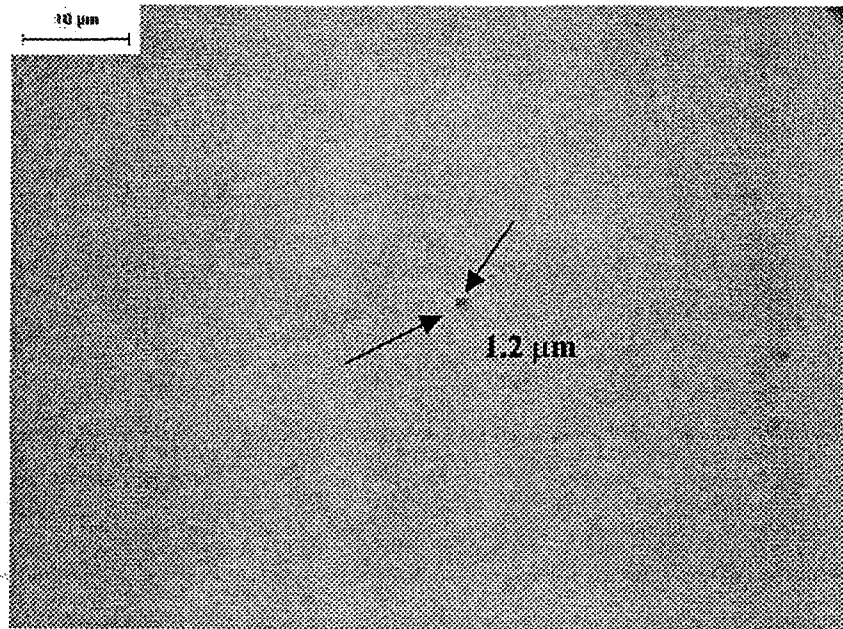
Figure 3-7 The most visible pores that were detected by optical microscope at a magnification of 500X.
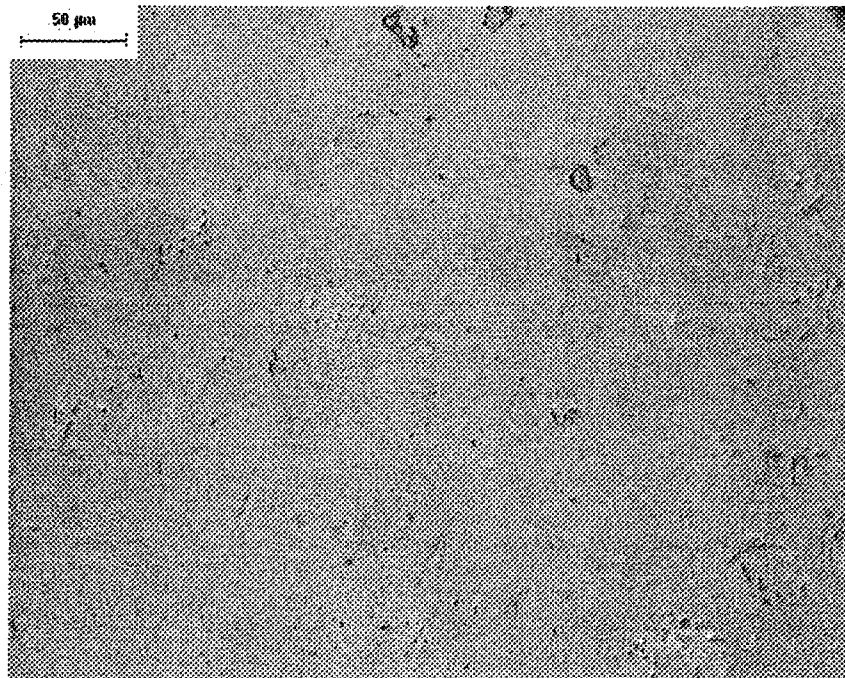
Figure 3-8 Membranes morphology of Nafion™ membranes (100X).

59
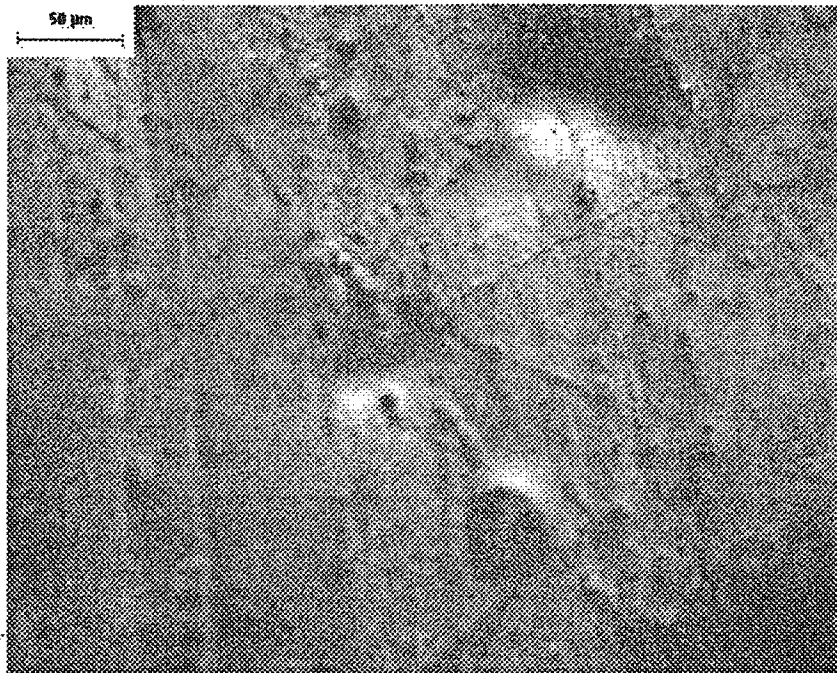
Figure 3-9 Morphology of PBI membranes after doping (100*X*).

To determine the effect of doping on the morphology of PBI membranes, the morphology of undoped membrane was compared with the same membrane after H_3PO_4 doping at 85 wt% acid concentrations and removal of excessive acid from the membrane surface using tissue paper. Figure 3-9 shows the membrane morphology after doping, at a magnification of 100*X*. It shows the difference in morphology after doping with H_3PO_4, when compared to that before doping (Figure 3-6). Figure 3-9 shows the formation of a thin layer of H_3PO_4 on the PBI membranes surface. This thin layer formation has prevented PBI membranes from being directly exposed to severe conditions, especially during fuel cell operation at elevated temperature. Therefore, doping improved the thermal stability of PBI membranes, because the membranes were protected by this thin phosphate layer.

3.3.4 Ionic Conductivity in PBI Membranes

There were several reasons for determining the ionic conductivity of membranes. One of the reasons was the wide range of values reported for ionic conductivities of doped PBI membranes by previous researchers (Section 2.4.3). Furthermore, no data

60

were available on the conductivity of H_3PO_4 doped PBI membranes for temperatures well over 200°C. Possible reasons for the lack of data include the decomposition of H_3PO_4 to form pyrophosphoric acid and polyphosphate by the elimination of water at temperatures above 200°C. This decomposition reaction would affect the conductivity of PBI membranes, although it was not known to what extent, nor the stability of conductivity with time.

3.3.4.1 Effect of Doping Level on PBI Membrane Conductivity

In the H_3PO_4/PBI system, the ionic conductivity of the membranes came from H_3PO_4 bonded within the polymer matrix. Therefore, a higher content of H_3PO_4 inside the PBI matrix would be expected to enhance the conductivity of H_3PO_4 doped PBI membranes. The effect of H_3PO_4 doping levels on conductivity of PBI membranes was investigated as a function of temperature under anhydrous conditions and data are presented in Figures 3-10 (a) and (b). Figure 3-10 (a) shows results obtained for 213 mol% doping level while Figure 3-10 (b) shows results for 335 mol% doping level.
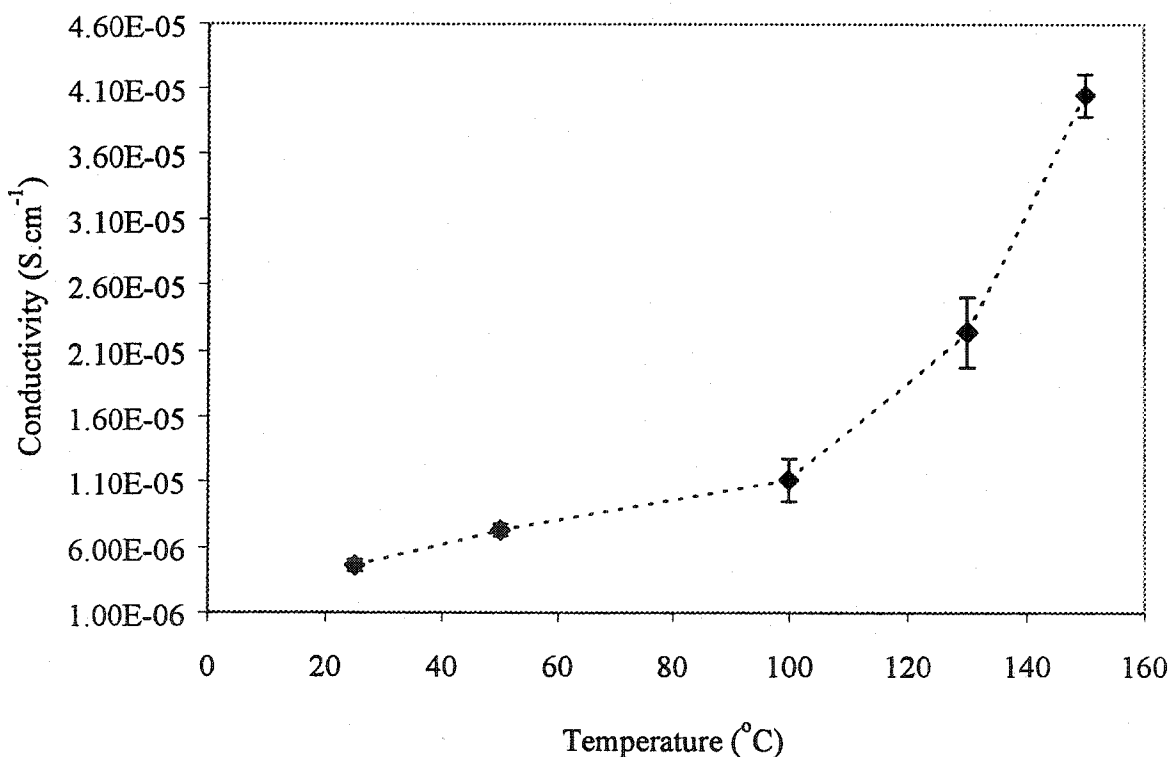
(a) Conductivity of H_3PO_4/PBI membranes at 213 mol% doping.
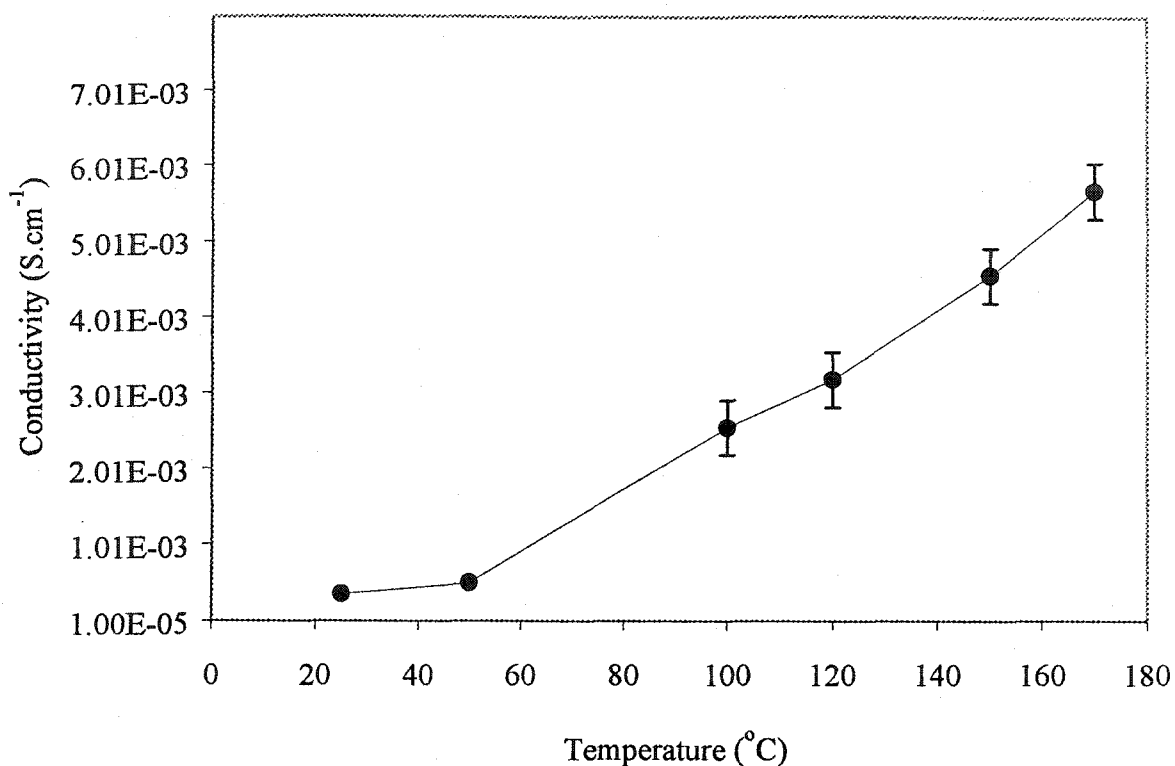
(b) Conductivity of H_3PO_4/PBI membranes at 335 mol% doping.

Figure 3-10 Effect of doping level on conductivity of H_3PO_4/PBI membranes as a function of temperature under anhydrous conditions.

Referring to Figure 3-10 (a), a low doping level, around 213 mol% H_3PO_4, produced PBI membranes with poor conductivity, which were about 10^{-6} S.cm^{-1} at room temperature and increased to about 4.0×10^{-5} S.cm^{-1} at 150°C.

A higher doping level, approximately 335 mol% doping enhanced the conductivity of H_3PO_4 doped PBI membranes. At room temperature, the conductivity of membranes was again poor, about 10^{-5} S.cm^{-1}, one order higher than the 213 mol% doping. But at higher temperatures, especially above 100°C, the conductivity improved to 10^{-3} S.cm^{-1} levels (Figure 3-10 (b)).

Although 335 mol% doping level exhibited higher conductivity, both PBI membranes with the specified doping levels were not suitable for use in fuel cells because of the low current densities obtained. For H_2-O_2 fuel cell operation, low internal resistance, about 0.2 to 0.4 Ohm, with conductivity of membrane about 10^{-2} S.cm^{-1} is a

62

prerequisite for high current flow (> 100 mA.cm^{-2}). Therefore, a higher doping level of H_3PO_4 was needed.

A previous report by Li et al. [8] described membranes with doping levels of 500 mol% to 600 mol% that exhibited good mechanical properties up to 200°C. Figure 3-11 shows the ionic conductivity variation of 550 mol% H_3PO_4 doped PBI membranes with temperature under anhydrous conditions.
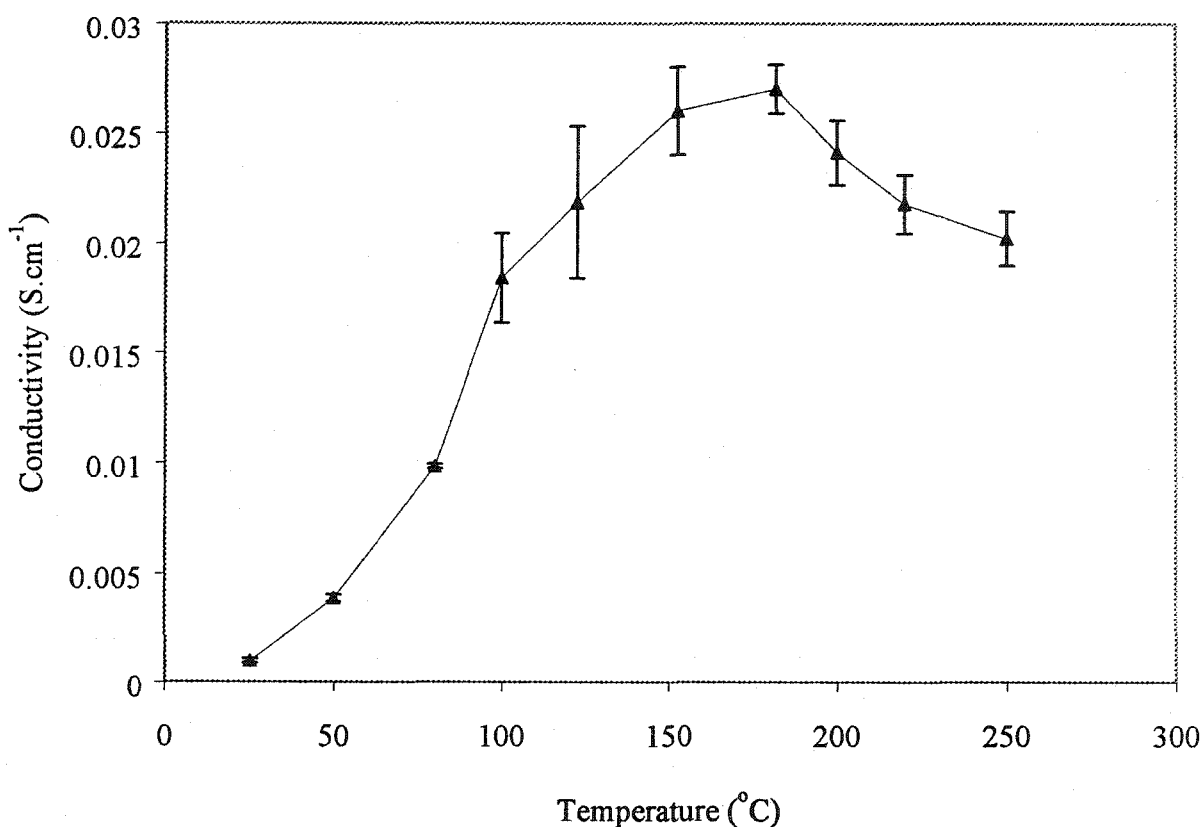
Figure 3-11 Ionic conductivity as a function of temperature under anhydrous condition (Doping level = 550 mol%), after stabilization for 2 to 3 h.

Typically, at temperatures below 80°C, PBI membranes exhibited poor conductivity, in the 10^{-3} S.cm^{-1} level. At room temperature, the conductivity was only about 10^{-4} S.cm^{-1}. The increase in temperature showed a beneficial effect towards the improvement of ionic conductivity. At about 80°C, the ionic conductivity reached nearly 10^{-2} S.cm^{-1} level and further increases in temperature resulted in even higher conductivity. The

enhancement of ionic conductivity is attributed to enhanced self-dissociation of H_3PO_4 to ions at temperatures higher than 100°C.

Nonetheless, drying up of membranes and condensation of H_3PO_4 to form pyrophosphoric acid and then polyphosphate in the region above 185°C resulted in drop in conductivity. The ionic conductivity of these membranes was still in the 10^{-2} S.cm^{-1} level, even at temperature as high as 250°C, which was acceptable for fuel cell operation. Membranes with conductivity of at least 10^{-2} S.cm^{-1} gave a better cell performance. Consequently, since PBI membranes with 550 mol% doping level exhibited very good ionic conductivity, all fuel cell conducted herein used PBI membranes with doping levels ranging from 500 mol% to 600 mol%.

At temperatures above 200°C, self-condensation of H_3PO_4 forming pyrophosphoric acid by water liberation was strongly favored [12, 13]. Figure 3-12 shows that formation of pyrophosphoric acid and polyphosphate by elimination of water molecule formed $P - O - P$ bonds.
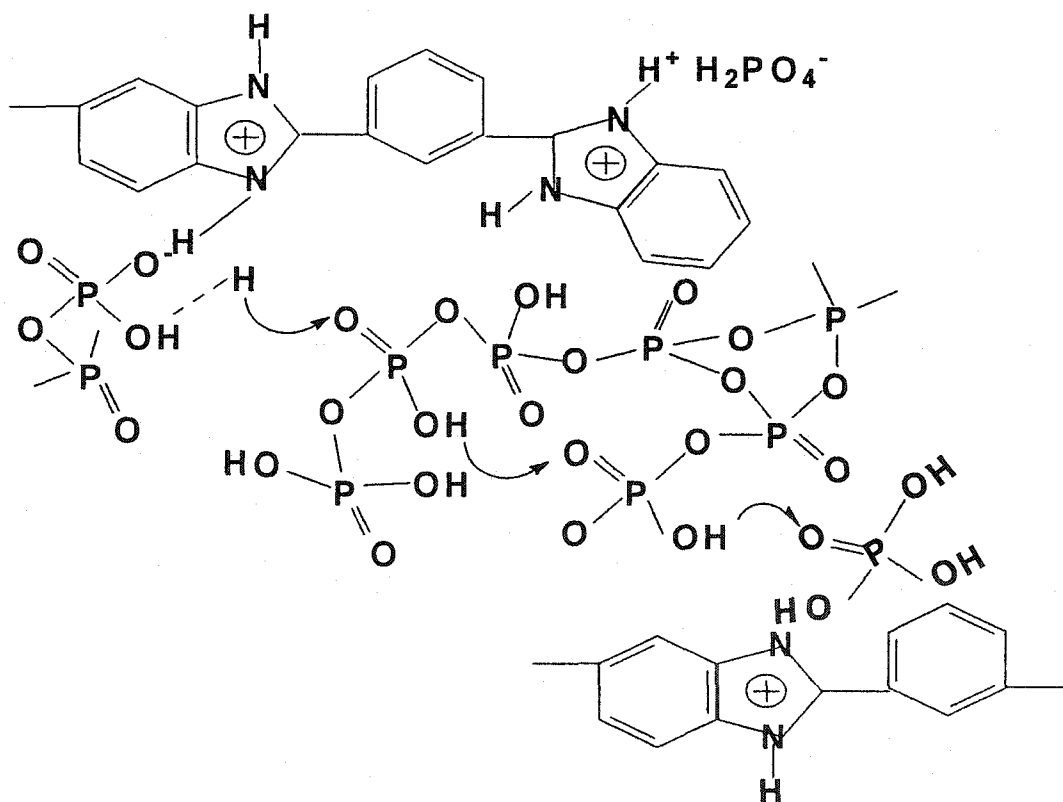
Figure 3-12 Illustration showing formation of polyphosphate chains inside PBI.

64

The elimination of OH groups contributed to the lower protonic conductivity behavior at high temperatures, because there were fewer acid sites available for proton hopping. This P – O – P polymer bond was stable, and dissociation into protonic ions thereafter became more difficult. Elimination of water meant that the amount of $H_2PO_4^-$ anion decreased. Thus, fewer ions were available to act as donors and acceptors in proton transfer.

3.3.4.2 Conductivity Stability of PBI Membranes

PBI membranes with high doping levels of 500 mol% to 600 mol% showed high conductivity ($> 10^{-2}$ S.cm^{-1}). Results presented in the previous section were obtained for the conductivity of PBI membranes in the first few hours in anhydrous condition after stabilization at each temperature. The conductivity stability of PBI membranes for extended periods was another important parameter that needed to be determined. The conductivity of PBI membranes, especially at high temperatures ($> 200°C$), always dropped after prolonged use, as shown in Figure 3-13.
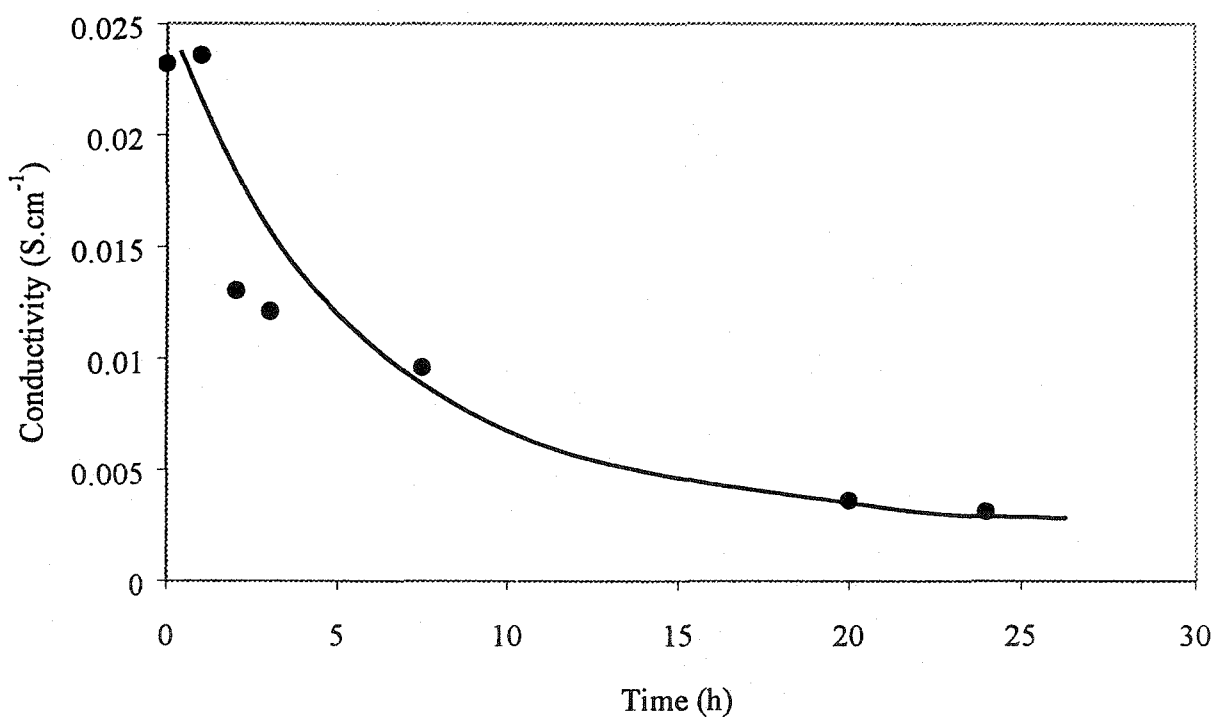
Figure 3-13 Conductivity versus time at 250°C under anhydrous conditions with doping level of 505 mol% H_3PO_4.

65

Figure 3-13 shows that, at 250°C under anhydrous condition, the conductivity of PBI membranes was not stable. After 24 h, conductivity dropped from 10^{-2} S.cm^{-1} to 10^{-3} S.cm^{-1}. This showed that the conductivity of PBI membranes was still influenced by water vapor because, as PBI membranes were subjected to high temperature, more and more water was eliminated from H_3PO_4 to form polyphosphate over time. Nevertheless, the conductivity had only dropped one order of magnitude under these conditions, and so was far superior when compared to the conductivity exhibited by Nafion^{TM} membranes, which depend strongly on R.H.

Through operation of these membranes in H_2-O_2 fuel cells, it was found that an option for maintaining the conductivity of H_3PO_4 doped PBI membranes was by humidification of the membranes resulting from water formation when a small current flows in the cell (Figure 3-14).
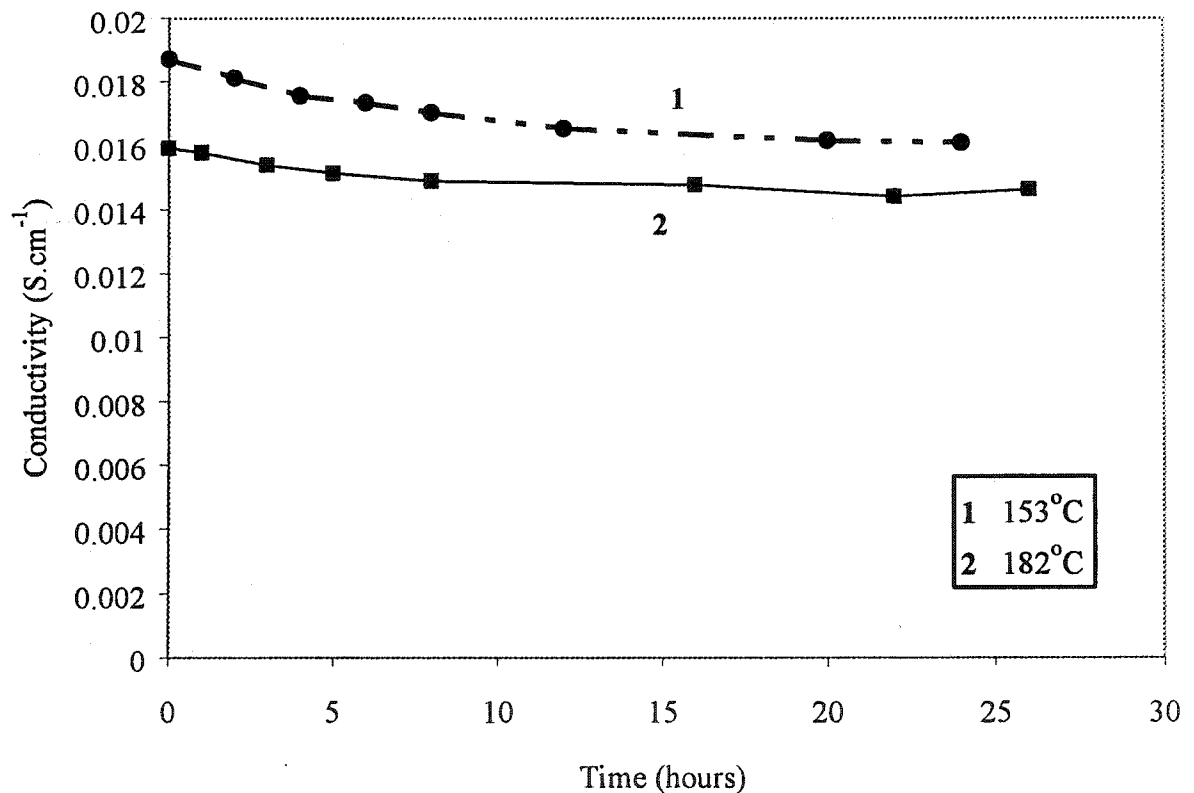
Figure 3-14 Conductivity stability versus exposure time at specified temperature with fuel cells working at 50 mA (Doping level ~ 500 mol%).

Figure 3-14 shows that by running H_2-O_2 fuel cells at 50 mA, the conductivity of PBI membranes with doping level of approximately 500 mol% at both 153°C and 182°C was maintained at 10^{-2} S.cm^{-1} levels, even after continuous use for 24 hours. Running the fuel cells ensured continuous production of water vapor in the cathode compartment. This water vapor was absorbed by H_3PO_4 doped PBI membranes, due to their hygroscopic nature, and thus maintained the membranes' conductivity.

An alternative method for maintaining the conductivity of PBI membranes was by humidifying the membranes with water vapor. A humidified PBI membrane was tested for conductivity stability at 250°C. Higher temperature not only favored rapid reaction kinetics, but at the same time also produced steam of 'high quality', if co-generation is implemented during fuel cell operation. H_3PO_4 doped PBI membranes exhibited good ionic conductivity at 250°C under conditions of slight humidification (Figure 3-15). This result was repeatable, and was confirmed during operation of hydrocarbon fuel cells (Chapter 5) at 250°C for several days. The data herein are a single, representative set from the accumulated data for a doping level of approximately 550 mol% H_3PO_4.
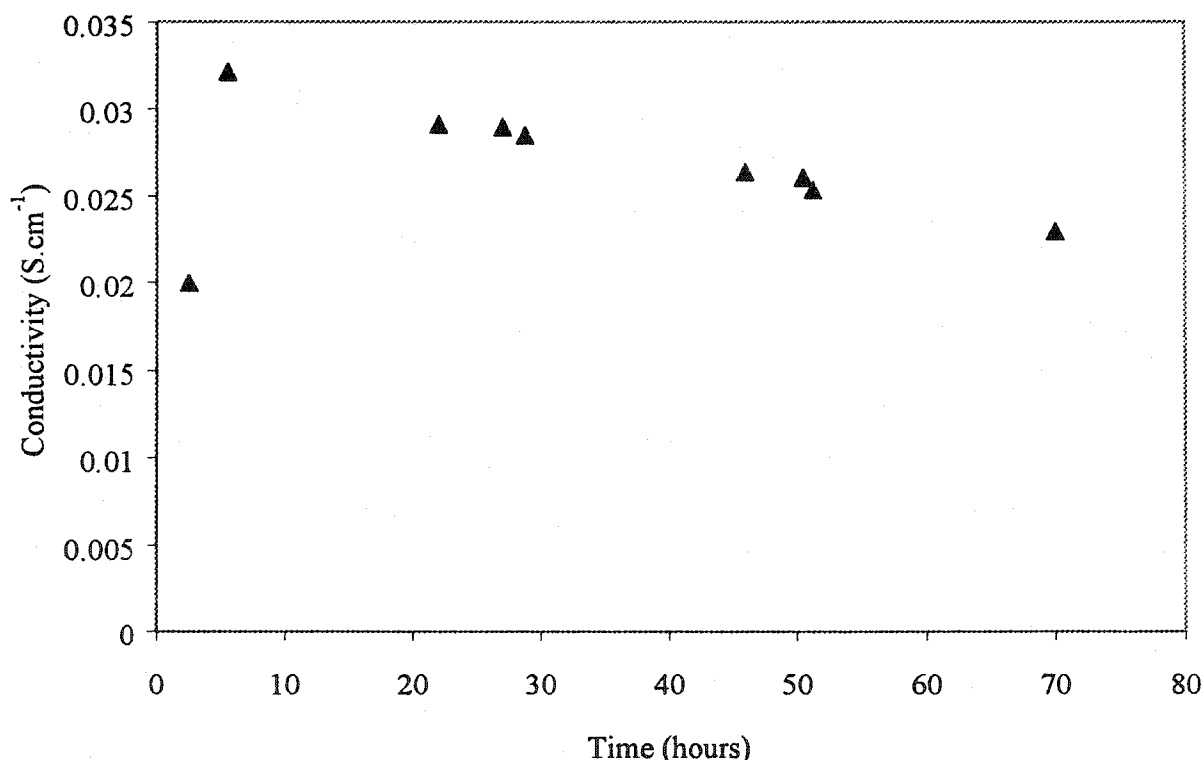
Figure 3-15 Stability of conductivity with time at 250°C, with water vapor activity of 0.0016 at both anode and cathode compartments.

Referring to Figure 3-15, the first data point was obtained after 2.5 hours at 250°C under anhydrous conditions. Addition of water vapor to the feed at temperature of 25°C slightly improved the ionic conductivity of PBI membranes. This was reflected by the second data point. Clearly, the conductivity of PBI membranes was stable under these conditions. After continuous operation for about 3 days, conductivity had only dropped slightly from 0.032 to 0.025 $S.cm^{-1}$. The conductivity stability shown by PBI membranes in this condition was indeed remarkable, considering that this membrane is humidified at water vapor activity of only 0.0016. During fuel cell operations, the continuous generation of water vapor at the cathode side enhanced and maintained the conductivity of the membranes.

3.3.4.3 Conductivity Mechanism inside H_3PO_4/PBI System

There are variety of opinions concerns the proton conduction mechanism in the PBI membranes. Conduction of H_3PO_4 inside PBI polymer has been reported to occur through proton hopping along the network of phosphate ion chains instead of segmental motions via the polymer chain [14, 15].

Since the conductivity of PBI membranes depends on free H_3PO_4 for good ionic conductivity, there is reason to believe that the proton conduction mechanism inside PBI membranes follows the same conduction mechanism as was found in concentrated H_3PO_4 solution (Section 2.4). In section 3.3.4.1, it was shown that low doping levels produced poor ionic conductivity. At low doping level, no free H_3PO_4 existed inside the polymer matrix since there was a high possibility that all H_3PO_4 was bonded to the available nitrogen sites of the polymer chain. With 500 mol% doping, 2 mol of H_3PO_4 are bonded to PBI to form the phosphate–PBI complex with strong interactions between them. The other 3 mol of acids are free acids, which are hydrogen-bonded to each other, and further hydrogen-bonded to the phosphate complex to form a network of H_3PO_4 chains.

Since low doping levels produced unsatisfactory membrane ionic conductivity, it was reasonable to conclude that there was no direct proton hopping between N–H sites. According to Li et al. [8], the average H_3PO_4 to H_3PO_4 distance was too large for proton hopping to occur at low doping, unlike at high doping levels when the average H_3PO_4 to

68

H_3PO_4 distance was small in comparison to the N–N separation between the imide groups, and thus the close distance allowed proton hopping between the anions.

Figure 3-16 is provided to illustrate schematically proton hopping during proton conduction in H_3PO_4 doped PBI membranes with a doping level of 500 mol% H_3PO_4. H_3PO_4 forms a network of acid chains inside the PBI polymer that connect one repeat unit to the other repeat units. Excess protons, from fuel cell operation, will be hydrogen bonded to one molecule of H_3PO_4. This proton will then hop to its neighboring H_3PO_4. Thus, transport of proton has taken place.
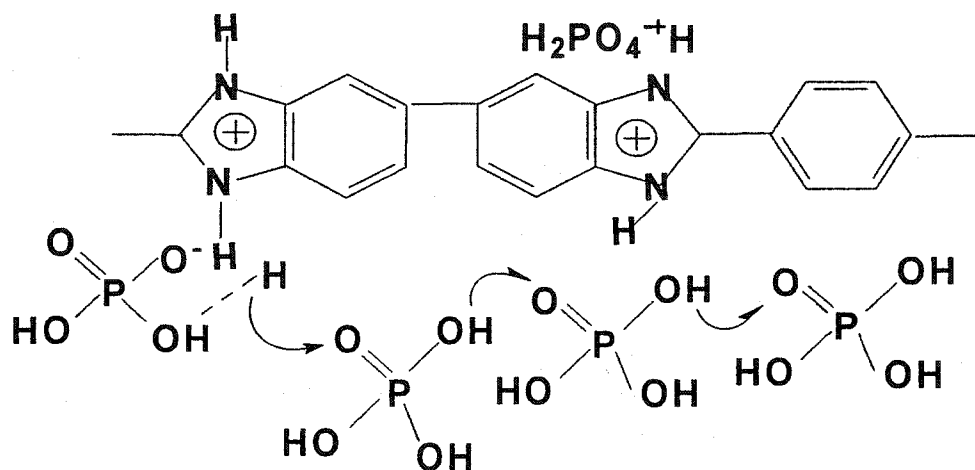
Figure 3-16 Proton hopping from one acid site to its neighboring acid at 500 mol% doping level.

From the conductivity measurements, PBI membranes with doping level of 200 mol% had poor membrane conductivity during fuel cells operation. This was because the 2 mol of H_3PO_4 acids in one repeat unit of PBI were chemical bonded to imide groups to form the PBI complex, and thus were weaker in terms of further ionizing ability. Without the presence of free H_3PO_4, the conductive network of phosphate chains was not formed.

It was very important to keep treated PBI membranes away from liquid water, since H_3PO_4 inside the PBI membranes was highly hygroscopic and so had high affinity for water. Liquid water, if present in excess, pulled out the free acid from the PBI matrix. As a consequence, it caused a drop in membrane conductivity. Operation of fuel cells which utilized PBI/H_3PO_4 acid membranes was thus preferably carried out under conditions that were liquid water free. Nonetheless, the presence of water vapor was highly favorable for

69

conductivity of H_3PO_4 doped PBI membranes, because water was required to minimize formation of condensed polyphosphates.

3.3.5 Thermal Stability of PBI Membranes

The majority of previous thermal stability studies conducted on PBI membranes were carried out using Thermal Gravimetric Analysis (TGA) methods. Furthermore, most of the analysis was only done on fresh H_3PO_4 doped PBI membranes. Comparisons were then made to see the effect of doping towards chemical stability of PBI, without consideration of the exposure time. To date, only Samms et al. [16] have reported analyzing thermal stability of acid doped PBI by heating in TGA while in an atmosphere of either nitrogen or 5% hydrogen (nitrogen balance), or air. There are no reports of any efforts to investigate the thermal stability of PBI membranes under severe reducing (pure H_2) and oxidizing environments (pure O_2). Furthermore, no data are provided on PBI membrane stability when kept under these conditions for extended periods.

Thus the objective of this study was to determine the thermal stability of PBI membranes under these severe environments during operation at 250°C. DSC analysis was performed to study the thermal stability of PBI membranes. The measurements were conducted under an atmosphere of N_2 and a temperature programme of $10°C.min^{-1}$. Comparison was made between PBI powder before casting, fresh PBI membranes after doping with H_3PO_4 and PBI after prolonged operation in fuel cell at 250°C.

Pure PBI, in powder form had remarkable thermal endurance (Figure 3-17). PBI powder showed an endothermic heat flow peak at about 118°C. This peak was assigned to the heat absorbed to evaporate water from PBI powder. The analysis confirmed that pure PBI powder indeed has the ability to retain water strongly. This water originated from the moisture in atmosphere. It happened as a result of long-term exposure as PBI powder was only stored under normal room conditions. There was no further chemical degradation up to 500°C. In addition, there was no obvious T_g peak. A small peak was observed around 420°C that may indicate a phase transition.

70
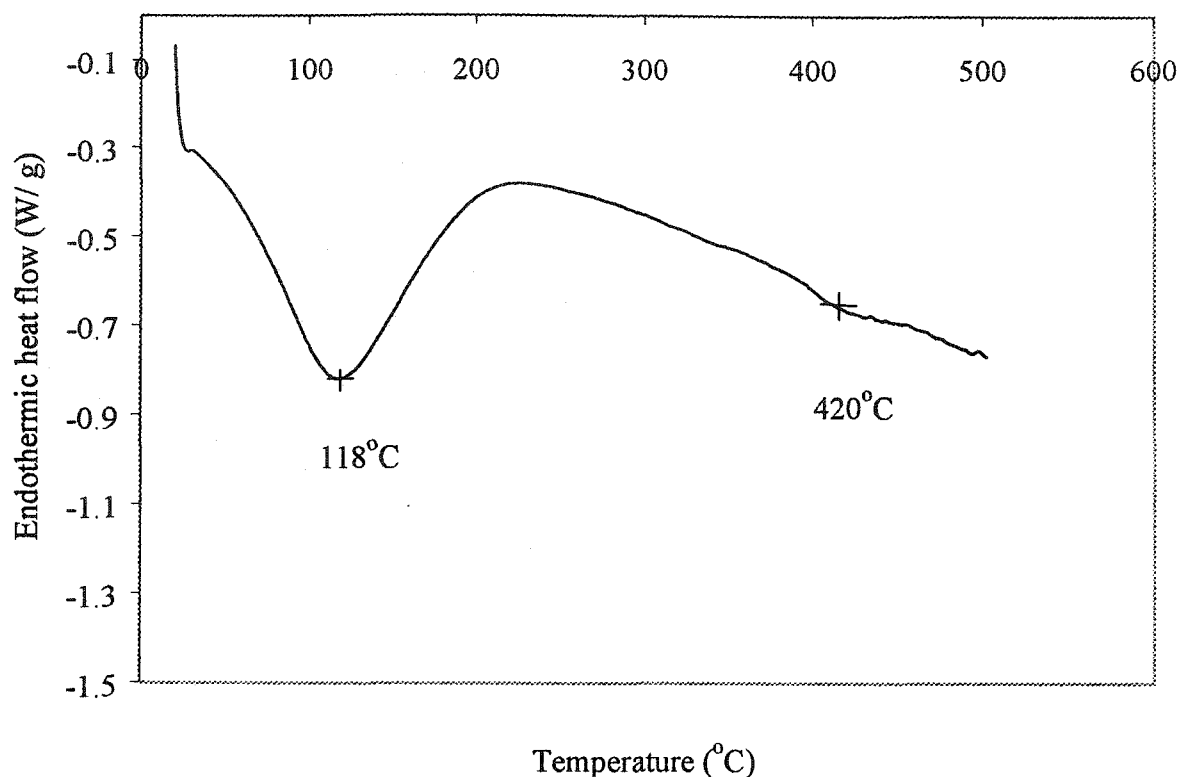
Figure 3-17 DSC analysis on pure PBI powder.

Figure 3-18 shows the DSC analysis of fresh H_3PO_4 doped PBI membranes under the same conditions. Two peaks were detected. The first peak at 104°C was attributed to the loss of water from the fresh PBI membranes. This water was either structural water or hydration water from H_3PO_4 because, as mentioned earlier, H_3PO_4 is a highly hygroscopic material that absorbs and retains water.

In addition, condensation of H_3PO_4 also occurred to produce water through the formation of pyrophosphoric acid. However, it was expected that the contribution from this process would be small at this low temperature. This endothermic heat value was greater than the endothermic heat that was absorbed by untreated PBI powder at the same peak, showing that a greater amount of water was eliminated from treated PBI membranes.

71
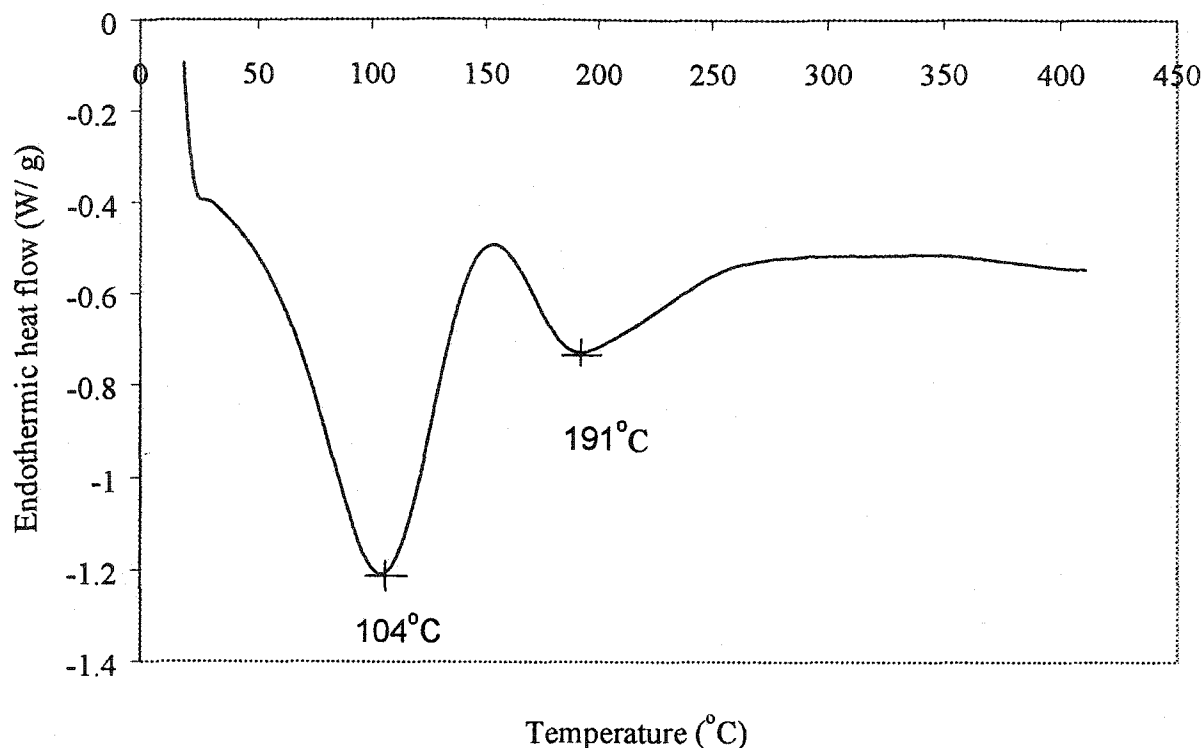
Figure 3-18 DSC analysis on fresh H_3PO_4 doped PBI membranes.

A second endothermic heat peak was observed at 191°C, consistent with extensive formation of pyrophosphoric acid and polyphosphate by condensation reactions. The elimination of water to form pyrophosphoric acid and polyphosphate at this high temperature was consistent with the drop in ionic conductivity of PBI membranes reported in the previous section. No other peaks were observed, showing that treated PBI membranes had similar thermal stability to the untreated PBI in powder form.

The analysis shown in Figure 3-19 was conducted on one of the H_3PO_4 doped PBI membrane after used in a fuel cell under severe operating conditions. The membranes analyzed had been exposed to highly oxidizing (pure O_2) and reducing environments (pure H_2 or a hydrocarbon such as ethane) continuously for about 5 days, at 200°C for 2 days then to 250°C for 3 days. The membrane after fuel cell use, had been left under ambient conditions for a period of time before DSC analysis, and so had absorbed moisture from the atmosphere. Thus the DSC analysis again showed loss of adsorbed water from these PBI membranes at both 110°C and 193°C. No other chemical decomposition reactions occurred, even up to 400°C. Thus I showed that H_3PO_4 doped

72

PBI can withstand use under severe operating conditions, and did not undergo any chemical degradation at 250°C during continuous operation for more than 5 days. If such membranes were not stable, the DSC analysis would not have shown the same analysis as had been found for the fresh acid doped PBI membranes.
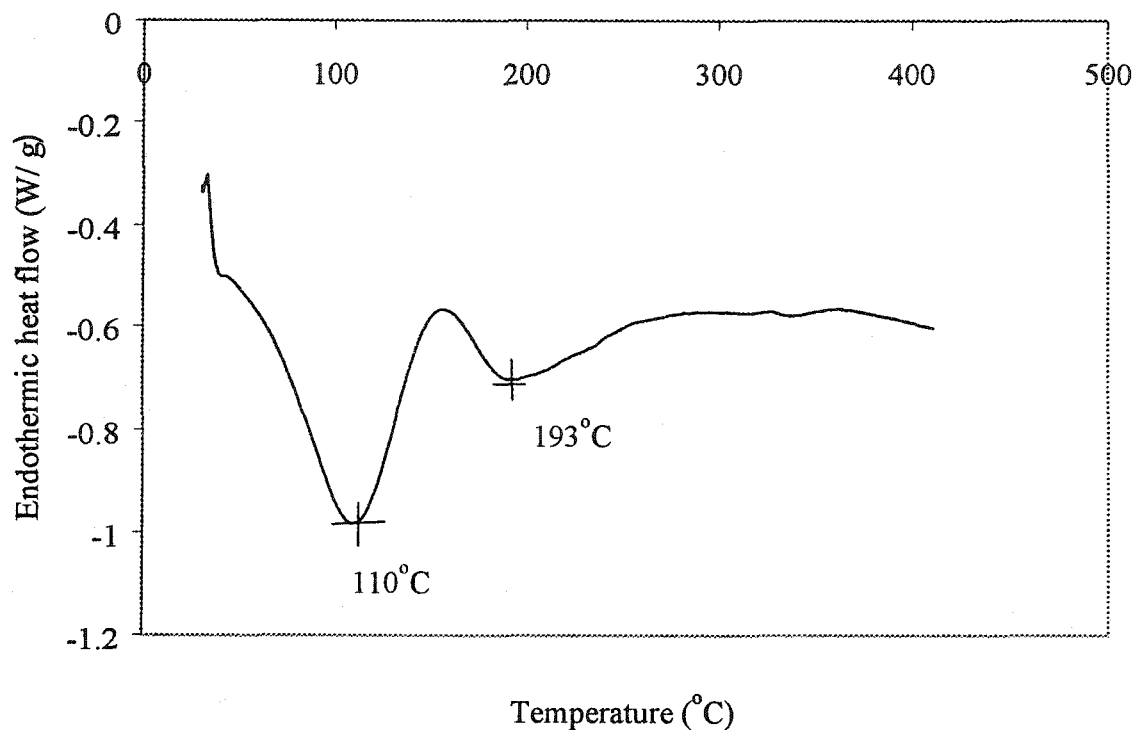
Figure 3-19 DSC analysis on H_3PO_4 doped PBI membranes after use in a H_2-O_2 fuel cell.

From all the DSC analysis presented here, I conclude that both new and used H_3PO_4 treated PBI membranes possessed high thermal stability. The only losses of water from PBI occurred at temperatures ranging from 100 to 200°C, and no other chemical degradation happened up to 400°C. The stability of treated PBI membranes during fuel cell application at 250°C was proven by the analysis on the used membranes, which had been exposed to severe oxidizing and reducing environments for 5 days. Again, no chemical degradation was observed from DSC analysis of this film.

3.3.6 Gas Permeability Tests

The main objective of these tests was to determine and compare the permeability of H_2 and O_2 through Nafion™ and H_3PO_4 doped PBI membranes. Figures 3-20 (a) and (b)

73

show the variation of oxygen and hydrogen permeability with temperature, respectively. H_3PO_4 doped PBI showed greater resistance to permeability of both gases when compared to Nafion™ membranes over the same temperature range. Furthermore, for H_3PO_4 doped PBI membranes, up to temperatures of about 170°C, the permeabilities of hydrogen and oxygen gases were substantially independent of temperature, proving that, in this temperature range, PBI membranes can be used at higher temperatures than Nafion™ membranes. This effect is attributed to the denser microstructure of PBI, which limited the passage of gases. At approximately 190°C, the permeability of gases through PBI membranes started to increase, and the increment in permeability was particularly more profound for the hydrogen gas compared to oxygen gas, indicating that at higher temperatures, the micropores had expanded to a larger diameter. As a result, membranes became more porous and permeability increased sharply.
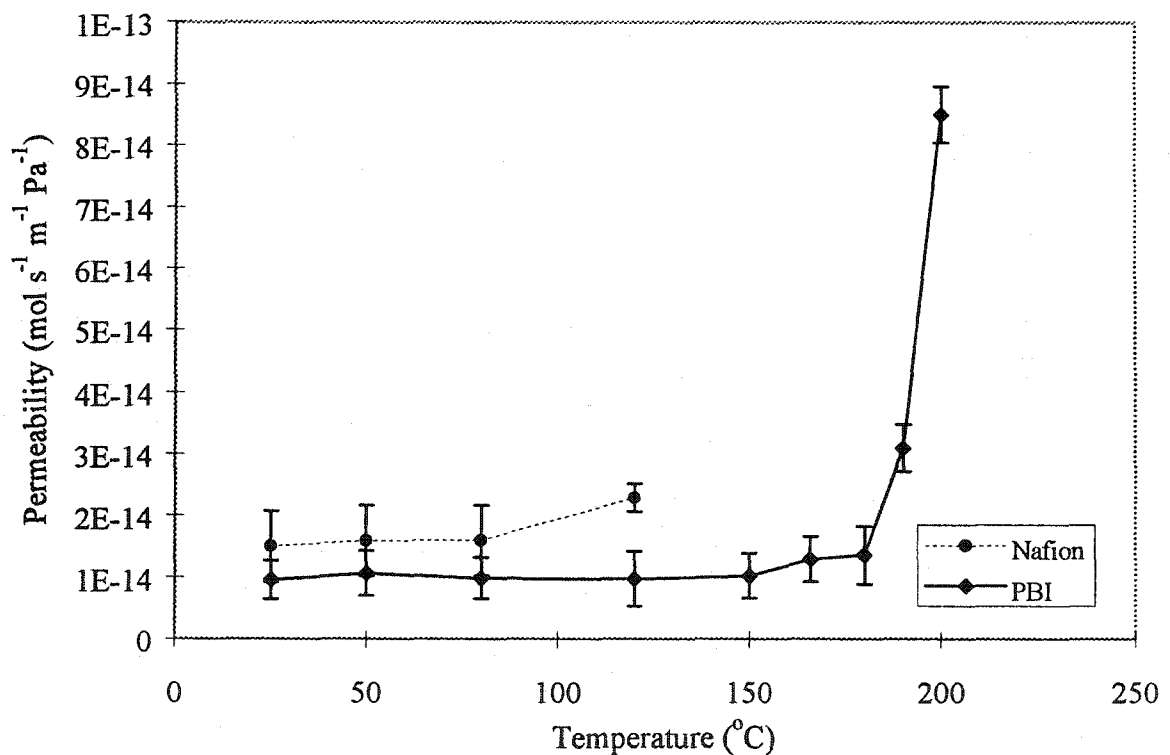
(a) Permeability of oxygen gas versus working temperature.

74
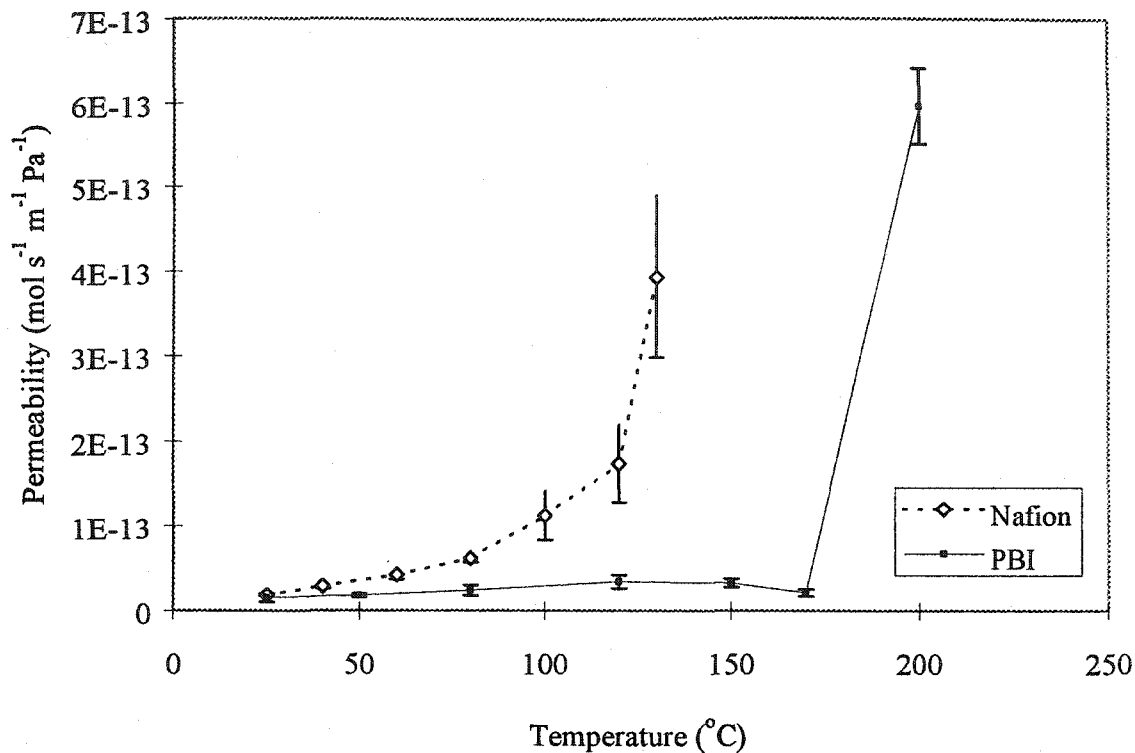
(b) Permeability of hydrogen versus working temperature.

Figure 3-20 Variation of oxygen and hydrogen gas permeability with temperature.

Methanol permeability data for PBI were reported by groups from CWRU [11, 17, 18]. However, there are only limited data available on the permeability of other gases through H_3PO_4 doped PBI membranes, in particular oxygen and hydrogen gas, although PBI membranes have been claimed to provide a better resistance to methanol permeability compared to Nafion™ membranes. In U.S. Patent 5,525,436 [11], the authors reported permeability tests on PBI membranes that they had prepared, but only at 150°C for hydrogen and at 140°C for oxygen. At 150°C, the PBI membranes that they prepared had a hydrogen permeability constant of about 6.03×10^{-14} mol.m^{-1}s^{-1}Pa^{-1} while permeability of O_2 at 140°C was about 3.5×10^{-15} mol.m^{-1}s^{-1}Pa^{-1}. All the reported results were for a doping level of 338 mol%.

In the present permeability tests, I have determined permeability over a far more extensive range of parameters for the H_3PO_4 doped PBI membranes. Permeability data from room temperature to as high as 200°C were obtained for PBI membranes with a high doping level, about 550 to 600 mol% H_3PO_4, since these are the doping levels for

75

membranes that I used in fuel cells. While the authors in ref. [11] only reported two data points for low doping level of 338 mol% H_3PO_4, in other publication, the same authors operated their H_2-O_2 or CH_3OH-O_2 fuel cells at 500 mol% doping level, because of enhanced ionic conductivity [1, 19]. Thus the permeability data are not representative of the actual PBI doping level for fuel cells operation. The gas permeability tests on the membranes used herein found that permeability of O_2 gas at 150°C was about 1.02×10^{-14} $mol.m^{-1}s^{-1}Pa^{-1}$, while for hydrogen gas the permeability was about 3.24×10^{-14} $mol.m^{-1}$ $s^{-1}Pa^{-1}$ at 150°C. These two values are comparable magnitude to the reported data. The differences maybe related to the different molecular weights of the PBI in the two studies.

More complete lists summarizing experimental data and calculated constants obtained from the gas permeability tests are presented in Appendix A1.

CONCLUSIONS

High temperature tolerant protonic conducting PBI membranes for fuel cell applications were prepared using PBI with a high M.W.~75,000. Morphology studies on these membranes indicated that the solution casting method was suitable for preparation of highly dense PBI membranes. The PBI membrane had few small micropores, and the structure appeared similar to that of commercial Nafion™ membranes. H_3PO_4 doped PBI membranes not only could withstand higher temperatures than Nafion™ membranes, but also provided greater resistance than Nafion™ membranes to permeability of hydrogen and oxygen. H_3PO_4 doped PBI membranes with a doping of 500 mol% to 600 mol% of H_3PO_4 showed good ionic conductivity up to 250°C under anhydrous conditions. The ionic conductivity was stable in the presence of small amount of water vapor due to the hygroscopic nature of H_3PO_4 embedded in the PBI matrix. No chemical decomposition was detected by DSC analysis on H_3PO_4 doped PBI membranes after prolonged use in fuel cell operated at 250°C under highly reducing and oxidizing conditions. Hence, these membranes have been shown for the first time to be suitable for fuel cell operations under rigorous conditions up to 250°C.

76

REFERENCES

[1]   Wang, J.-T., R.F. Savinell, J. Wainright, M. Litt and H. Yu, "A H_2O/O_2 fuel cell using acid doped polybenzimidazole as polymer electrolyte", Electrochim. Acta, **41 (2)**, 193 – 197 (1996).

[2]   Bouchet, R., S. Miller, M. Duclot, J.L. Souquet, "A thermodynamic approach to proton conductivity in acid-doped polybenzimidazole", Solid State Ionics, **145**, 69 – 78 (2001).

[3]   Asensio, J.A., S. Borros and P.G.-Romero, "Polymer electrolyte fuel cells based on phosphoric acid-impregnated poly(2,5-benzimidazole) membranes", J. Electrochem. Soc., **151 (2)**, A304 – A310 (2004).

[4]   Xing, B., and O. Savadogo, "Hydrogen/oxygen polymer electrolyte membranes fuel cell (PEMFCs) based on alkaline-doped polybenzimidazole (PBI)", Electrochem. Communications, **2**, 697 – 702 (2000).

[5]   Bhadeshia, H.K.D.H., (2002). "Differential Scanning Calorimetry". University of Cambridge, Materials Science & Metallurgy. Retrieved February 09, 2004 from the website: http://www.msm.cam.ac.uk/phase-trans/2002/Thermal2.pdf

[6]   Nicula, R., (2000). "Introduction to Differential Scanning Calorimetry". Retrieved February 09, 2004 from the website:
http://wwwswt.informatik.unirostock.de/englisch/projekte/Physik2000/Experimen tII/ta2web001.pdf

[7]   Wadha, L., M. Bitritto and E.J. Powers, "High performance thermally stable polybenzimidazole film", U. S. Patent #5,017,681 (1991).

[8]   Li, Q., H.A. Hjuler and N.J. Bjerrum, "Phosphoric acid doped polybenzimidazole membranes: Physiochemical characterization and fuel cells applications", J. Appl. Electrochem., **31**, 773 – 779 (2001).

[9]   Hasiotis, C., V. Deimede and C. Kontoyannis, "New polymer electrolytes based on blends of sulfonated polysulfones with polybenzimidazole", Electrochim. Acta, **46**, 2401 – 2406 (2001).

[10] Xing, B., and O. Savadogo, "The effect of acid doping on the conductivity of polybenzimidazole (PBI)", J. New Mat. Electrochem. Systems, **2**, 95 – 101 (1999).

[11] Savinell, R.F., and M.H. Litt, "Proton conducting polymers used as membranes", U. S. Patent #5,525,436 (1996).

[12] Bozkurt, A., M. Ise, K.D.Kreuer, H.H. Meyer and G. Wegner, "Proton-conducting polymer electrolytes based on phosphoric acid", Solid State Ionics, **125**, 225 – 233 (1999).

[13] Bouchet, R., S. Miller, M. Duclot and J.L. Souquet, "A thermodynamic approach to proton conductivity in acid-doped polybenzimidazole", Solid State Ionic, **145**, 69 – 78 (2001).

[14] Pu, H., W.H. Meyer and G. Wegner, "Proton transport in polybenzimidazole blended with H_3PO_4 or H_2SO_4", J. Polym. Sci.: Part B: Polym. Phys., **40**, 663 – 669 (2002).

[15] Fontanella, J.J., M.C. Wintersgill, J.S. Wainright, R.F. Savinell and M. Litt, "High pressure electrical conductivity studies of acid doped polybenzimidazole", Electrochim. Acta, **43**, 1289 – 1294 (1998).

[16] Samms, S.R., S. Wasmus and R.F. Savinell, "Thermal stability of proton conducting acid doped polybenzimidazole in simulated fuel cells environments", J. Electrochem. Soc., **143 (4)**, 1225 – 1232 (1996).

[17] Wainright, J.S., J.-T. Wang, D. Weng, R.F. Savinell and M. Litt, "Acid-doped polybenzimidazoles: A new polymer electrolyte", J. Electrochem. Soc., **142**, L121 – L123 (1995).

[18] Wainright, J.S., R.F. Savinell and M.H. Litt, "Acid doped polybenzimidazole as a polymer electrolyte for methanol fuel cells" in "Proceedings of the 2nd International Symposium on New Materials for Fuel cells and Modern Battery Systems", Eds. O. Savadogo and P.R. Roberge, Montrèal, Canada, July 6 – 10, 1997, pp. 808 – 817.

[19] Wang, J.-T., J.S. Wainright, R.F. Savinell and M. Litt, "A direct methanol fuel cell using acid-doped polybenzimidazole as polymer electrolyte", J. Appl. Electrochem., **26**, 751 – 756 (1996).

CHAPTER 4

FUEL CELL DESIGN AND APPLICATIONS
USING H₃PO₄ DOPED PBI MEMBRANES

4.1 INTRODUCTION

The objective of this chapter is to present results obtained from the application of H_3PO_4 doped PBI membranes in self-designed fuel cells system. The discussion in this chapter covers the experimental apparatus setup for the fuel cells testing and the design layout as well as material selections for the homemade single cell. In addition to these, this chapter also contains information on the MEA preparation procedure. The technique used to prepare electrodes for fuel cells applications is also included.

The H_3PO_4 doped PBI membranes, that were synthesized as described in Chapter 3, were applied in H_2-O_2 fuel cells to test whether the fuel cell system was functioning well.

If the design of homemade single cell was satisfactory, better performance for H_2-O_2 fuel cells could be obtained. Then, when the design was satisfactory, that design could be used to investigate use of the same fuel cell system to conduct experiments using hydrocarbon as fuel to replace hydrogen. This part is included in Chapter 5.

4.2 FUEL CELL TESTING

4.2.1 Fuel Cell Electrode Preparation

Fuel cell electrodes consist of at least two layers; one is a catalyst layer while the other one is a gas permeable layer. To prepare the catalyst layer for the system used herein, dry catalyst powder was thoroughly mixed with appropriate proportions of Nafion™ solution, water and ethanol to create an ink. Typically, for this catalyst layer, a mixture was prepared containing Nafion™ ionomer (5 wt%, Aldrich), Pt/C catalyst (20 wt% Pt/Vulcan XC-72, Alfa Aesar) or Pt black catalyst, and ethanol in weight ratio of

79

1:3:10 respectively. For all experiments, platinum loading was set at 1 $mg.cm^{-2}$ for each electrode.

Water was needed, especially when preparing platinum-based catalysts. Burning can occur on direct addition of ethanol (as dispersion agent) to platinum catalyst, or direct addition of Nafion™ solution to platinum catalyst [1]. The reason is oxygen atoms adsorbed onto the Pt surface were highly reactive. Therefore, when ethanol and Nafion™ solution (contains methanol) are added, reactions leading to the burning on the catalyst surface can occur to form agglomerated Pt. In order to avoid this, water was mixed with Pt/C first. This prevented the catalyst from directly contacting ethanol, Nafion™ solution and air. After that, ethanol and Nafion™ solution in the desired ratio were added to this mixture and a homogeneous paste was obtained upon stirring.

The ink was then directly applied on to the membrane surface by brushing [2]. Then 5 $mg.cm^{-2}$ of H_3PO_4 was added to the ink to create an ionic pathway, at both electrodes. This catalyst layer was then dried for approximately 20 min. using an infra-red lamp.

To prepare the gas permeable layer, a solution of Teflon (~50 wt%) containing carbon black (Vulcan) XC-72 was mixed thoroughly in a ratio of 6:4 by weight [3]. Then it was directly brushed onto carbon cloth (Electrochem). This electrode backing layer was sintered at a temperature of $350°C$ for 30 min. [4]. The treated carbon cloth was then cold-pressed onto the catalyst layer. Sintering allowed the PTFE to form an evenly distributed gas diffusion network, and acted as a binder to bind carbon black to the carbon cloth.

4.2.2 MEA Preparation

Since the catalyst layer was directly painted onto the membranes surface, the conventional 'hot-press' method was not required. A 'cold-press' method was preferred here, involving assembling membranes (with catalyst on it) and electrode-backing layer together after accurate placement. The advantage of this procedure was that it eliminated any damage that could have occurred during hot pressing of the membranes.

Referring to Figure 4-1, the phosphonated PBI membrane was red brown in color. Also shown in the figure is carbon cloth, which was used to provide intimate contact

80

between the current collector (mesh) and PBI membrane, and also functioned as membrane protector as the carbon cloth had a soft texture.
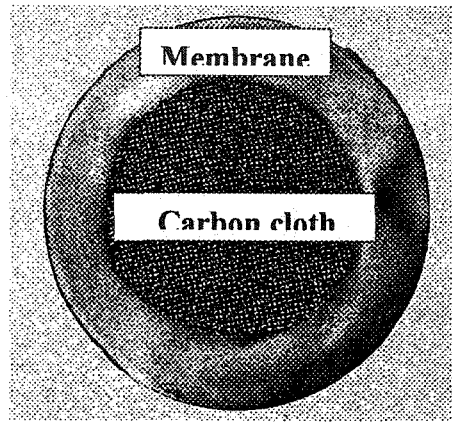
Figure 4-1 MEA of PBI polymer.

At high temperatures PBI membranes became soft, and the mechanical strength was reduced compared to ambient conditions. When stainless steel mesh is used as current collector in direct contact with the membrane, it crushed the membrane, because membranes not only became soft at high temperature, but also underwent thermal expansion as the temperature increased.

The thermal expansion of PBI membranes and mesh were not compatible with each other. The direct interaction between them crushed the membranes, causing gas leaks. To improve the situation, non-metallic materials like carbon cloth and Teflon gaskets with soft textures, were used during the cell design development stage.

4.2.3 Fuel Cell Design

A single cell was designed in our laboratory, which specially catered to the operation of low temperature polymer membrane fuel cells.

Figure 4-2 shows the design layout of a homemade single cell. This single cell comprised two bipolar plates, which were fabricated from stainless steel SS316, a material having 18% chromium and 12% nickel [5]. It is preferred over SS304, a

81

commonly used stainless steel material, because SS316 can better withstand a corrosive environment, which was introduced here by the acidic electrolytes.
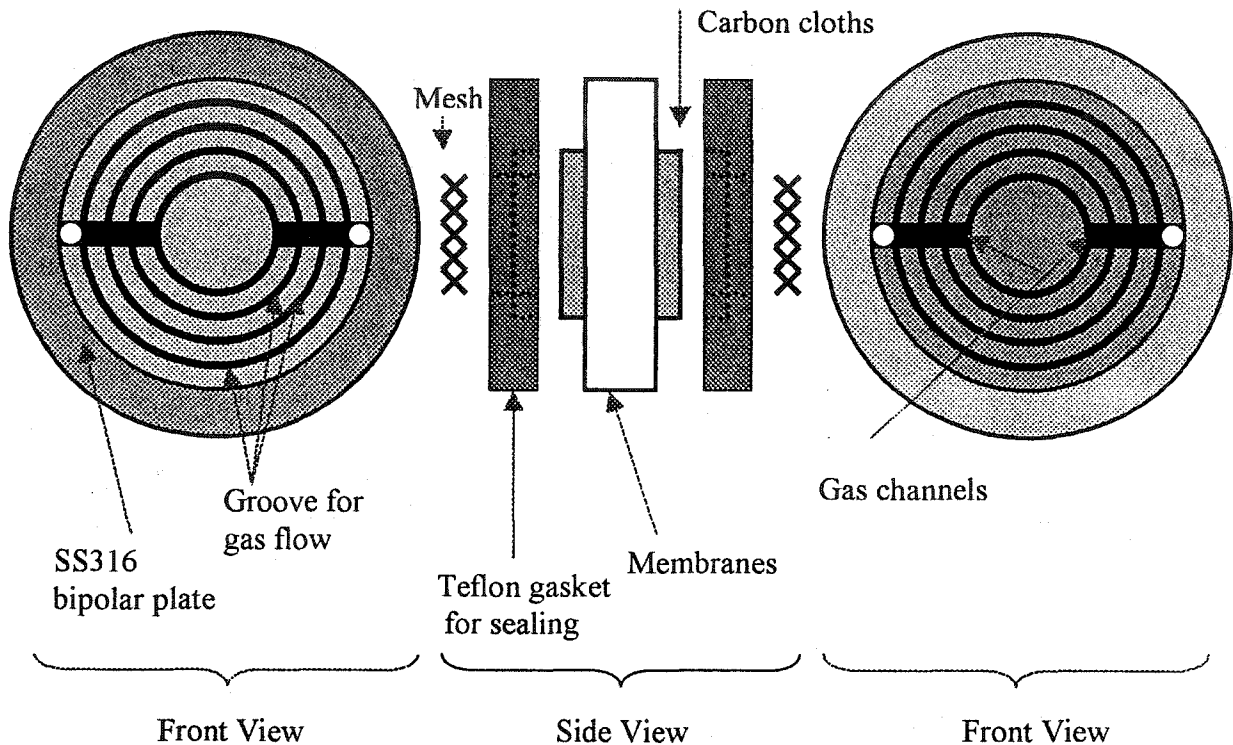
Figure 4-2 Exploded view of homemade polymer fuel cell.

Fuel cell operation revealed that, while SS316 bipolar plates did not suffer any corrosion problem after prolonged operation period, the same operation carried out by using SS304 had inflicted severe corrosion to the cell's surface. This passive film affected the ohmic losses of the fuel cell because it increased the interfacial resistance. Stainless steel material was chosen over graphite because graphite material is brittle, far expensive and difficult to machine although it has high resistance to corrosion and has no tendency to form passive oxide layers in air, which would have increased the interfacial resistance compared to stainless steel [6].

Besides providing electrical conductivity and cell protection, bipolar plates also functioned to supply reactants to the gas diffusion electrodes via a flow field etched directly into the bipolar plate's surface. These bipolar plates also provided high mechanical strength to the whole cell assembly as a result of high density, impermeable to reactant gases to curb gas leaking problems, and were easy of manufacture.

Construction of single cells for testing had to be carefully carried out to ensure the planarity of bipolar plates. Any non-planarity in these plates would have resulted in poor gas sealing. In addition to this problem, it was very easy to crush the MEA during cell assembling if the surface was not planar. This cell was connected to the load outside the test station by electrical wires connected to the outer surface of both bipolar plates. The inner surface of the bipolar plates was connected to the mesh which formed part of the current collector. The mesh provided intimate contact between bipolar plates and MEA once the whole assembly was tightened.

To provide good sealing, two thin Teflon gaskets were designed to accommodate both mesh and carbon cloths. The thickness of each gasket was adjusted to be equal to the overall thickness of both mesh and carbon cloths. The typical thickness of each Teflon gasket was about 31 mils. Figure 4-3 shows the complete assembly of a single cell inside the oven housing. It consisted of two streams, inlet and outlet for each anode and cathode compartments. These gas streams provided a continuous flow of reactants and tailing gases. The oven functioned using a temperature controller to maintain the operation of cell at specified temperatures. An external electrical wire was connected to the bipolar plates. The other end of this wire was connected to a Gamry Electrochemistry instrument.
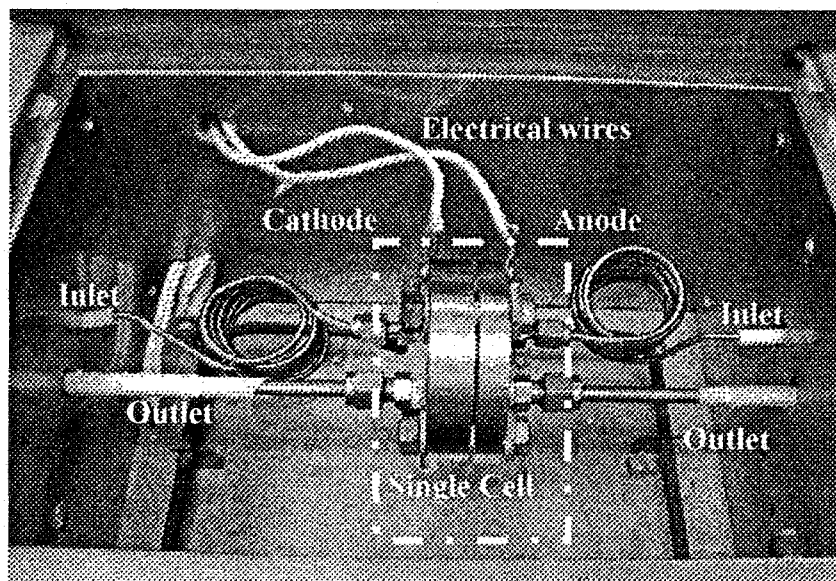
Figure 4-3 Fuel cell testing system.

83

4.3 EXPERIMENTAL PROCEDURE

4.3.1 Experimental Setup for Fuel Cell MEA Testing
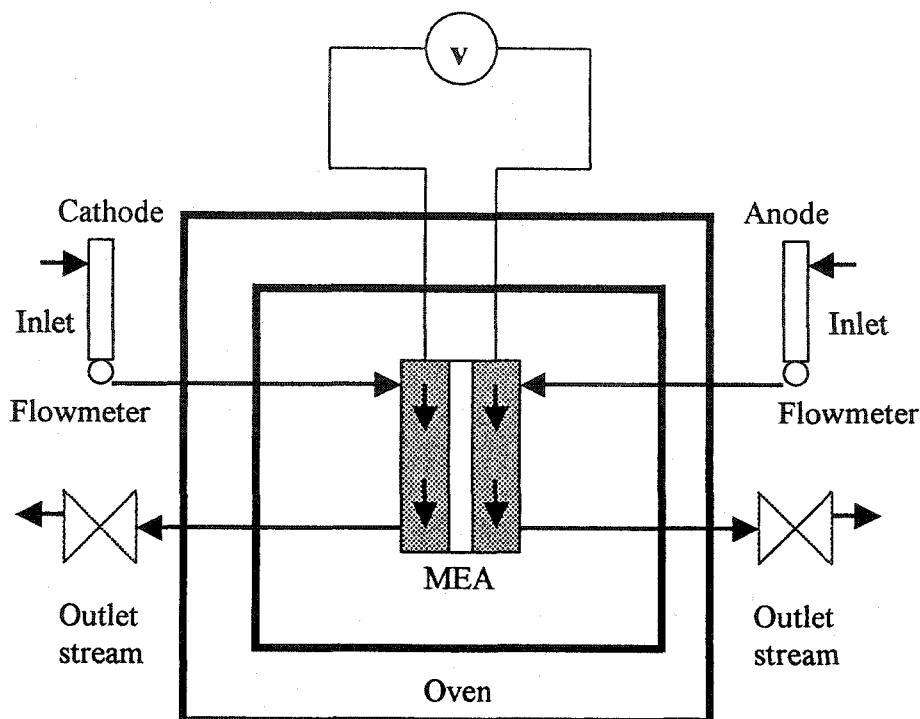
Figure 4-4 Experimental setup for fuel cell testing.

A polymer fuel cell testing system has been developed in our laboratory to test the performance of MEA composed of H_3PO_4 doped PBI membranes, and to evaluate their suitability for fuel cell applications. The performance of this MEA was gauged using H_2-O_2 fuel cells first, and later on using hydrocarbon-O_2 fuel cells. A digital Voltmeter (Fluke 175) was used to measure the potential of cell during the operation of fuel cells.

Figure 4-4 shows the configuration of the fuel cells testing station for atmospheric pressure experiments. All experiments utilizing PBI membranes have been carried out at 1 atm pressure since PBI membranes do not require 100% humidification to maintain good ionic conductivity, as shown in Chapter 3. The whole fuel cell apparatus was placed inside the oven, which also housed stainless steel gas manifolds, with two-way valves on each exit line. This test station also controlled the cell's working temperature.

84

The flow-rates for each gas stream was controlled using a volumetric flowmeter. To ensure that both reactant streams achieved the desired operating temperature, a coiled feed line was situated before both inlets, to increase the travel distance of feeds within the heated zone. The bolt-tightened single cell was connected to these gas manifolds. Before an experiment commenced, the whole assembly was checked to ensure that it was electrically insulated. The insulation was done by covering the stainless steel gas manifolds by tape, so that it had no direct contact with the test station.

Gamry Electrochemistry Instrument Version 3.20 © 2000 software was used in all conducted experiments to evaluate electrochemical experiments in fuel cell testing. Particular attention has been given to the following measurements:

- Cell potential of fuel cells.
- EIS, to determine the resistance of cell.
- Potentiodynamic scans.
- Potentiostatic scans.

In all cases, measurements have been optimized for accuracy. In addition, AC~DC Decade Resistor from Leeds & Northrup Co., was used occasionally, especially during H_2-O_2 fuel cell operation, to provide accurate electrical loads. These loads enabled the measurement of current flows. The Gamry Instrumentation could only measure the current flow up to 820 mA. Normally, this value can be exceeded.

For H_2-O_2 fuel cells testing, the following gases were used:

Table 4-1 Specifications for gases utilized in H_2-O_2 fuel cells.

Hydrogen	PP 4.5 Grade	99.995% purity
		O_2 < 5 ppm
		H_2O < 5 ppm
Oxygen	2.6 Grade	99.6% purity
		H_2O < 10 ppm

Source: *Praxair Canada Ltd.*

85

4.4 RESULTS AND DISCUSSION

4.4.1 Cell Potential

The experimental results for H_2-O_2 cell potential are presented in Figure 4-5. When the single cell was properly installed, high cell potentials were obtained during fuel cell operation. The results were repeated at least five to six times. The results showed that the single cell did not have any gas sealing problems. If sealing had been poor, gases would have leaked from the anode to cathode compartment or vise versa, resulting in low cell potentials. Another observation was that the temperature of the cell did not remain constant at the set temperatures when gas leaking happened. This was most probably because the exothermic reaction to produce water had increased the temperature of the cell.
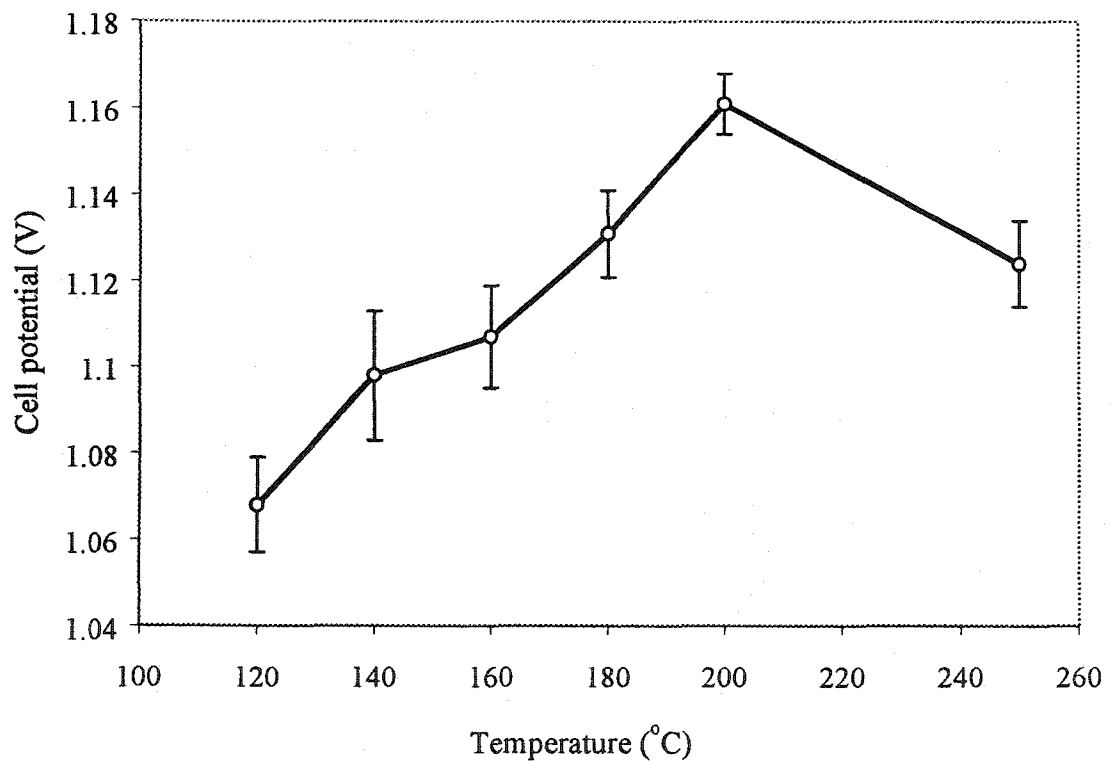
Figure 4-5 Cell potential of H_2-O_2 fuel cells at 1 atm after stabilization for more than 6 h at OCV.

High cell potentials of more than 1.0 V also indicated that the H_3PO_4 doped PBI membrane was not permeable to either hydrogen or oxygen. If the PBI membranes had not been dense enough, hydrogen would have transported from anode to cathode compartment. This is because hydrogen has a smaller molecule diameter and can be easily transported through the micropores, causing loss of cell potential due to reactant crossover. The high cell potential also confirmed that the whole fuel cell assembly did not have any 'electrical leaking' problem. Electrical leaking would have had a direct impact on potential because it would have made the cell come into direct contact with stainless steel material.

The potential of H_2-O_2 fuel cells increased with temperature. This reflected the behavior of the platinum catalyst, which had become more active for chemisorption as the temperature increases. Nonetheless, at 250°C, the potential dropped, but still remained at a reasonably high value. This drop in cell potential was attributed to a 'crossover' problem at high temperatures. When temperature increased, the micropores of membranes gradually become larger. At 250°C, the micropores had become large enough that the crossover of hydrogen molecules to cathode compartment had a significant impact. This resulted in a loss of about 30 mV in cell potential compared to the cell potential at 200°C.

Figure 4-6 shows the variation in theoretical cell potentials of H_2-O_2 fuel cells with temperature. These values were calculated based on Eqn. (2.6) for the following chemical reaction equation:

$$2\,H_2\,(g) + O_2\,(g) \rightarrow 2\,H_2O\,(g) \qquad\qquad (4.1)$$
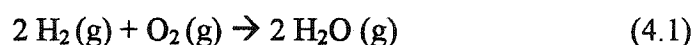
All theoretical cell potentials presented in Figure 4-6 were calculated using the thermodynamic data available from HSC Chemistry, Version 1.12 by Outokumpu Research. The values obtained were on the basis of 1 atm pressure for each chemical species present.

87
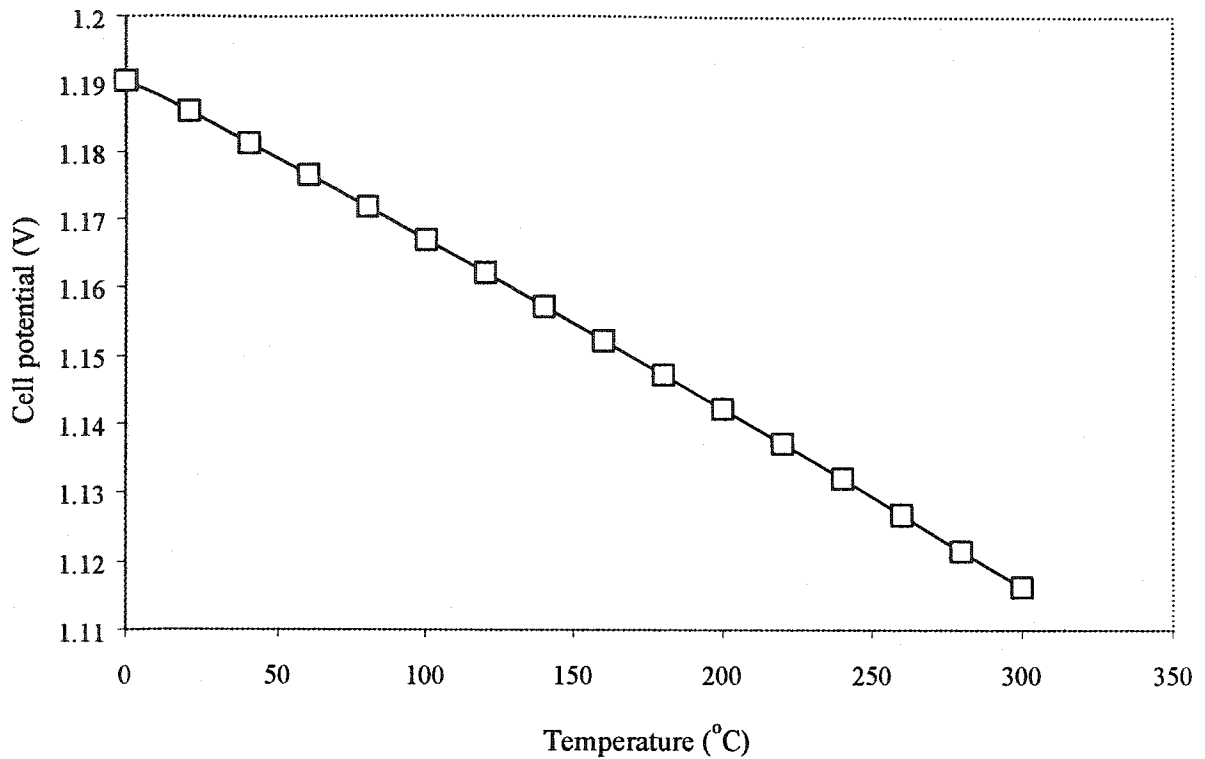
Figure 4-6 Theoretical cell potentials of H_2-O_2 fuel cells with temperature.

Theoretically, the cell potential at standard condition is close to 1.19 V and declines linearly as the temperature increases. Although the theoretical trend is not same as those obtained experimentally, the theoretical cell potentials were only slightly higher or lower than the values obtained experimentally at those operating temperatures. For example, at 120°C, the theoretical cell potential was 1.162 V compared to the experimental value of 1.068 V. At 200°C, the theoretical value was 1.142 V while experimental value was 1.161 V.

A significant reason for the disparity is that the above theoretical values were based on 1 atm pressure for each chemical species reacting. But in our fuel cell system, the overall pressure for either anode or cathode was 1 atm. Thus the partial pressure for water was definitely less than 1 atm. Based on Eqn. (2.7), for H_2-O_2 system, the following equation applied:

$$\Delta U = \Delta U^{\circ} - \left(\frac{RT}{2F}\right) \ln \left[\frac{P_{H_2O}}{P_{H_2} P_{O_2}^{1/2}} \right] \tag{4.2}$$

88

The above equation relates the cell potential of H_2-O_2 system at temperatures other than 25°C and partial pressure, which was not 1 atm for every chemical species. As the partial pressure of water during the running of cell was not 1 atm, this certainly contributed to the difference between cell potentials.

Theoretical cell potentials are based on participation by reactants which have reached equilibrium in a closed system. This equilibrium needs certain period of time to be established. For fuel cell operation, hydrogen and oxygen are continuously fed into the system with certain residence time inside the "reactor". Therefore, fuel cell operation will not achieve the real "maximum equilibrium" which is the basis for theoretical values. The equilibrium in a fuel cell system is a dynamic equilibrium. For example, a dynamic equilibrium between adsorbed hydrogen atoms on catalyst surface with the hydrogen in the gas surface or a dynamic equilibrium of adsorbed oxygen atoms with oxygen in the gas phase.

Thus, theoretical cell potentials only serve as a benchmark for actual cell potentials.

4.4.2 Polarization Curves for H_2-O_2 Fuel Cells

Hydrogen is a very reactive fuel. In the anode compartment, hydrogen molecules chemically dissociated and adsorped rapidly on to the platinum surface. Each hydrogen molecule donated two electrons to form two protons, and these protons were transported through the PBI membranes to the cathode compartment where they recombined with oxygen and electrons to form water molecules. The driving force behind this proton transport was mainly the electromotive force generated between anode and cathode compartment through the H_2-O_2 reaction. Below is a reaction sequence showing how the proton transportation through PBI polymer membranes occurred:

$$H_2 + 2\,Pt \rightarrow 2\,H - Pt \;\; \text{(Anode chemisorption reaction)} \qquad (4.3)$$

$$2\,(H - Pt) \rightarrow 2\,H^+ + 2\,e^- + 2\,Pt \;\; \text{(Fast oxidation reaction)} \qquad (4.4)$$

$$H^+(\text{anode side}) \rightarrow \text{membranes} \rightarrow H^+ \;(\text{cathode side}) \;\text{(Slow process)} \qquad (4.5)$$

$$O_2 + 4\,H^+ + 4\,e^- \rightarrow 2\,H_2O \;\; \text{(Reduction process at cathode)} \qquad (4.6)$$
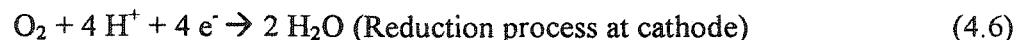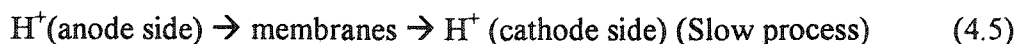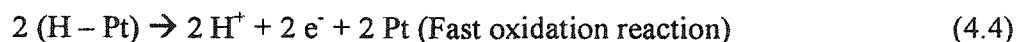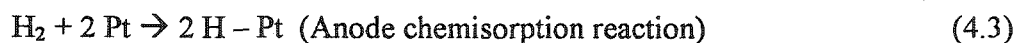
The last reaction at the cathode compartment was slow when compared to the reaction in the anode side because oxygen molecules did not adsorb well on the platinum

89

surface compared to the adsorption of hydrogen. Although the third reaction was the slowest among the reaction mechanisms, nonetheless, it was comparable to that in other types of fuel cell. Transport of protons in proton conducting polymer like Nafion™ is the fastest, since this polymer is thin and also because of the nature of acid, which has a high conductivity. Figure 4-7 shows the performances of H_2-O_2 fuel cells constructed in our laboratory, using single cells at 200°C with internal resistance of approximately 0.18 Ohm.
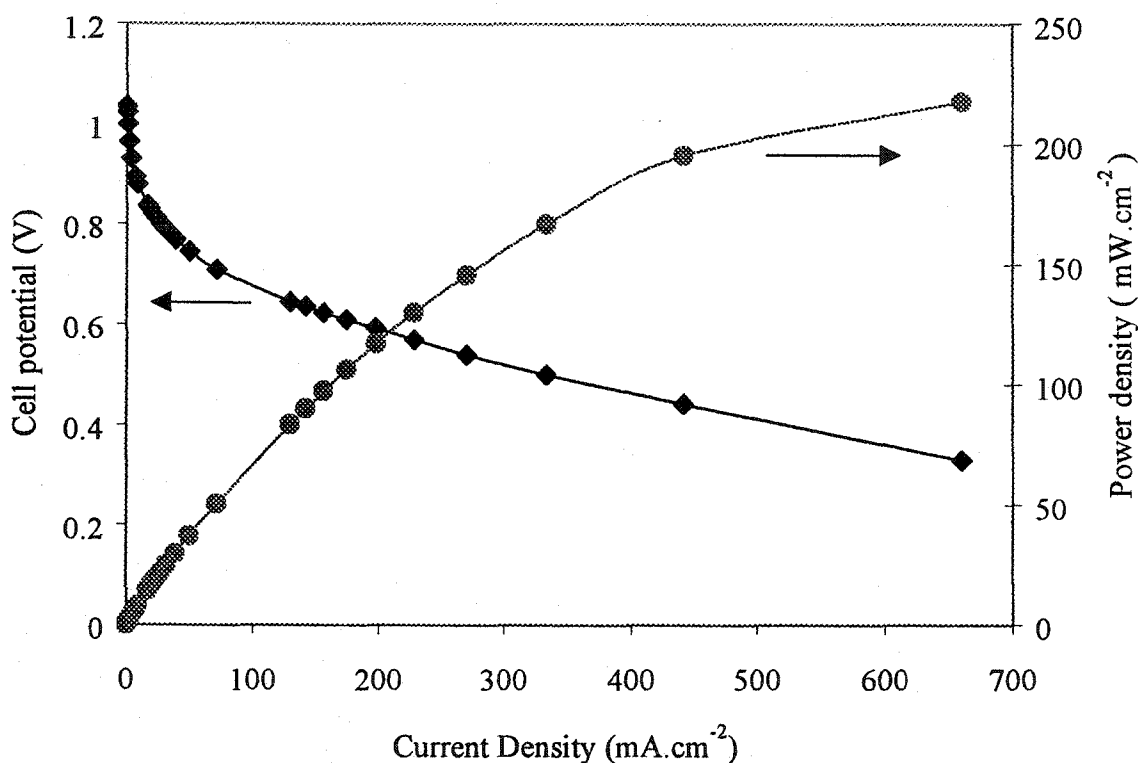
Figure 4-7 H_2-O_2 fuel cells at T = 200°C without humidification (Doping level = 550 mol% H_3PO_4 with I.R. 0.18 Ohm).

The performance chart shown above was obtained using a digital voltmeter (Fluke 175) and a AC~DC Decade Resistance Box from Leeds & Northrup Co. At the specified operating temperature of 200°C, high current density was obtained from the single cell. At around 330 mV, the working cell had a current density flow reaching nearly 700 $mA.cm^{-2}$. Power density was nearly 230 $mW.cm^{-2}$ at a current flow of 700 $mA.cm^{-2}$. This result was obtained under non-optimized conditions.

Power densities obtained using the present PBI membranes in the fuel cell testing system constructed in our laboratory were slightly lower than those in previous reports of H_2-O_2 fuel cells utilizing H_3PO_4 doped PBI membranes. Li et al. has reported the highest power density, about 0.55 $W.cm^{-2}$ at a current density of 1.2 $A.cm^{-2}$ at 190°C [7]. Wang et al. reported maximum power density of 0.25 $W.cm^{-2}$ at a current density about 700 $mA.cm^{-2}$ at 150°C [8]. Savadogo et al. obtained optimum power output of 0.65 $W.cm^{-2}$ at 1.5 $A.cm^{-2}$ at 185°C [9].

The operation of these fuel cell systems was not under optimized conditions. It is anticipated that, with optimization, an improvement in performance of cell could be obtained, especially at 200°C. These results were easily reproducible if the I.R. of cell was about 0.20 to 0.30 Ohm. A single representative set of those results has been presented here. The main focus of this chapter is on the design of homemade cell and fuel cells system apparatus layout.

CONCLUSIONS

H_3PO_4 doped PBI membranes showed very promising results during the H_2-O_2 fuel cell operation using a low temperature fuel cell system developed in our laboratory. Fuel cell operations did not encounter any major problems, signaling that the design of the single cell was satisfactory. Good sealing and dense membranes contributed to attainment of high cell potentials. The experimental cell potentials were very closed to the theoretical values. This was further proof of good cell design. The performance of fuel cells improved slightly at higher operating temperatures because the catalyst became more active. All results obtained were under non-optimized conditions.

REFERENCES

[1]   Qi, Z., and A. Kaufman, "Low loading high performance cathodes for PEM fuel cells", J. Power Sources, 113, 37 – 43 (2003).

[2]   Wilson, M.S., "Membranes catalyst layer for fuel cells", U. S. Patent #5,211,984 (1993).

91

[3]   Watanabe, M., S. Motoo, N. Furuya and T.K. Kogyo, "Gas permeable electrode",
        U. S. Patent #4,931,168 (1990).

[4]   Easton, E.B., "Chemical modification of fuel cell catalysts and electrochemistry
        of proton exchange membranes fuel cell electrodes", PhD Thesis Memorial
        University of Newfoundland, pp. 41 (2003).

[5]   Davies, D.P., P.L. Adcock, M. Turpin and S.J. Rowen, "Stainless steel as a
        bipolar plate material for solid polymer fuel cells", J. Power Sources, 86, 237 –
        242 (2000).

[6]   Hentall, P.L., J.B. Lakeman, G.O. Mepsted, P.L. Adcock and J.M. Moore, "New
        materials for polymer electrolyte membranes fuel cell current collectors", J.
        Power Sources, 80, 235 – 241 (1999).

[7]   Li, Q., H.A. Hjuler and N.J. Bjerrum, "Phosphoric acid doped polybenzimidazole
        membranes: Physiochemical characterization and fuel cell applications", J. Appl.
        Electrochem., 31, 773 – 779 (2001).

[8]   Wang, J.-T., R.F. Savinell, J. Wainright, M. Litt and H. Yu, "A H_2/O_2 fuel cell
        using acid doped polybenzimidazole as polymer electrolyte", Electrochim. Acta,
        41, 193 – 197 (1996).

[9]   Savadogo, O., and B. Xing, "Hydrogen/oxygen polymer electrolyte membranes
        fuel cell (PEMFC) based on acid-doped polybenzimidazole (PBI)", J. New Mat.
        Electrochem. Systems, 3, 343 – 347 (2000).

CHAPTER 5

HYDROCARBON FUEL CELLS

5.1 INTRODUCTION

The conventional way to exploit hydrocarbon fuels is through combustion. Direct oxidation of hydrocarbons, such as propane and ethane, is an exothermic reaction and provides useful energy, for example; combustion of propane and ethane can yield 2044.0 kJ.mol^{-1} and 1427.81 kJ.mol^{-1} respectively at STP [1]. Alternatively, energy can be generated by oxidation of hydrocarbons in fuel cells. Hydrocarbon fuel cells offer several advantages compared to conventional heat engines; e.g. controlling the reaction rate and product selectivity through the manipulation of cell potential and variable resistor, the possibility of deep oxidation of hydrocarbon could be curbed and the potential danger of explosion is greatly reduced since the reactants are separated from each other [2].

In this chapter, I will discuss the application of PBI membranes in hydrocarbon fuel cells. The purpose of this study is to look into the prospect of using H$_3$PO$_4$ doped PBI polymer fuel cells as co-generator for electricity and olefins as products from conversion of paraffins under mild conditions. In Chapter 3, I show that the membranes have good ionic conductivity at high temperature. High temperatures, in the range of 200 to 250°C promote activation of dehydrogenation of alkenes by noble metal catalysts. Herein, I will describe conversion of ethane and propane in PBI fuel cells.

5.2 PRINCIPLES OF CONVERSION OF HYDROCARBONS IN FUEL CELLS

Catalytic dehydrogenation of light hydrocarbon on noble metals is well known and has been widely used in industry. Studies have shown that dehydrogenation of ethane and propane to ethylene and propylene occurs through a dissociative chemisorption process on catalyst surface [3].

93

The Fuel Cells Group at the University of Alberta is trying to develop low temperature fuel cells for highly selective dehydrogenation of alkanes. In principle, use of fuel cells overcomes equilibrium limitations as hydrogen atoms from dehydrogenation chemisorb at the catalyst surface, and are then rapidly conducted through the protonic exchange PBI membranes in proton form to the cathode side, where they recombine with oxygen and electrons to produce water. The proposed transport mechanism ensures the continuous production of ethylene and propylene from ethane and propane, and the electrochemical system is not equilibrium limited.

The electrochemical reactions of the hydrocarbon feed resemble the catalytic dehydrogenation reaction. In an electrochemical system, shown schematically in Figure 5-1(a), propane fuel, C_3H_8, for example, first chemisorbs on the catalyst surface. This dissociative chemisorption is forming propylene, C_3H_6 and two hydrogen atoms. In Figure 5-1(b), the hydrogen atoms will be transformed into protons that are conducted through the membrane to the cathode side. Propylene desorbs from the catalyst surface and makes available the active surface for further reaction (Figure 5-1(c)).
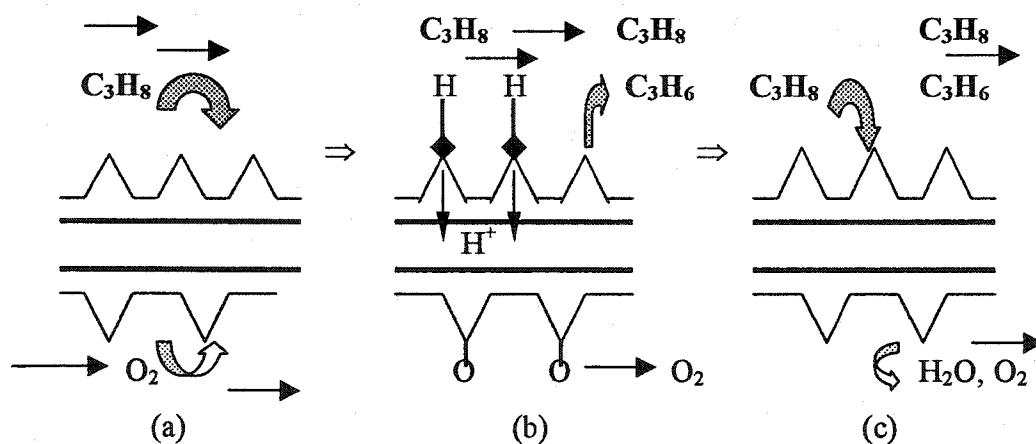
Figure 5-1 Schematic of proposed electrochemistry reactions utilizing propane.

5.3 THERMODYNAMICS OF HYDROCARBON FUEL CELL REACTIONS

The spontaneity of an electrochemical reaction is determined by the change in ΔG. If ΔG is negative, then the reaction is deemed a spontaneous electrochemical reaction. A

94

spontaneous electrochemical reaction will generate electricity; a non-spontaneous electrochemical reaction requires an external source of electricity.

Oxidative conversion of both ethane (Eqn. 5.1) and propane (Eqn. 5.2) to the corresponding alkenes is spontaneous, and thus it is possible in principle to generate electricity from these reactions. The relationship of ΔG and theoretical potential to temperature for each of these reactions is illustrated in Figure 5-2.

$$2\ C_2H_6\ (g) + O_2\ (g) \rightarrow 2\ C_2H_4\ (g) + 2\ H_2O\ (g) \qquad (5.1)$$

$$2\ C_3H_8\ (g) + O_2\ (g) \rightarrow 2\ C_3H_6\ (g) + 2\ H_2O\ (g) \qquad (5.2)$$
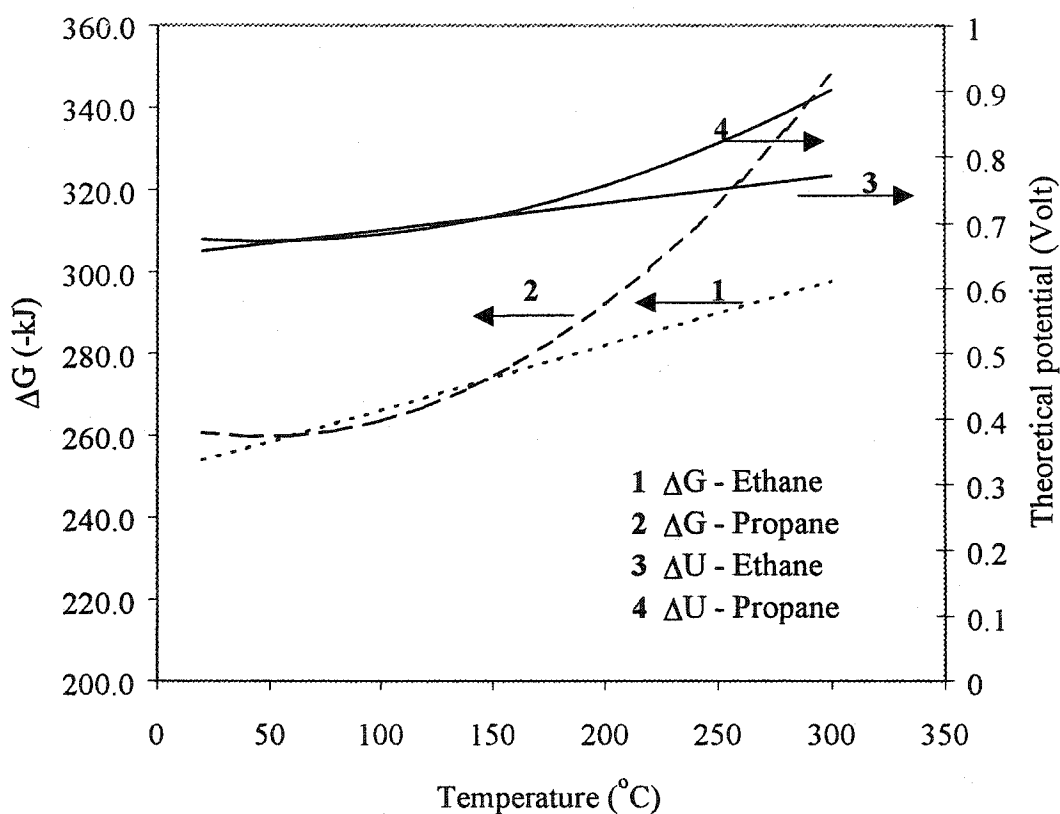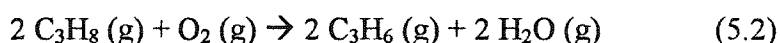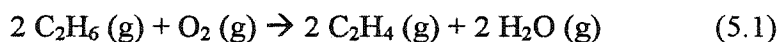
Figure 5-2 Variation of ΔG and theoretical potentials with temperature.

5.4 EXPERIMENTAL PROCEDURE

The fuel cell testing system was the same as that previously described in Chapter 4. The test cell had an area of 4.9 cm^2. The exit gas stream was analyzed using on-line G.C.

95

(Hewlett Packard Series II 5890), equipped with packed bed column and connected to an integrator (HP 3396 Series II). Products were determined using a thermal conductivity detector (TCD) with helium as a carrier gas. Analyses were performed isothermally at 80°C for 15 min. The specifications for the gases (Praxair Canada) used for the experiment are shown in Table 5-1.

Table 5-1 Gas specifications for hydrocarbon fuel cells experimental work.

Ethane	Grade 2.0	99.0% purity
C_2H_6		Methane < 50 ppm
		Ethylene < 4000 ppm
		Propane < 400 ppm
		Propylene < 1000 ppm
		C-3's < 1500 ppm
		Sulfur < 1 ppm
Ethylene	Grade 3.0 Polymer	99.9% purity
C_2H_4		O_2 < 10 ppm
		N_2 < 50 ppm
		CO < 3 ppm, CO_2 < 10 ppm
		C_2H_2 < 6 ppm
		C_2H_6 < 100 ppm
		Other HC < 100 ppm
		H_2O < 5 ppm, Sulfur < 1 ppm
Propane	Instrument Grade 2.5	99.5% purity liquid phase
C_3H_8		H_2O < 3 ppm, n-Butane < 20 ppmw
		Methane < 300 ppmw, Sulfur < 1 ppmw
		Ethane < 600 ppmw, Isobutane < 3000 ppmw

5.5 RESULTS AND DISCUSSION

5.5.1 Ethane-Oxygen Fuel Cells

5.5.1.1 Cell Potential

The dependence of OCV or cell potential on temperature for an ethane-oxygen fuel cell is shown in Figure 5-3. The cell potential confirms that the fuel cell reactions are spontaneous, provides proof concept of hydrocarbon fuel cell. The OCV for C_2H_6-O_2 fuel cells is stable over the whole range of operating conditions and normally ranged from about 600 mV to 780 mV at 1 atm pressure. Data were acquired after the cell had stabilized for more than 6 h at 1 atm pressure, when the system has reached steady state conditions.
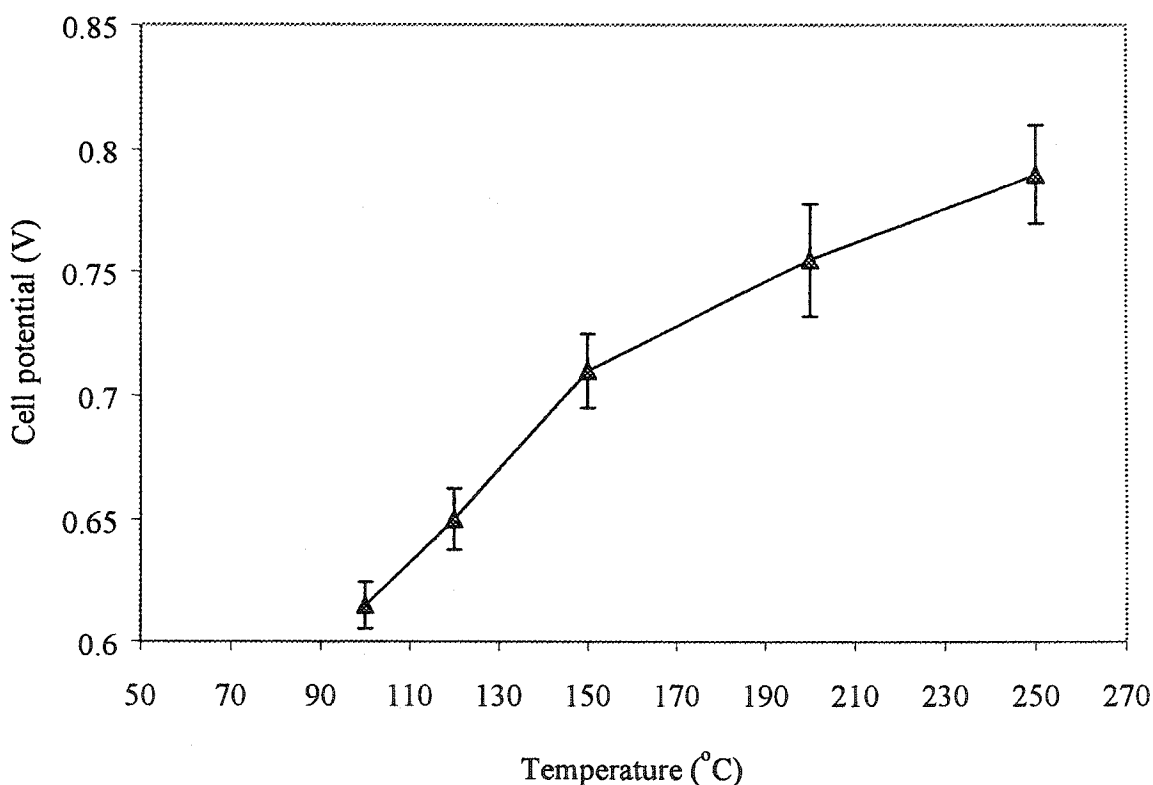
Figure 5-3 Variation of C_2H_6-O_2 fuel cells potential with operating temperature at 1 atm pressure after stabilization for at least 6 h under OCV condition.

If we compare the results between experimental values presented in Figure 5-3 and theoretical values in Figure 5-2, apparently, both exhibit the same variation trend. Both

97

show an increase in cell potential with temperature, which reach nearly 800 mV. The increases in cell potentials imply that higher temperature provided larger driving force for reactions to proceed. Higher temperatures also lead to the catalyst activation where more reactants can readily chemisorb on catalyst surface, thus increasing the reaction rate.

5.5.1.2 Polarization Curves for Ethane-Oxygen Fuel Cells

Referring to Figure 5-4, ethane and oxygen were fed to the respective compartments of H_3PO_4 doped PBI membrane fuel cell under anhydrous conditions using Pt-black as catalyst for both electrodes. It was found that only small current densities were produced, even though the I.R. of the cell was only about 0.4 Ohm. Furthermore, this current density was not sustainable, and gradually decreased with time.
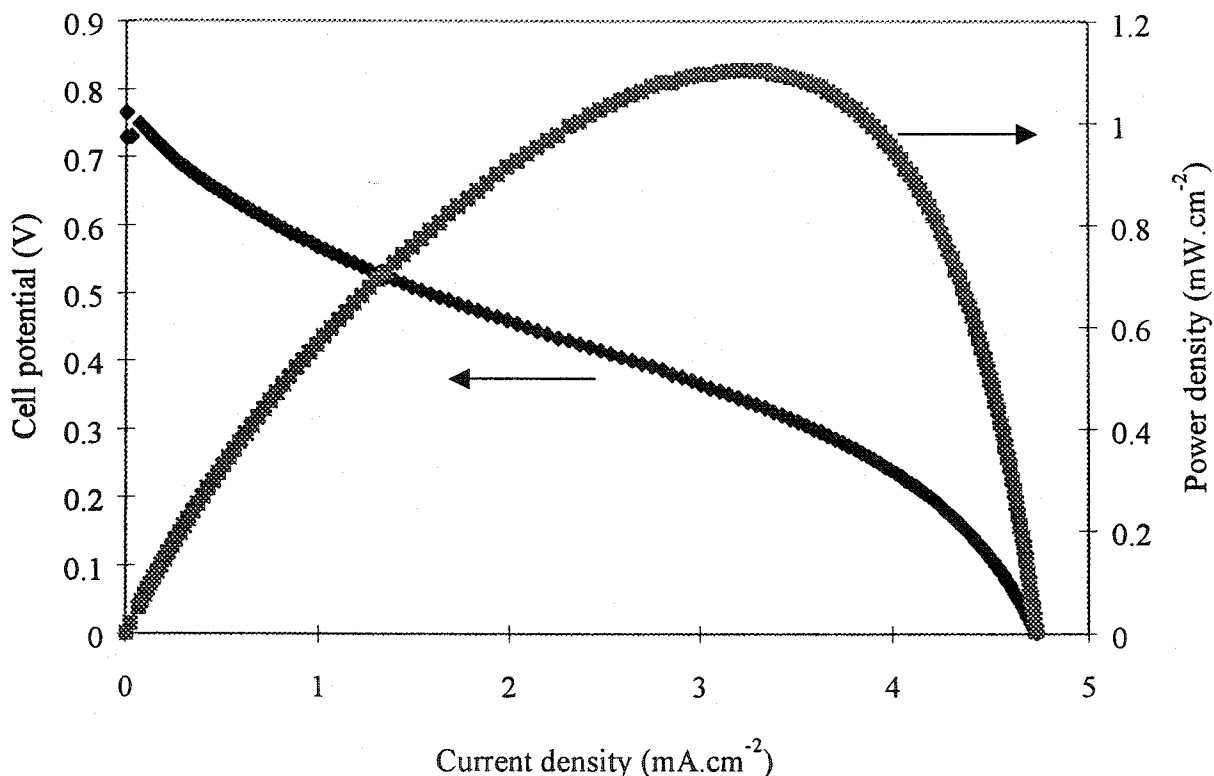
Figure 5-4 Polarization curve of C_2H_6-O_2 fuel cells at 200°C under anhydrous condition (I.R. of cell was 0.411 Ohm).

Although the polarization curve in Figure 5-4 shows a maximum current density of nearly 5 mA.cm^{-2}, when the same fuel cell was operated in potentiostatic mode, even this low current density was unstable, and dropped to a few µA.cm^{-2} after several minutes of

98

operation. Consequently, any products generated were greatly diluted, and on-line G.C. was unable to detect these products. In contrast, adding water to the anode feed humidified the anode compartment at 25°C. Humidification improved the ionic conductivity of PBI membranes, and significantly increased the current density in C_2H_6-O_2 fuel cell (Figure 5-5).
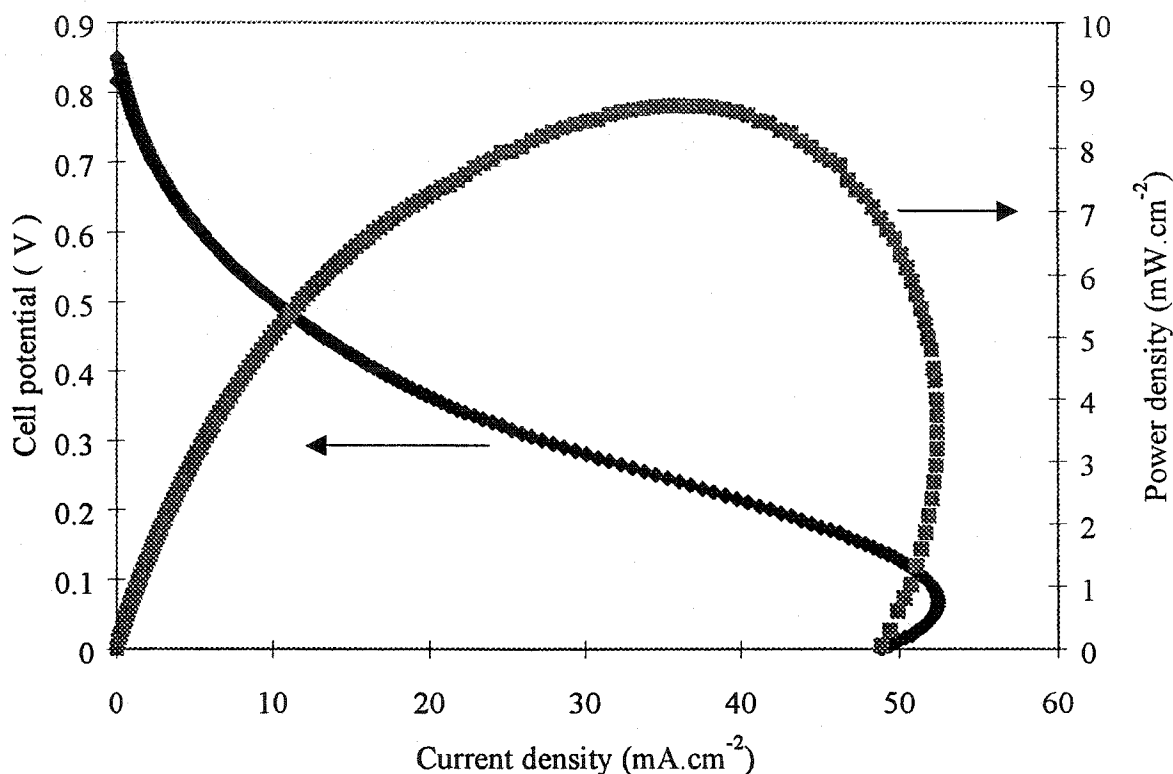
Figure 5-5 Polarization curve of C_2H_6-O_2 fuel cells at 200°C after the addition of water at the anode side with temperature of 25°C (I.R. of cell was 0.19 Ohm).

Comparison of Figure 5-4 with Figure 5-5 shows that water take part in the electrochemical reactions of hydrocarbon fuel cells. These data suggest that water plays an active role in surface reactions. Most probably, the electrochemical reactions of ethane at the anode side produce intermediate products which are strongly chemisorbed onto the platinum catalyst surface, thus blocking the active sites. The higher current density found when the anode feed is humidified suggests that water interacts with the chemisorbed species to promote regeneration of active sites.

Figure 5-5 also shows that the onset of limiting current density occurred between approximately 100 mV to 200 mV. At this low potential (around 100 to 200 mV) and

high current density region, the anode became severe polarized. This may be a consequence of formation of poisonous intermediate products that blocked the catalyst surface sites, thereby limiting access by reactants to the active catalyst sites. This caused the current density to drop further.

Another possibility is that the rate-determining step in this potential region is the adsorption of ethane onto the catalyst surface. This is because low potential conditions might not have provided ideal surface electronic state for ethane adsorption. Furthermore, H_2O species adsorb strongly on platinum surfaces at potentials below 200 mV [4]. As a result, ethane has to compete with water to access sites on the catalyst. So, the presence of water reduces the amount of ethane reactant that can be adsorbed onto the platinum surface, resulting in a drop in current density.

The preliminary results indicate that kinetics for the electrochemical reactions for use of ethane as fuel are slow. To examine whether the slow reaction was due to poisoning of catalyst sites by intermediate products, the system was left to operate continuously at OCV overnight. The current density dropped significantly. This phenomenon was readily reproducible.

This suggested that, after the chemisorption step, intermediates formed from the ethane reactant were strongly retained by acidic platinum metal. As a result, performance of C_2H_6-O_2 fuel cells always deteriorated from initial performance after continuous operation overnight at OCV. This was because potentially active surface of catalyst sites had been blocked to electrochemical reactions.

Figures 5-6 and 5-7 show the polarization curves for C_2H_6-O_2 operated by PBI fuel cells at 250°C with water at 25°C entering the anode side.

100
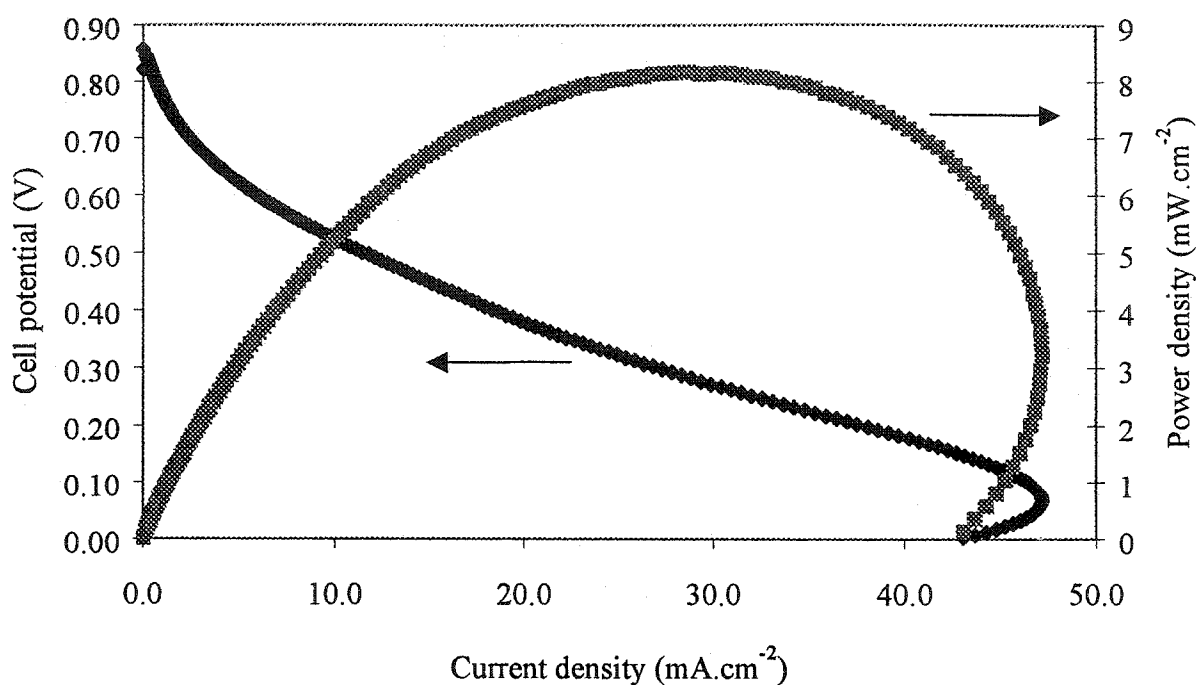
Figure 5-6 Polarization curve of C_2H_6-O_2 fuel cells at 250°C after 3 h running with water added at the anode side, 25°C (I.R. was 0.24 Ohm).
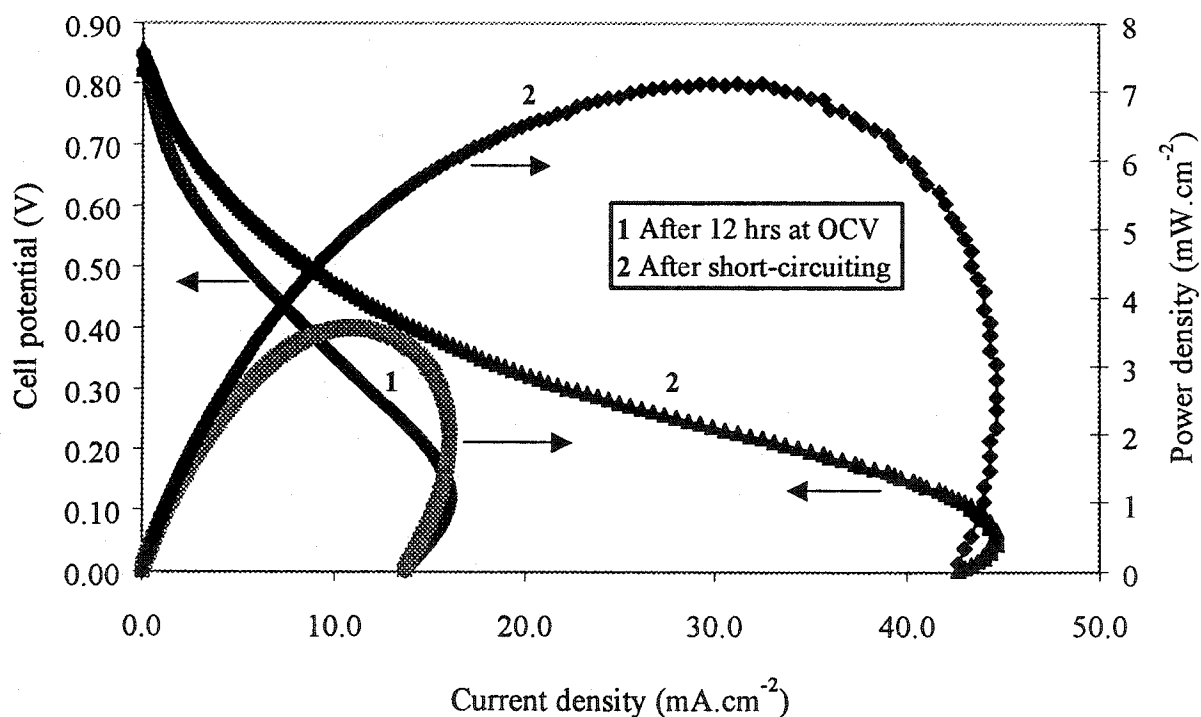
Figure 5-7 Polarization curve of C_2H_6-O_2 fuel cells after (1) more than 12 h at OCV and (2) after short-circuiting (same conditions with I.R. was 0.20 Ohm).

101

The data in Figure 5-6 were obtained after operation for several hours at the specified conditions, while data in Figure 5-7 show the performance of the same cell after 12 h at OCV. The current density was less than half of the value obtained initially. This is consistent with the formation of very stable intermediate products on the catalyst surface during OCV condition. In an attempt to re-generate the original performance level (Figure 5-6), the surface was refreshed by deep oxidation (low potential, 0.0 to 0.05 V) for 0.5 to 1 h to remove any poisonous intermediate products. It was found that, although regeneration restored performance to a high level (Figure 5-7), it did not fully recover all activity. Another important criterion for evaluation of fuel cells is current sustainability. After operation for about 200 s, the current flow reached steady state within the test duration (Figure 5-8).
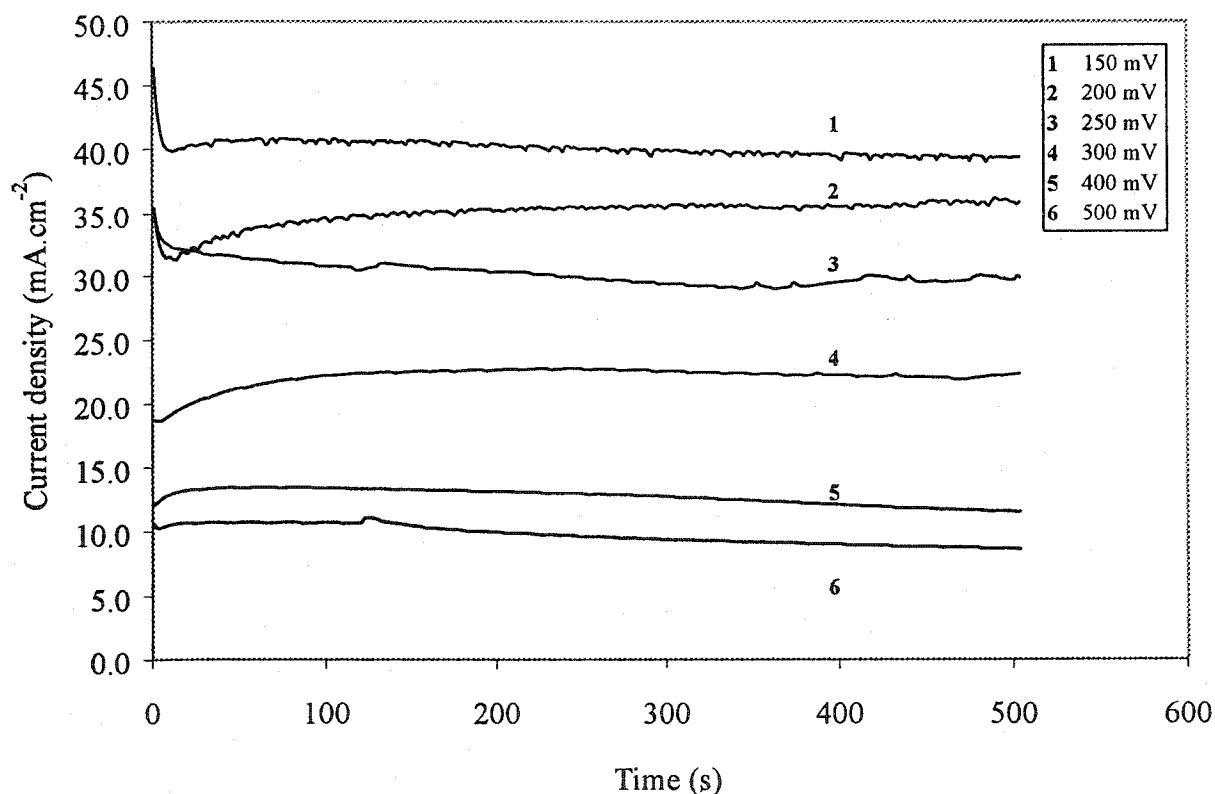
Figure 5-8 Sustainability of current flow with time in C_2H_6-O_2 fuel cells operated at $250°C$ and 1 atm pressure.

Whereas current flow obtained using fuel cell under anhydrous conditions was not sustainable, when the same cell was used with anode feed humidified, the current flow

102

had much better sustainability. Further, there was improved current flow at reduced cell potential.

An objective was to convert ethane to ethylene. However, the role of ethylene as probable intermediate product was not known. Consequently, to better understand the electrochemical reaction mechanisms in C_2H_6-O_2 fuel cells, performance using C_2H_4-O_2 as feeds was also tested in fuel cells in the presence of water vapor. Higher current density was achieved. Ethylene is reactive and is easily adsorbed onto the catalyst surface due to the existence of its double bond.

However, the C_2H_4-O_2 fuel cells did not achieve high power density, because large increments in current density only happened at low potential, typically below 300 mV (Figure 5-9).
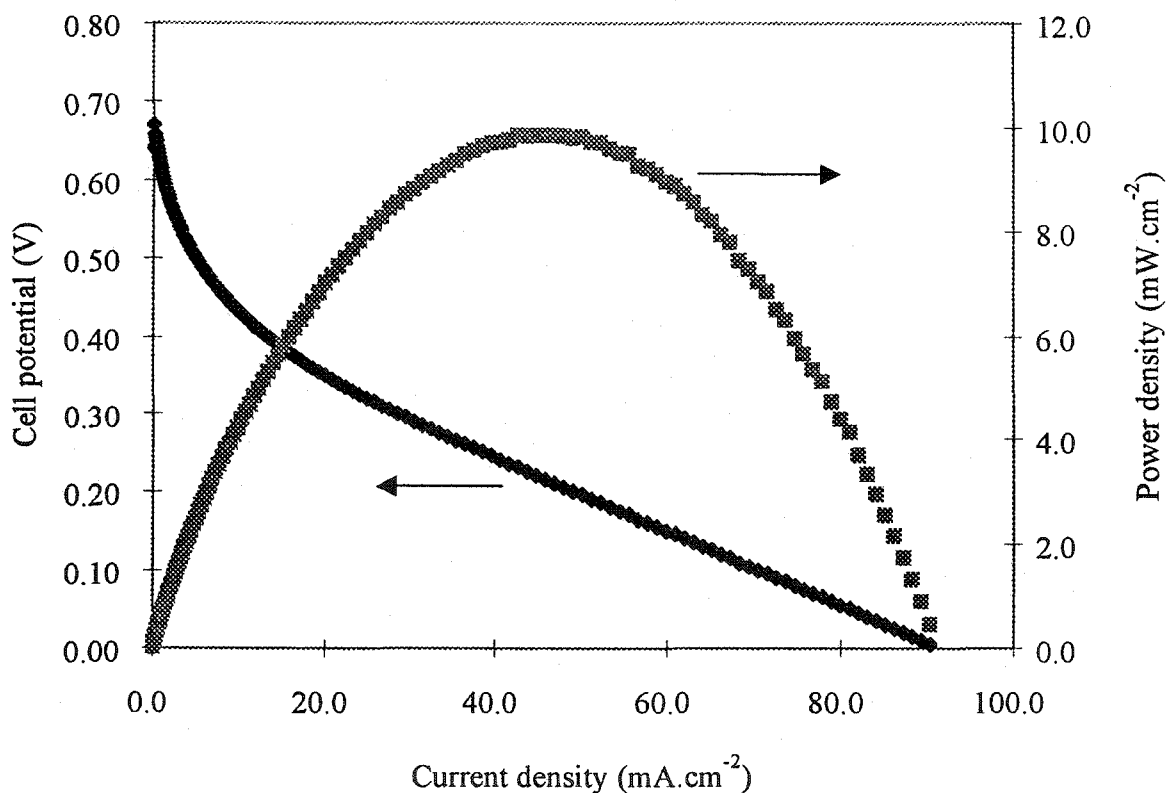
Figure 5-9 Polarization curve of C_2H_4-O_2 fuel cells at 200°C with addition of water at anode side, 25°C (I.R. was 0.40 Ohm).

103

Figure 5-10 shows another polarization curves for C_2H_4-O_2 fuel cells at an operating temperature of 200°C after continuous operation overnight. Both Figures 5-9 and 5-10 are characteristic of a process not having 'limiting current density', in contrast to ethane. Further, C_2H_4-O_2 fuel cells do not show any significant decay in cell performance with time. Figure 5-10 clearly shows that unlike C_2H_6-O_2 fuel cells, the polarization curve for C_2H_4-O_2 fuel cells was stable, without having to apply low cell potential to perform deep oxidization, even after operating continuously for more than 12 h at 200°C. The differences in both performance and stability, strongly indicated that the adsorption mechanisms were different for alkanes and alkenes.
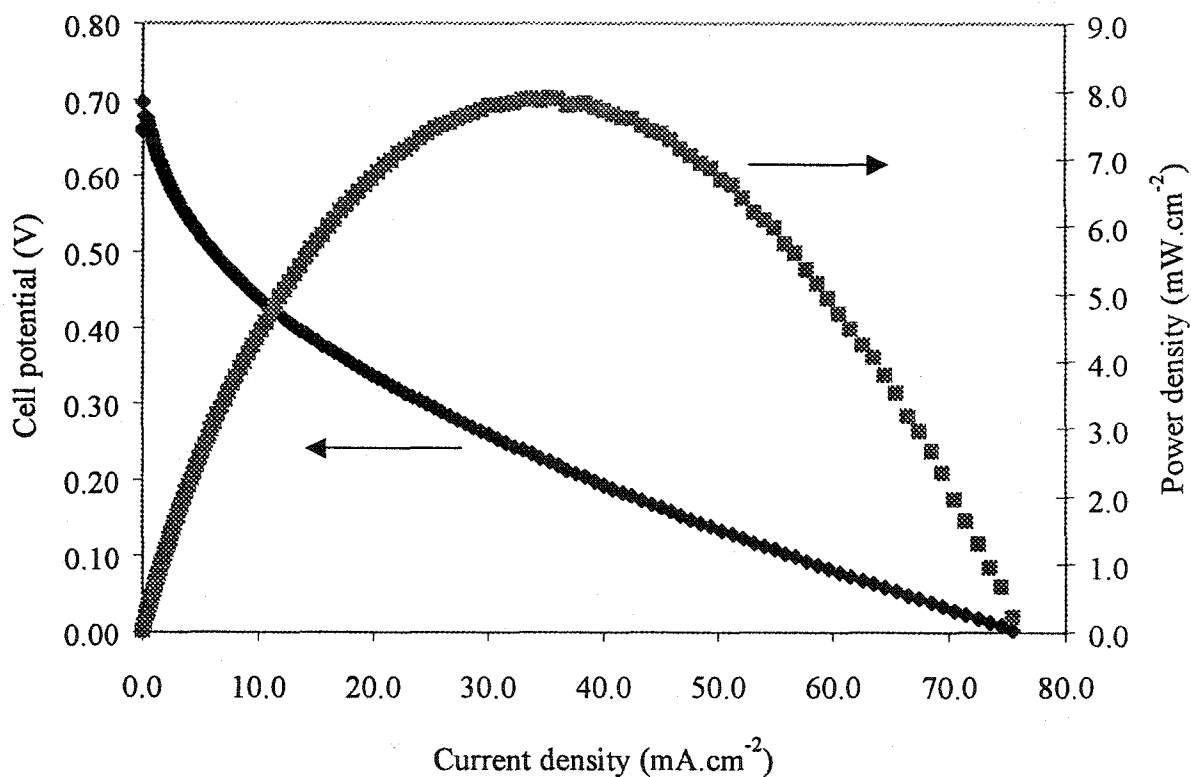
Figure 5-10 Polarization curve of C_2H_4-O_2 fuel cells after continuous operation at OCV overnight at 200°C; water added at the anode side, 25°C (I.R. was 0.41 Ohm).

Both graphs also showed a sudden increase in current density below 300 mV. This strongly indicated that ethylene, due to its more reactive double bond, was more easily chemisorbed on the platinum surface, compared to ethane, especially in the region below 300 mV. This was also the region where water species were easily adsorbed. Because both ethylene and water were adsorbed very strongly on the platinum surface, this

104

contributed towards larger current density because more reactants were absorbed onto the catalyst surface and ready to take part in the electrochemical reaction compared to ethane as fuel.

The rate-limiting steps in the overall electrochemical reactions for conversion of ethane and ethylene appeared to be different. The rate-limiting step for ethane most probably involved dissociative chemisorptions of ethane on platinum surface to form ethylene-like intermediate species during electrochemistry reaction. Once it had overcome this limitation, the subsequent reactions were faster. For ethylene, adsorption happened rapidly on the platinum surface, so the rate limiting step was the electrochemical reaction that occurred on the surface of platinum.

In terms of current flow sustainability, it was determined that current flow of C_2H_4-O_2 fuel cells reached a steady-state condition after operating at a fixed cell potential for about 150 s. Here, I provided one set of data that represent current sustainability behavior shown by C_2H_4-O_2 fuel cell with slight humidification.
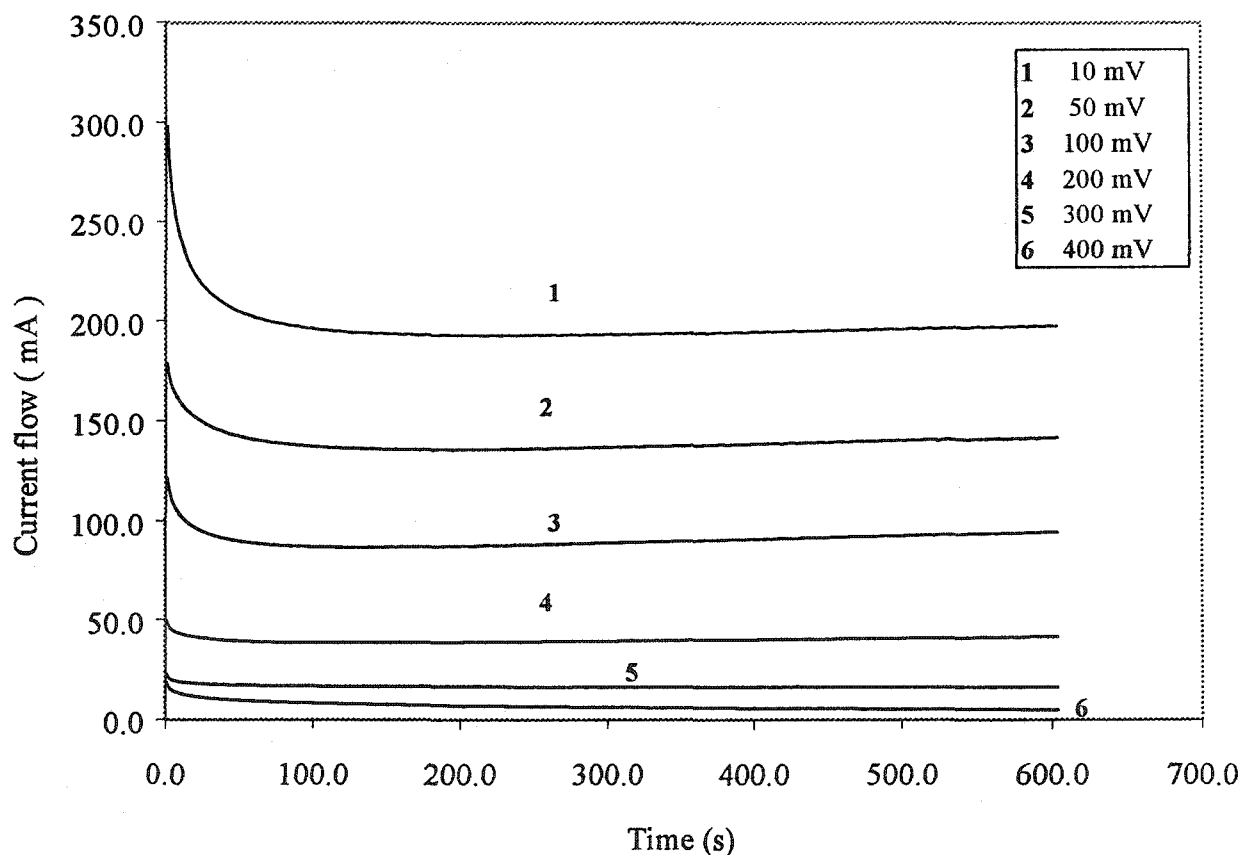
Figure 5-11 Current sustainability with time of C_2H_4-O_2 fuel cells operating at 200°C.

105

To confirm the earlier proposition that C_2H_4 adsorbed more strongly than C_2H_6 on platinum surfaces, another experiment was performed, in which the anode side was fed with H_2 and the cathode side fed with C_2H_4. Figure 5-12 was obtained.
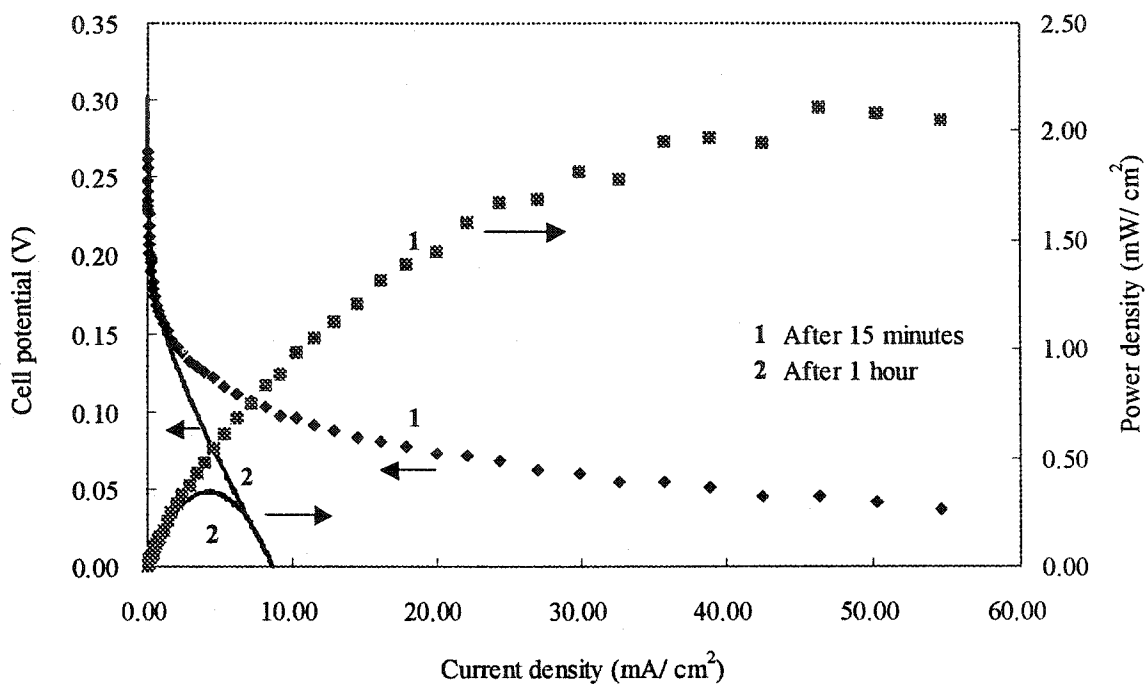
Figure 5-12 Polarization curve of H_2-C_2H_4 fuel cells at 160°C under anhydrous condition (I.R. was 0.39 Ohm).

Referring to Figure 5-12, since the cell potential of H_2-O_2 fuel cells mode is above 1.0 Volt and cell potential of C_2H_6-O_2 fuel cells mode is about 0.7 Volt at 160°C, the cell potential for H_2-C_2H_4 should be approximately 0.3 Volt. Using G.C. analysis, ethane product was detected at the cathode side. Several conclusions can be drawn. This experiment proved that, below a potential of 300 mV, C_2H_4 easily chemisorbed onto the platinum surface, where it was hydrogenated by proton transfer from the anode side, and desorbed freely from the platinum surface as C_2H_6. This is the reverse process to that proposed for conversion of ethane. Thus, because C_2H_6 easily desorbed, this showed that adsorption of C_2H_6 was relatively difficult. Similarly, because C_2H_4 was adsorbed easily, then desorption of C_2H_4 was relatively hard because of the strong bond formed to platinum.

106

5.5.1.3 Electrochemical Products for Ethane-Oxygen Fuel Cells

So far, the concept of C_2H_6-O_2 fuel cells has been described with reference to electrical performance, and not products. G.C. analysis showed that instead of the anticipated ethylene product from conversion of ethane during fuel cell operation, use of either ethane or ethylene only produced final products consisting of carbon monoxide and carbon dioxide. No other products have been detected under this acidic environment.

The concentration of CO and CO_2 obtained varied with cell potential. At high cell potential, the amount of CO was slightly higher than the amount of CO_2. As potential of the cell gradually decreased, consistent with deep oxidization, the amount of CO_2 increased while CO gradually diminished. The amounts of products detected were consistent with the current density generated. Thus, there were no others undetected products.

Figure 5-13 shows the dependence of product selectivity on cell potential. Operations at both 200°C and 250°C showed the same trend of product composition (G.C. analysis). For electrochemical reactions, cell potential always has influence over product distribution if there are more than single reactions taking place.

As cell potential declined, formation of CO_2 increased while the formation of CO decreased. From the Figure 5-13, the products' ratio is more favored towards CO at 250°C than 200°C. These differences can be attributed to the prolonged operation of cell at 200°C before shifting to 250°C, which decreased the activity of platinum black catalyst by the time of measurement.

The long-term performance of platinum catalyst during fuel cells operation at elevated temperature still can be affected by the formation of intermediate species. Measurements at 200°C were taken after fuel cells had been working continuously for 2 days, while the measurements at 250°C were taken on the 3rd day of operation. For both cases, rapid formation of CO_2 occurred at low cell potential, approximately 300 mV and below. Once again, this is consistent with the fact that an 'O' donating species, which was probably water, was adsorbed strongly in this low potential region, thus promoting the formation of CO_2 from CO.

107

Figure 5-13 Dependence of CO_2 to CO ratio on cell potential for C_2H_6-O_2 fuel cells at 200°C and 250°C.
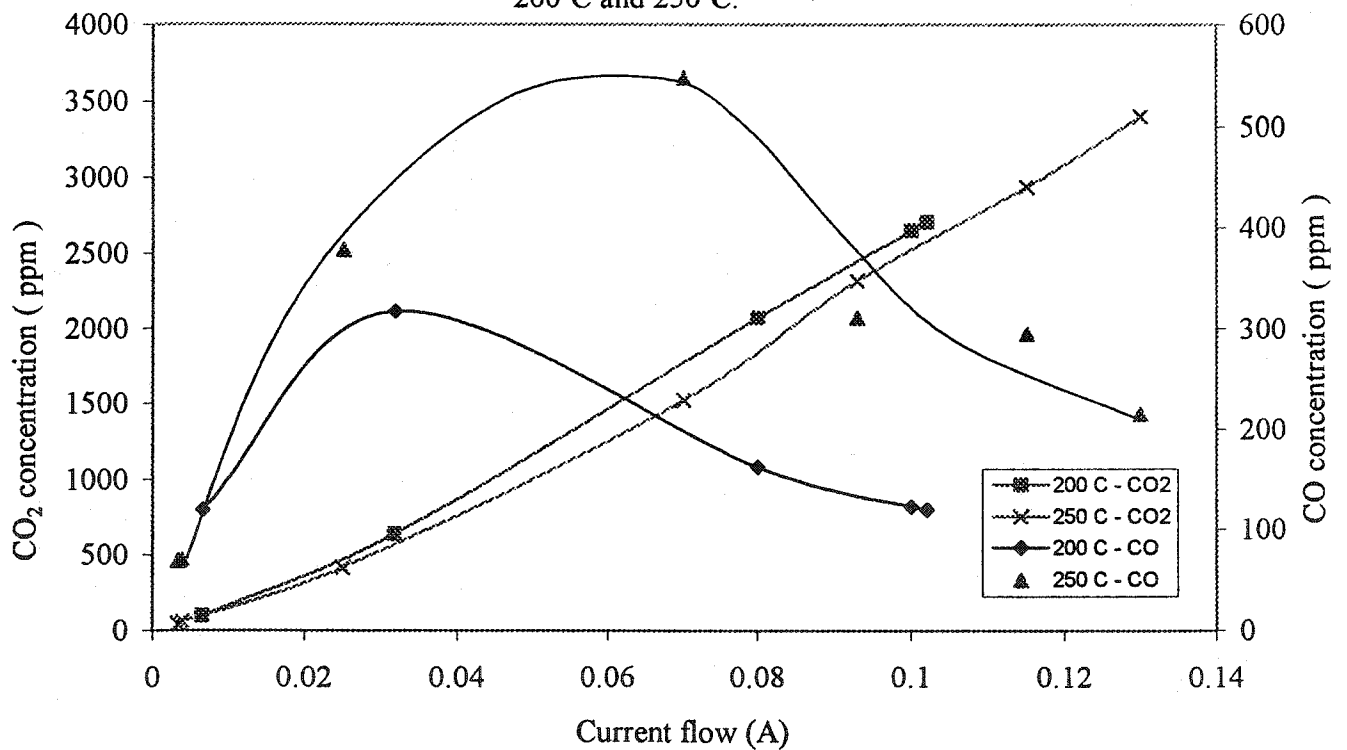
Figure 5-14 Calculated concentrations of CO_2 and CO with variation in current flow.

108

Figure 5-14 shows the correlation between product amounts and current density. As current flow increased, the total amount of products also increased. This showed that the current flow generated was equivalent to the amount of electrochemical products. The amount of CO_2 produced always increased with current flow, while the amount of CO increased at high cell potential and decreased as current flow increased (at low potential).

Although the detailed electrochemical reaction mechanisms are not fully understood, nonetheless, from the present data, it appears that, in an acidic environment, the overall electrochemical reactions at anode side resemble the steam reforming reaction. The following reaction sequence is proposed for the electrochemical reactions taking place at the anode side, consistent with the observed experimental results:

$$C_2H_6 \text{ (g)} + 2 \text{ } H_2O \text{ (g)} \rightarrow 2 \text{ CO (g)} + 10 \text{ H}^+ + 10 \text{ e}^- \quad (5.3)$$

$$CO \text{ (g)} + H_2O \text{ (g)} \rightarrow CO_2 \text{ (g)} + 2 \text{ H}^+ + 2 \text{ e}^- \quad (5.4)$$
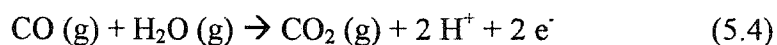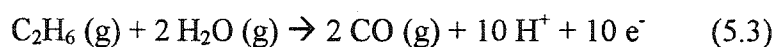
The reaction equations above imply that both electrochemical reactions were actually reactions in series. The first electrochemical reaction produced CO and released 10 mol of electrons, which were drawn away through the external electrical circuit. Then, depending on the cell potential, a further portion of CO was converted to CO_2 with a release of two additional electrons per mole of CO converted. The protons were then conducted through the electrolyte to the cathode.

Figure 5-15 presents two graphs comparing the concentrations of CO_2 and CO (using the reaction sequence in Eqns. (5.3) and (5.4)) with the concentration of these products detected by G.C. analysis (in molar basis). Details of the complete calculations are presented in Appendix A2. The calculated values agree well with the analytical data. From these comparisons, it is seen that the current flow produced by electrochemical reactions always tallied with the amounts of generated products. It also showed that the above reaction equations represent the overall electrochemical reactions for the use of ethane as hydrocarbon fuel.
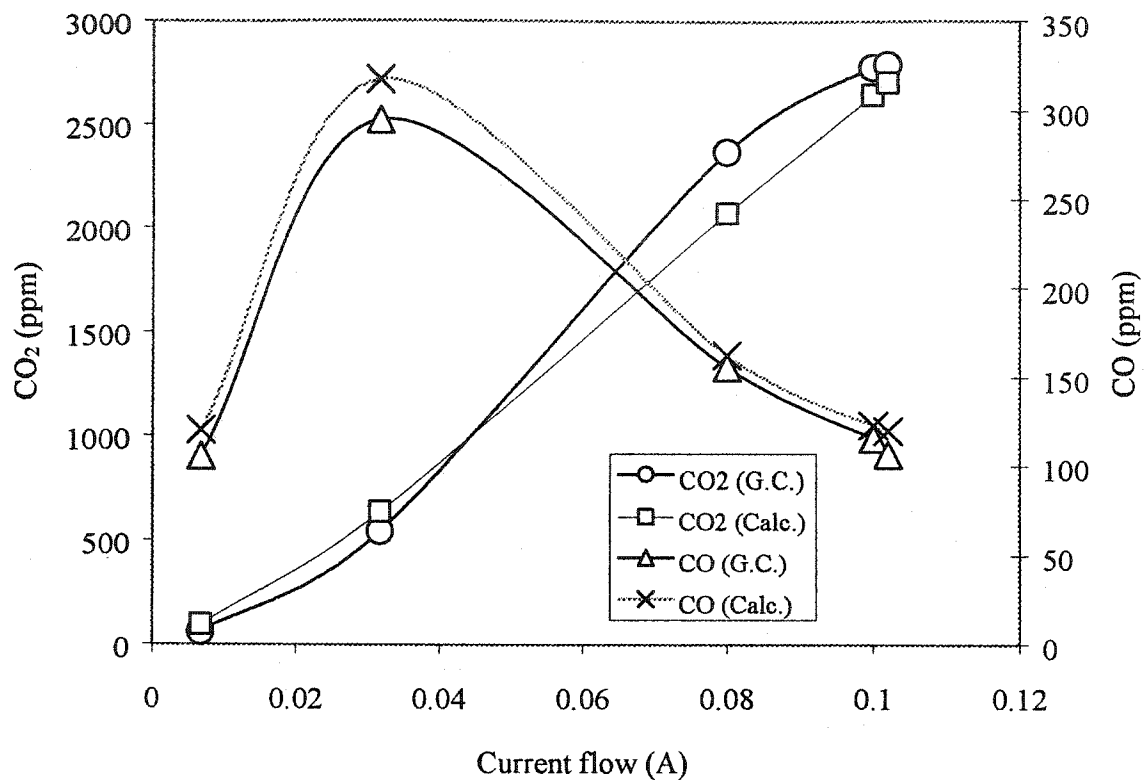
(a) C_2H_6-O_2 fuel cells at 200°C.
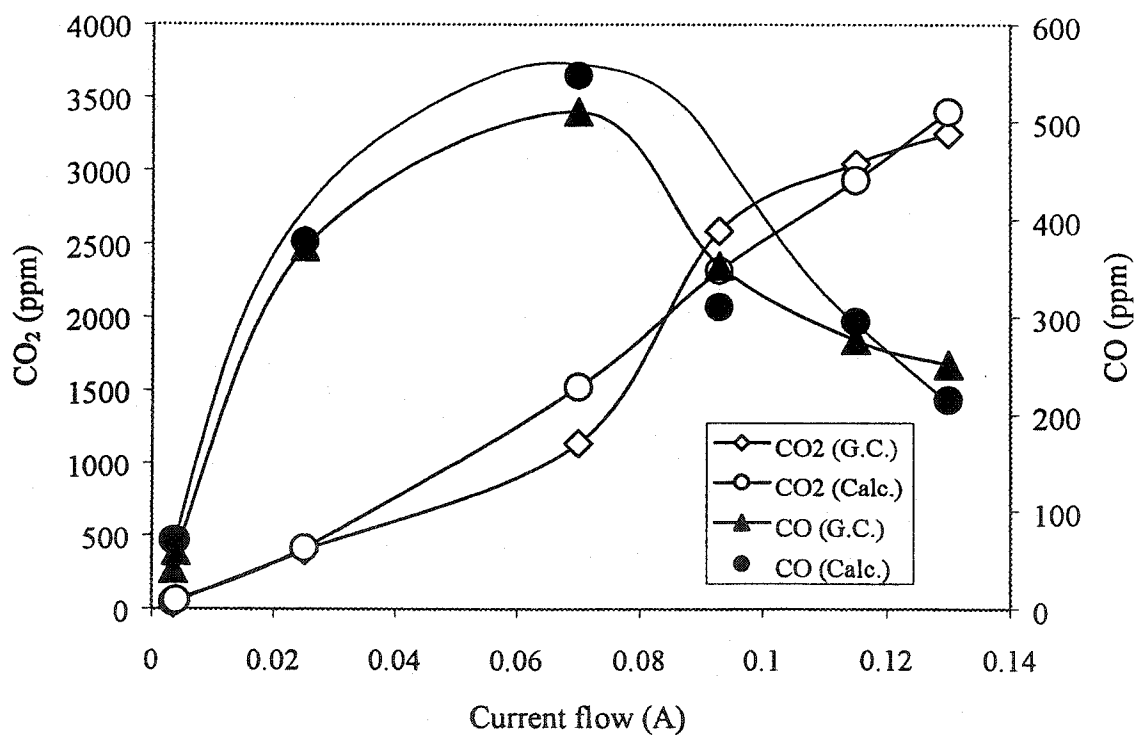
(b) C_2H_6-O_2 fuel cells at 250°C.

Figure 5-15 Comparison between calculated and detected concentration of products.

110

The presence of acid on catalyst surface enhanced the cracking of ethane [5]. Acidic condition provided an electron deficient environment. As a result, although ethane was dehydrogenated, an ethylene-like intermediate species with double bond became strongly adsorbed on the platinum surface, which was hard to desorb from the catalyst surface. Further reactions involving water then led to the final products of CO and CO_2, which finally were evolved from the catalyst surface.

When ethylene was used as hydrocarbon fuel, it produced the same products. No other products were detected. The dependence of product selectivity on cell potential was identical to that with ethane as fuel. Selectivity towards CO_2 again increased dramatically at potentials below 300 mV. Figure 5-16 shows the dependence of product selectivity on cell potential of fuel cells operated using ethylene and oxygen.
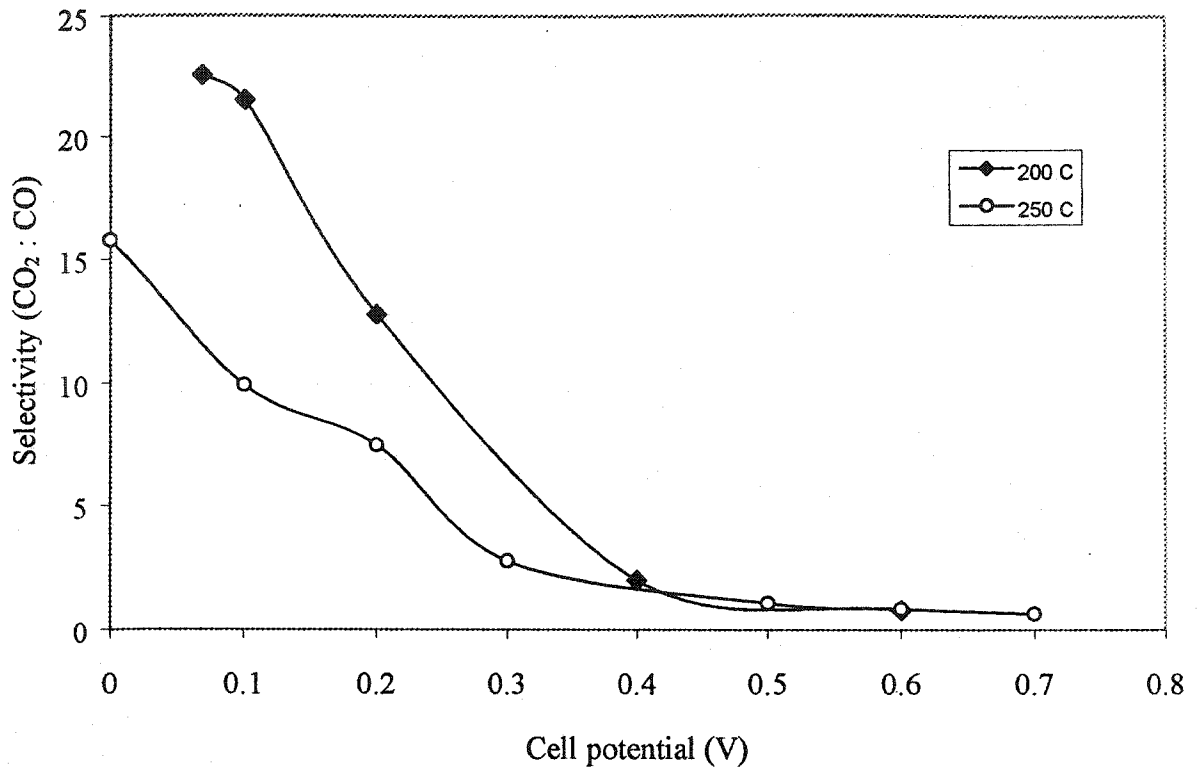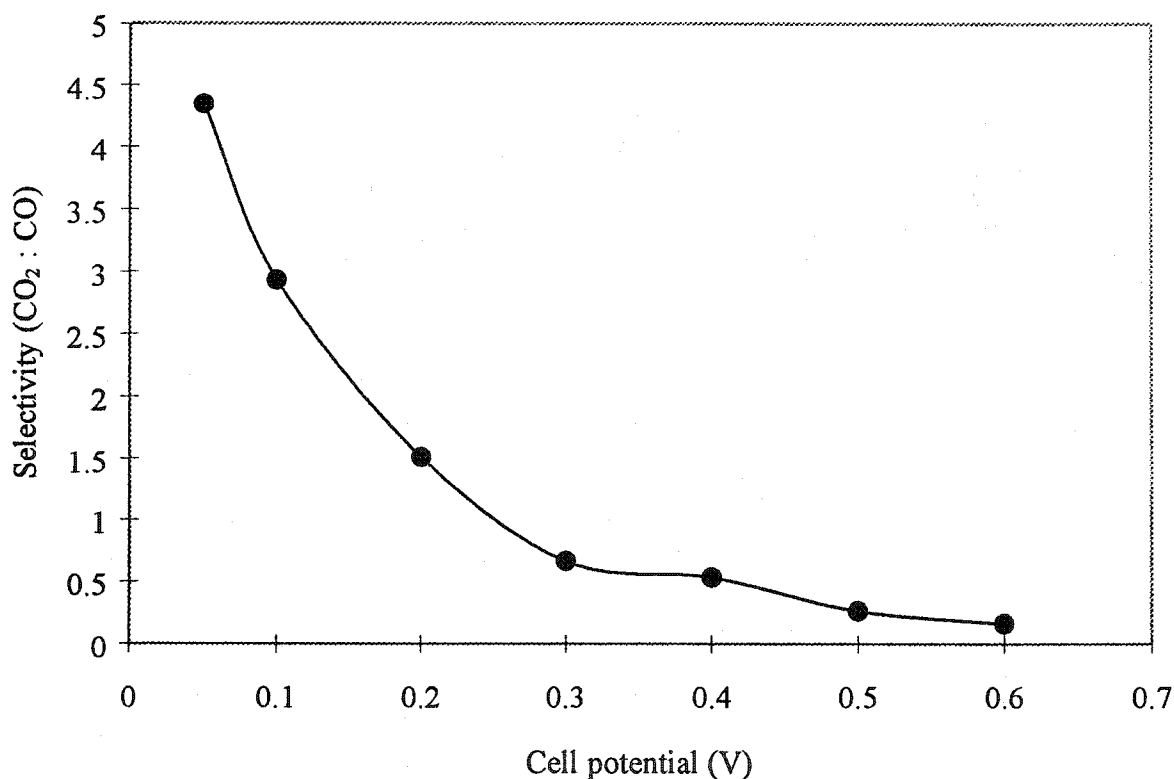

Figure 5-16 Dependence of CO_2 to CO ratio on cell potential for C_2H_4-O_2 fuel cells at 150°C and 1 atm pressure with water added at anode side, 25°C.

111

Referring to Figures 5-16 and 5-17, both graphs, which were obtained from the fuel cells operation using ethylene as fuel, exhibited the trend that matched to the results obtained using ethane fuel cells. Although the same products were obtained, in fuel cells operated using C_2H_4, higher concentrations of CO were produced when compared to C_2H_6. This is attributed to the stronger adsorption of C_2H_4 compared to C_2H_6 to form intermediate products, which were then converted into CO-alike species on platinum surface by reaction with H_2O. Further oxidation to CO_2 was hindered by the lower amount of H_2O adsorbed due to competition with strongly bonded C_2H_4. Consequently, the rate of conversion of CO to CO_2 was limited by the relatively lower concentration of water on the catalyst surface when C_2H_4 was also present.
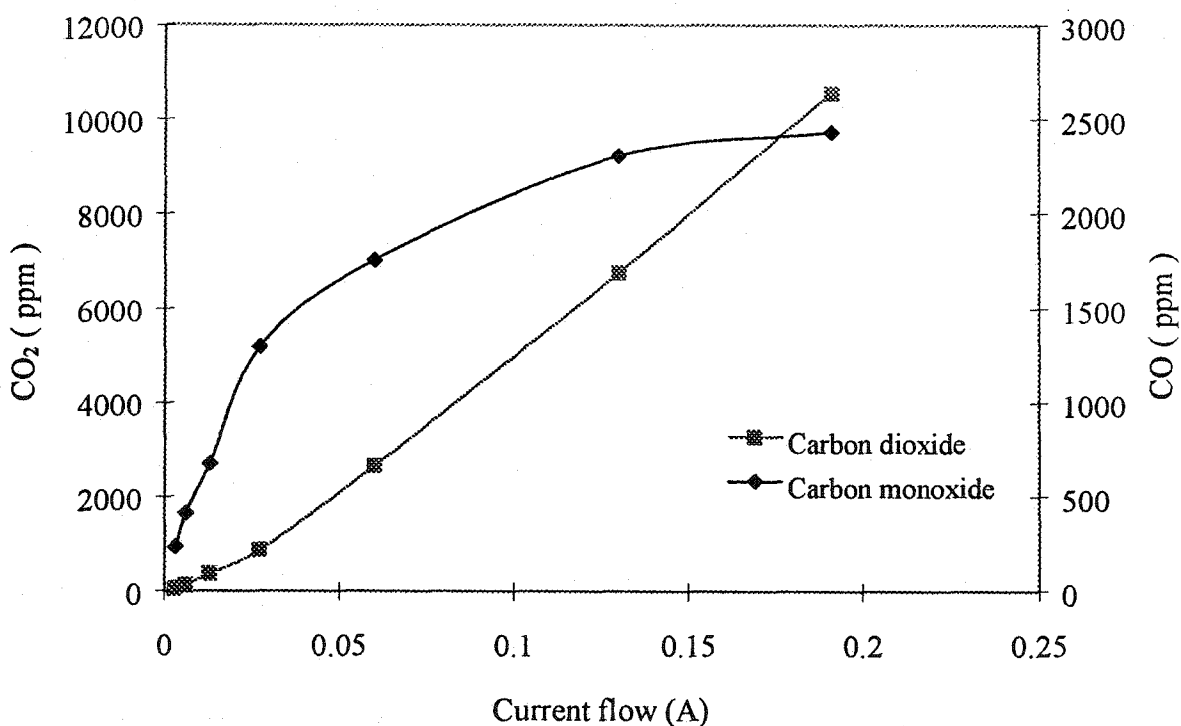
Figure 5-17 Correlation between current flow and concentration of products produced by C_2H_4-O_2 fuel cells operated at 150°C and 1 atm.

From these results, one possibility exists that ethylene indeed formed as intermediate species during the electrochemical reaction of ethane. But, the acidic metal catalyst provides an electron deficient environment which bond strongly to this intermediate species, resulting in further reaction, undergoing cracking of the C–C bond to form C_1 species, which finally formed CO and CO_2 before being detached freely from the catalyst surface. Further detailed discussion will be presented in Section 5.5.3.

112

5.5.2 Propane-Oxygen Fuel Cells

5.5.2.1 Cell Potential

The potentials attained with C_3H_8-O_2 fuel cells were as stable as those for C_2H_6-O_2 fuel cells. In addition, the cell potentials for C_3H_8-O_2 fuel cells at 1 atm pressure had values close to those obtained from C_2H_6-O_2 fuel cells. The potentials increased with temperature, consistent with the prediction from ΔG and Nernst equation as a function of temperature (Figure 5-2).

Figure 5-18 shows the cell potentials obtained at different temperatures, after stabilization for at least 6 h. Cell potentials for both propane and ethane fuel cells always increased with temperature, ranging from below 600 mV at 100°C to above 700 mV at 200°C. Then, over 230°C, the cell potential increased to above 800 mV.
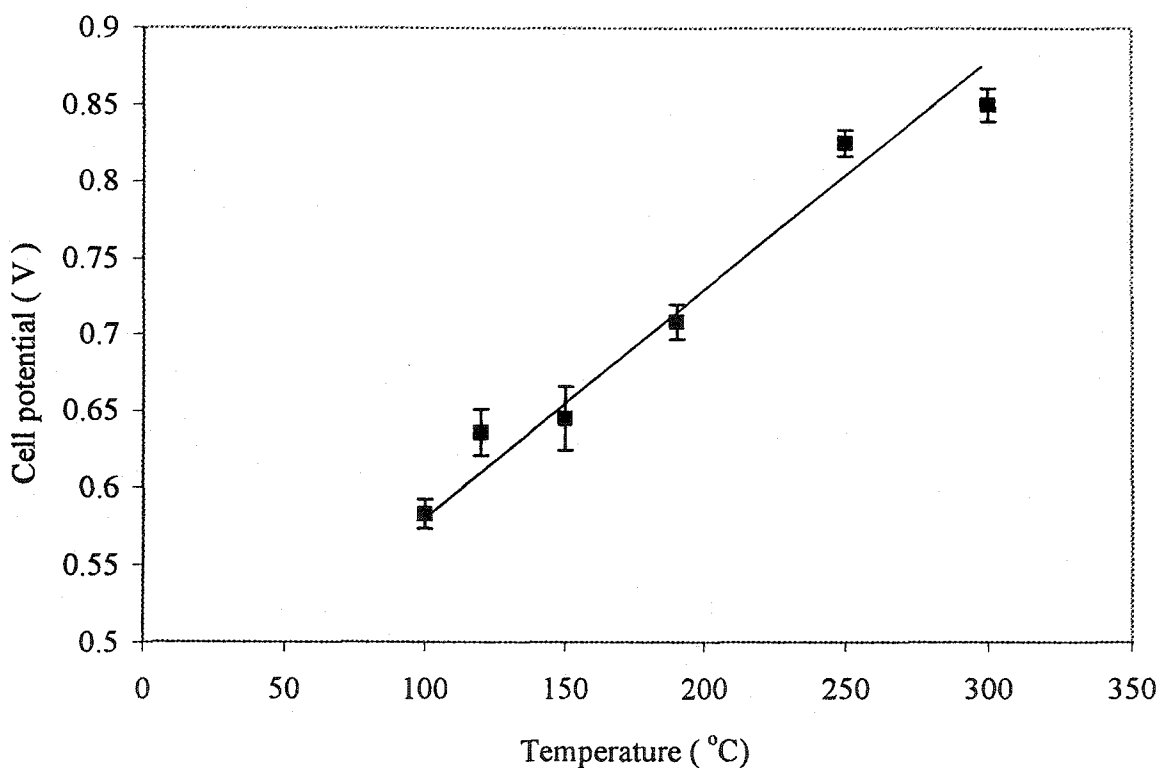
Figure 5-18 Variation of C_3H_8-O_2 fuel cells OCV with operating temperature at 1 atm after stabilization for at least 6 h.

113

The cell potential attained values over 800 mV at temperatures higher than 200°C, consistent with larger ΔG values that can be manipulated from the cell, thus providing a significant driving force for electrochemical reactions to take place.

5.5.2.2 Polarization Curves for Propane-Oxygen Fuel Cells

Under anhydrous condition, C_3H_8-O_2 fuel cells exhibit very small current flow, typically in the range of several $mA.cm^{-2}$, similar to those found for C_2H_6-O_2 fuel cells. In the absence of water, the electrochemical reactions cannot proceed to completion. Consequently, there was only a limited amount of reaction happened.

Figure 5-19 shows an example of a typical polarization curve obtained whenever operation was carried out under anhydrous conditions. Not only was the current density low, the current flow was also not sustainable.
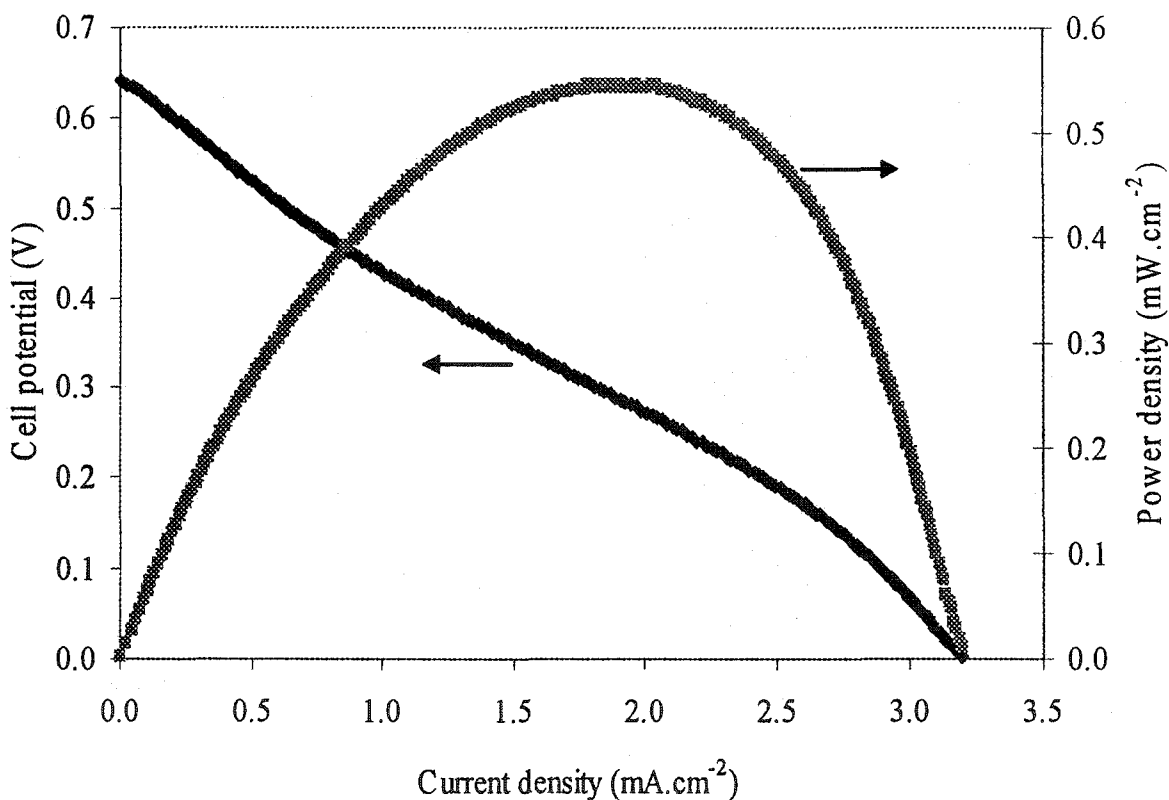
Figure 5-19 Polarization curve of C_3H_8-O_2 fuel cells under anhydrous conditions at 250°C and 1 atm pressure (I.R. was 0.26 Ohm).

114

Over an extended operating time, the current flow was reduced to a few microamperes. This is depicted in Figure 5-20.
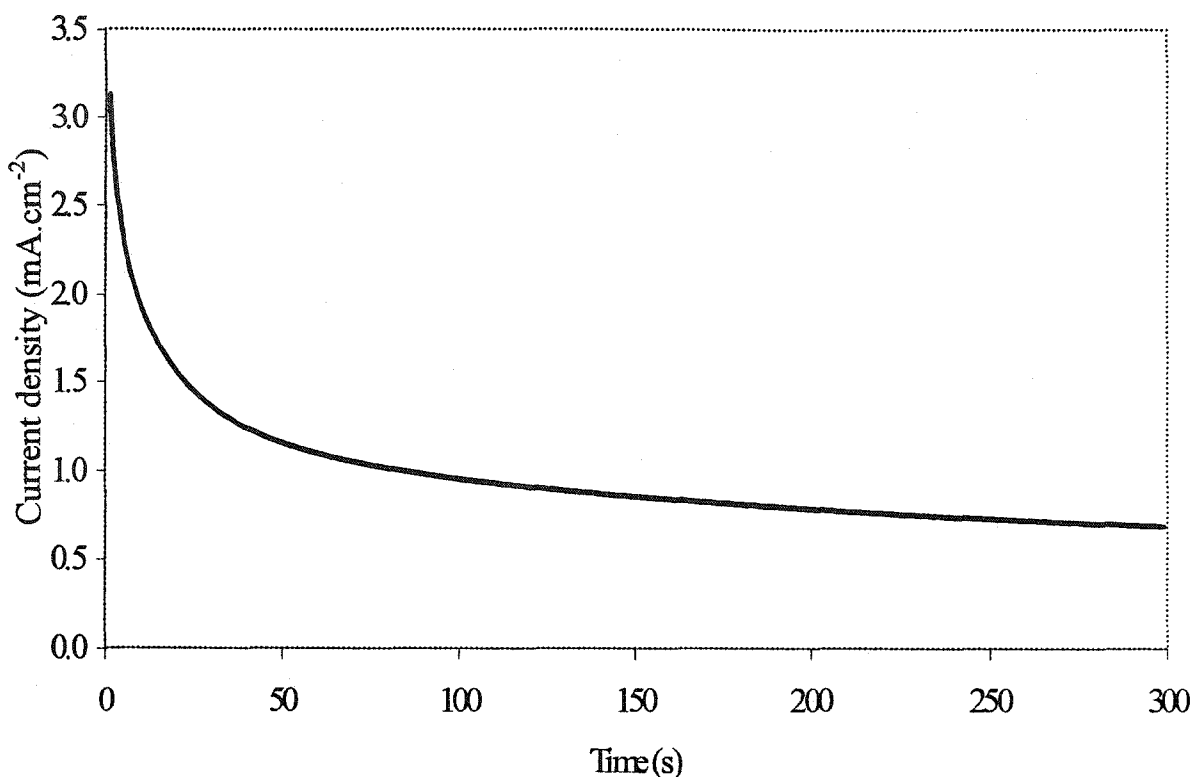
Figure 5-20 Current flow versus operating time at 100 mV potential for C_3H_8-O_2 fuel cells operated at 250°C and 1 atm pressure (anhydrous condition).

Figure 5-20 shows a typical trend of current flow under anhydrous conditions. As can be observed, the current flow diminished with time. After the cell had been working for 300 s at 100 mV, the current flow gradually became smaller. The operation of C_3H_8-O_2 fuel cells under anhydrous conditions was not sustainable, and the current flow did not attain steady state value. As for C_2H_6-O_2 fuel cells, this can be attributed to the formation of intermediate species on catalyst surface which blocked the majority of active catalyst surface sites for reactant adsorption and reaction.

Polarization curves for C_3H_8-O_2 fuel cells operated with humidification showed a significantly increase in current flow. The addition of water had the effect of enabling the progress of electrochemical reactions, resulting in increased current flow as was also found for C_2H_6-O_2 fuel cell systems. A typical polarization curve is shown in Figure 5-21.

115
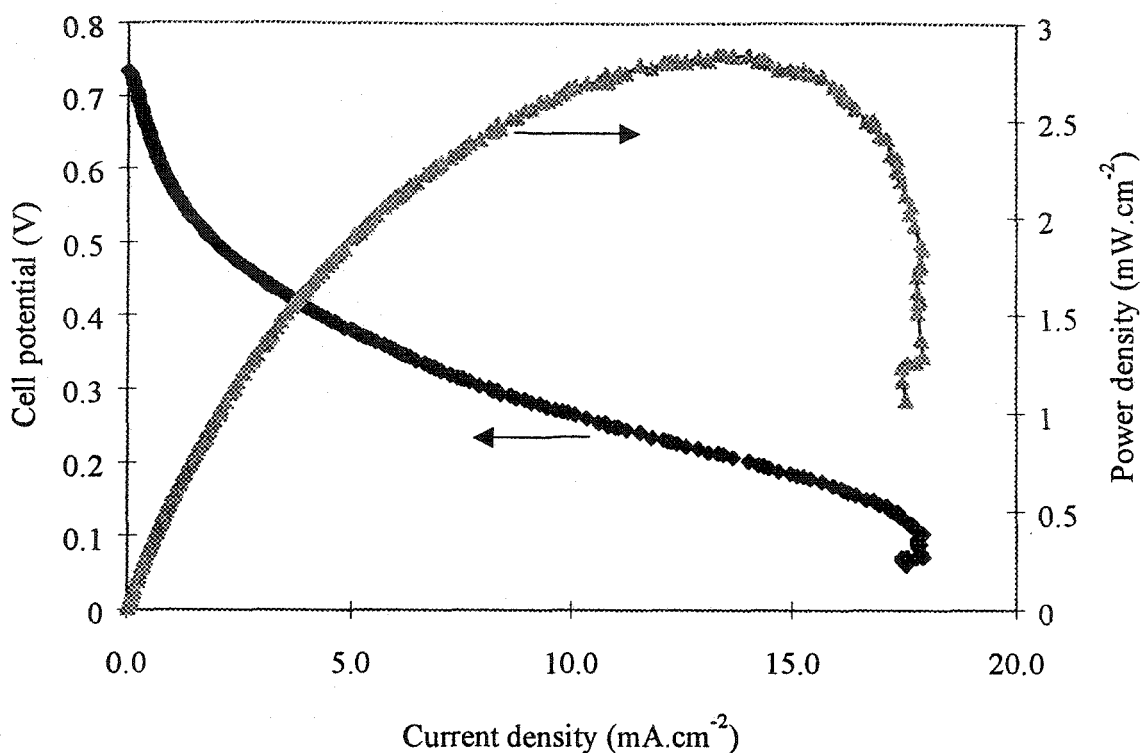
Figure 5-21 Polarization curve of C_3H_8-O_2 fuel cell at 250°C and 1 atm pressure with humidification of anode feed at 25°C (I.R. was 0.36 Ohm).

Figure 5-22 shows the variation of current flow at different potentials with operating time. Once again, with the addition of water, the current flow was sustainable. Current flow increased with decreased cell potential. Interestingly, when operation was carried out at low potential, 100 mV or short-circuit condition for an extended time (> 10 min.), the current flow increased gradually. This is an indication of the effect of low cell potential towards catalyst's surface condition where it can 'clean' the surface from stable intermediate products.

In Figure 5-23, throughout the high cell potentials and low current flow region, the molar amounts of CO_2 and CO generated were quite similar. At lower cell potential, below 0.3 Volt, the amount of CO_2 became predominant. Again, this behavior followed the same trend shown by ethane and ethylene fuel cells. Cell potentials generated altered the electronic properties of the platinum catalyst, thus influencing the activation of propane and the further reactions of intermediate products, as shown for ethane in Eqns. (5.3) and (5.4).

116
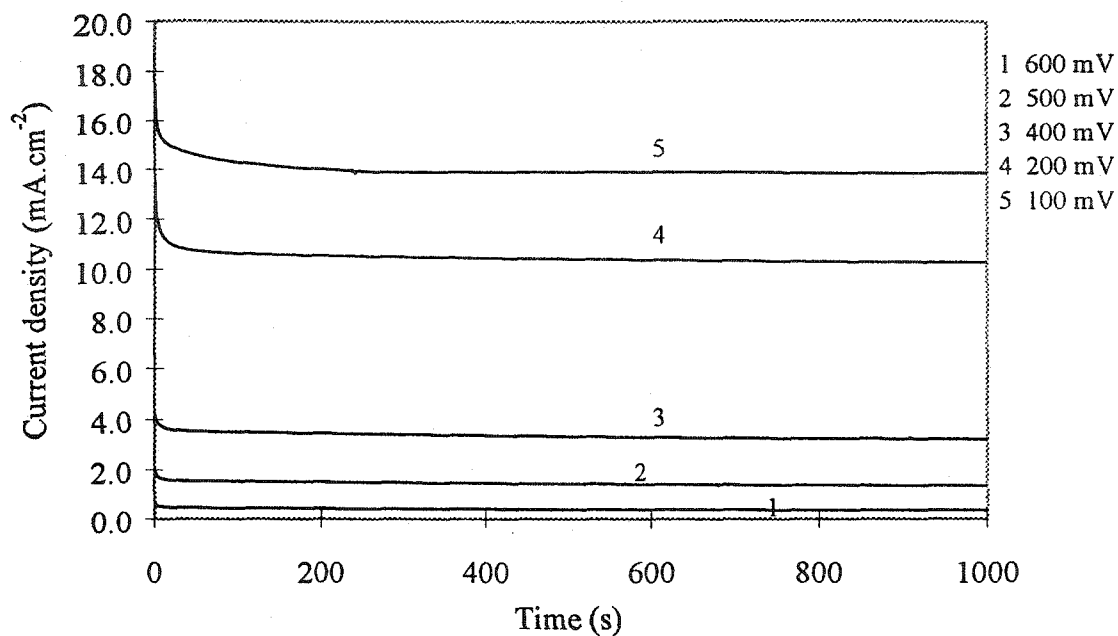
Figure 5-22 Current flow versus operation time for C_3H_8-O_2 fuel cells at 250°C with humidification of anode feed at 25°C.
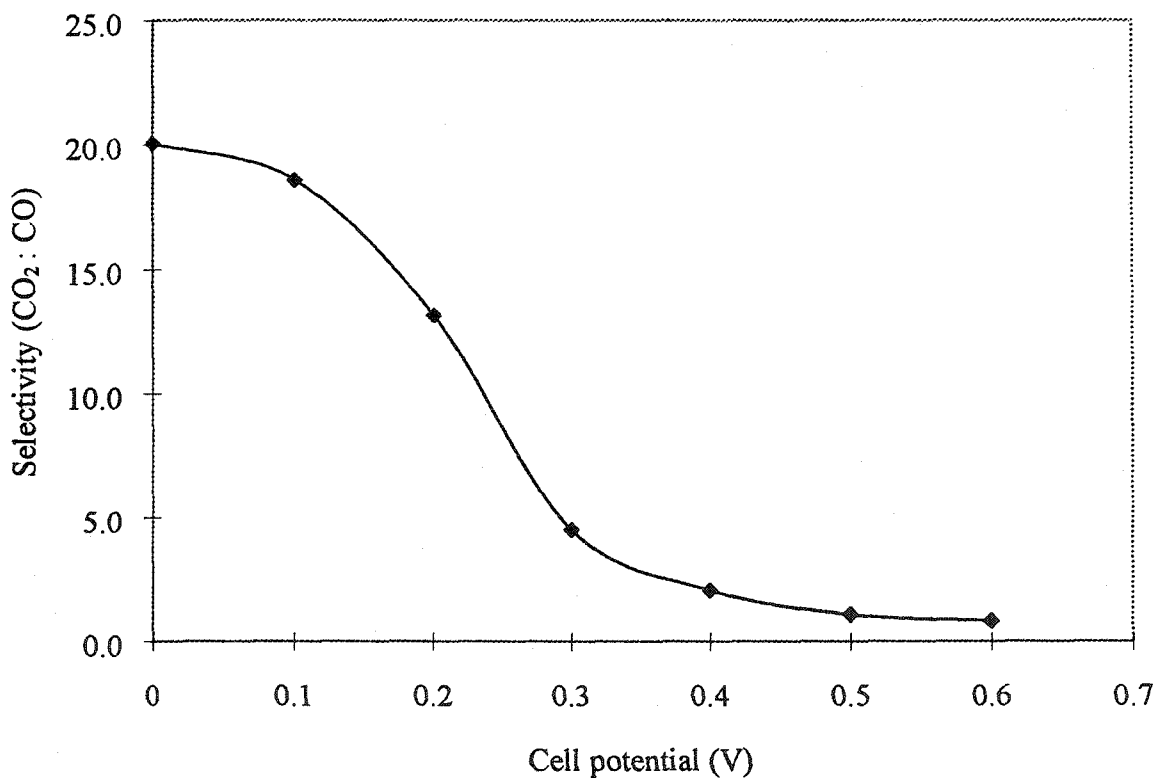
Figure 5-23 Dependence of CO_2:CO ratio on cell potential of C_3H_8-O_2 fuel cells operated at 250°C and 1 atm pressure, with anode humidification at 25°C.

117

At low potentials, easily desorbable electrochemical products were formed, so, the rate of formation of final products increased as current flow also increased (Figure 5-24). The concentration of CO_2 in the effluent increased linearly with current, while that of CO reached a maximum value before declining at high currents.
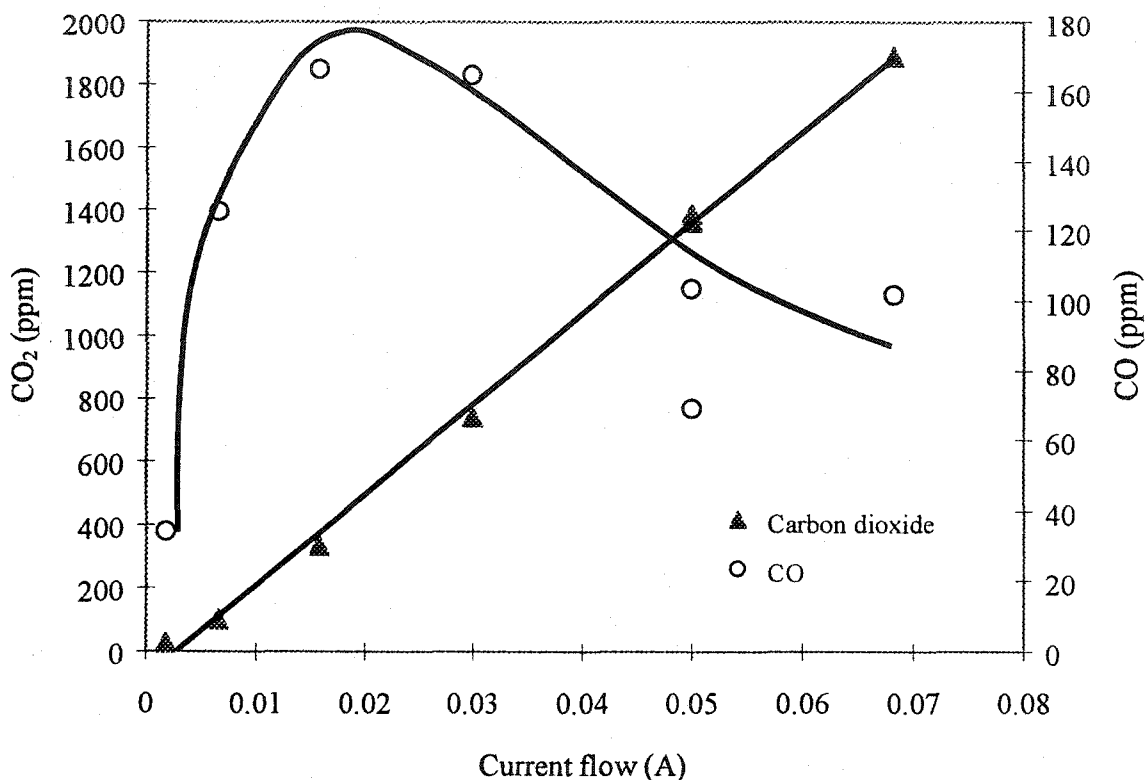
Figure 5-24 Variation of products concentration with current flow for C_3H_8-O_2 fuel cells operated at 250°C, 1 atm with humidification of the anode feed at 25°C.

5.5.3 Mechanisms of Reactions in Hydrocarbon Fuel Cells

The results obtained for C_2H_6-O_2, C_2H_4-O_2 and C_3H_8-O_2 fuel cells were each reproducible. Although the procedures were substantially the same for making all membranes, the I.R. of the fuel cells varied between 0.2 Ohm and 0.4 Ohm. In each case, significant current density was obtained when the anode feed was humidified, but much lower values were obtained when the cell was operated under anhydrous conditions. A large I.R., 1 to 2 Ohm indicated that the cell was not properly installed. No further testing was performed in such cases, as no significant improvement in current flow could be

118

obtained, even in the presence of water. The results reported herein were reproduced at least three times.

Since fuel cell experiments conducted using different light paraffins have shown similar trends and very similar results, there is reason to believe that the electrochemical reactions taking place followed similar mechanisms. Fuel cell operation carried out using propane and ethane as fuels each resulted in the formation of CO_2 and CO. This was consistent with the results obtained by Savadogo and Varela (2001), who reported the formation of only CO_2 from direct propane fuel cells [6].

Thus, water, which initially was introduced to humidify the membranes, has been identified instead as a participant in the electrochemical reactions in the present acidic environment. Without water, the electrochemical reactions did not proceed readily or extensively.

I now propose that the electrochemical reactions occurring in hydrocarbon fuel cells follow two reaction paths. One path is a sequence of reaction in series, as described in section 5.5.1.3. The other path involves parallel reactions to produce CO_2 and CO (Eqns. (5.5) and (5.6)).

$$C_2H_6 \text{ (g)} + \tfrac{7}{2} \, O_2 \text{ (g)} \rightarrow 2 \, CO_2 \text{ (g)} + 3 \, H_2O \text{ (g)} \qquad (5.5)$$

$$C_2H_6 \text{ (g)} + \tfrac{5}{2} \, O_2 \text{ (g)} \rightarrow 2 \, CO \text{ (g)} + 3 \, H_2O \text{ (g)} \qquad (5.6)$$
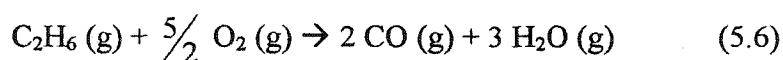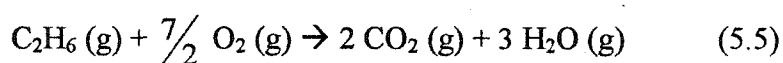
From Eqn. (5.5), we can separate the overall reaction into two half-cell reactions at both anode and cathode side:

Anode side: $\quad \tfrac{1}{2} \, C_2H_6 \text{ (g)} + 2 \, H_2O \text{ (g)} \rightarrow CO_2 \text{ (g)} + 7 \, H^+ + 7 \, e^-$ \quad (5.7 a)

Cathode side: $\tfrac{7}{4} \, O_2 \text{ (g)} + 7 \, H^+ + 7 \, e^- \rightarrow \tfrac{7}{2} \, H_2O \text{ (g)}$ \qquad (5.7 b)
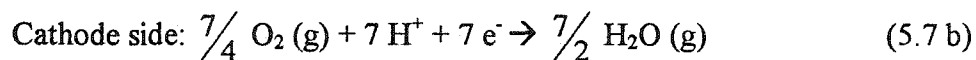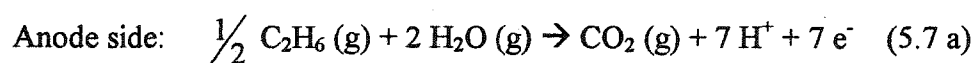
Production of one molecule of CO_2 requires the transfer of 7 protons to the cathode side, as evident from Eqns. (5.7 a) and (5.7 b). The electrochemical reactions at the anode side donate all these seven protons. This proposition provides another alternative way to calculate electrochemical reactions without having to know the prior reaction mechanisms at the anode side.

For overall reaction shown in Eqn. (5.6), five electrons are conducted for each molecule of CO formed (Eqns. (5.8 a) and (5.8 b)).

$$\text{Anode side:} \quad \tfrac{1}{2} \, C_2H_6 \, (g) + H_2O \, (g) \rightarrow CO \, (g) + 5 \, H^+ + 5 \, e^- \qquad (5.8 \, a)$$

$$\text{Cathode side:} \quad \tfrac{5}{4} \, O_2 \, (g) + 5 \, H^+ + 5 \, e^- \rightarrow \tfrac{5}{2} \, H_2O \, (g) \qquad (5.8 \, b)$$

Overall, the electrochemical reactions involve the transfer of 12 mol of electrons to produce CO_2 and CO, consistent with Eqns. (5.3) and (5.4).

Figure 5-25 shows the structures of proposed intermediates on the platinum surface, for both ethane (a, b) and propane (c, d) after dissociative adsorption.

Figure 5-25 Proposed intermediate species on platinum surface: (a) and (b) – from ethane; (c) and (d) – from propane.

The intermediate species formed at the platinum sites are not expected to retain the double bond characteristic of π-bonded alkenes, for two reasons. The first reason is adsorption of an alkene on platinum surface typically involves interaction with two metal atoms, and results in formation of a single $C - C$ bond oriented parallel to the surface as shown in Figure 5-25 (b) [7]. The analogous structure resulting from adsorption of propane is shown in Figure 5-25 (d).

The second reason is that, even if species (a) and (c) exist under these conditions, drawing of electrons away from the platinum surface results in electron deficiency in the vicinity of the metal surface sites. Thus, under acidic conditions, the electrons in the π bond, which is rich in electrons cloud, will be attracted toward the catalyst surface to form σ-bonds. Consequently, it is anticipated that species such as (b) and (d) are expected to prevail.

120

Conclusions can be drawn from the combination of polarization curves and electrochemical products obtained. The first conclusion is that intermediate species like the one shown in Figures 5-25 (b) and 5-25 (d) are probably formed initially by dissociative chemisorption of alkane feed, and that these species bond strongly to the platinum catalyst sites. The detection of only C_1 products (C_1 refers to species with one carbon atom) suggests that the C_2 and C_3 intermediates so formed then react further rather than desorb as alkenes once they are thermally activated [8]. Thus the mechanism necessarily involves a C – C bond breaking step.

The second important conclusion is that the cleavage of C – C bond happened during the electrochemical reaction sequence. It probably occurs as a result of the strong bonding of intermediate species to multiple sites at the platinum surface, resulting in weakening of the carbon-carbon bonds, and leading to the fragmentation of the intermediates. Unlike C=C bond, less energy was required to break the C – C bond. According to Wade Jr. [9], the bond energy of a carbon-carbon double bond is about 611 $kJ.mol^{-1}$ while the single bond energy is about 347 $kJ.mol^{-1}$. Furthermore, Fahmi et al. reported that the C – C bond strength was weakened upon adsorbing onto the catalyst surface compared to when it was in gas phase [10].

Another important conclusion is that the intermediate species formed by dehydrogenation are strongly bonded to the surface of platinum, and consequently have sufficient time to react further with water to form oxide species.

5.5.4 High Temperature Hydrocarbon Fuel Cells

To date, the concept for low temperature hydrocarbon fuel cells has been based on the perturbation of equilibrium limitation of the thermal process to produce olefins from paraffins, and at the same time generate satisfactory current flow. Although conceptually achievable, kinetically, the process has been proven very difficult to implement.

Operation at low temperatures requires use of expensive noble metals as effective dehydrogenation catalysts. Noble metal catalysts that have been tried include platinum, palladium black and platinum-ruthenium black. However, none of these catalysts have provided improved performance in terms of larger and sustainable current flow under anhydrous conditions. At temperatures of 200 to 250°C, dehydrogenation of light alkanes

121

to alkenes is still not highly favorable. Further, when the same catalysts are used under humidified conditions, the products are CO and CO_2.

Because of these limitations on conversion of alkanes in low temperature fuel cells, I have now tried a new approach. Like previous case, perturbation of the equilibrium limitation was still attempted by removal of hydrogen as protons from catalyst active sites so that the electrochemical reaction will keep moving forward. In addition to this, another layer of catalyst was used for converting propane to propylene first through catalytic thermal dehydrogenation. This will produce hydrogen which will then diffuse and selectively adsorbed onto another catalyst layer for further electrochemical reaction. Activation of propane to undergo a dehydrogenation process is thermodynamically easier when compared to ethane. Consequently, propane was selected as fuel for this component of the study.

A modification was made to the anode structure. Two layers of catalyst were applied consisting of two platinum layers. One layer was directly applied onto the membrane surface, to serve as the catalyst layer for electrochemical reactions. For this layer, 5 $mg.cm^{-2}$ of phosphoric acid was added to serve as proton carrier across the electrode-membrane interface. Another layer was applied onto the external surface of the anode, and acted as a catalyst layer for thermal catalytic dehydrogenation process. A total of 100 mg of 20 wt% Pt/C was applied for this catalyst layer. Platinum was again used as the cathode electrocatalyst for O_2 gas.

Before fuel cells experiments were carried out, the effectiveness of Pt/C (20 wt%) as dehydrogenation catalyst was tested. Figure 5-26 shows the results obtained at different operating temperatures compared to theoretical H_2 generated from dehydrogenation of propane at equilibrium. The hydrogen concentration in the effluent increased with temperature, increasing rapidly over 250°C.

At temperatures lower than 200°C, particularly 150°C, no propylene was detected using G.C. analysis. Different catalyst loadings also affected the amount of hydrogen and propylene produced. Generally, the higher the platinum loading, the higher was the yield. Figure 5-27 shows the polarization curve obtained during cell operation. Clearly, cell performance improved as a result of the presence of thermally generated hydrogen. Hydrogen was selectively oxidized in preference to propane.
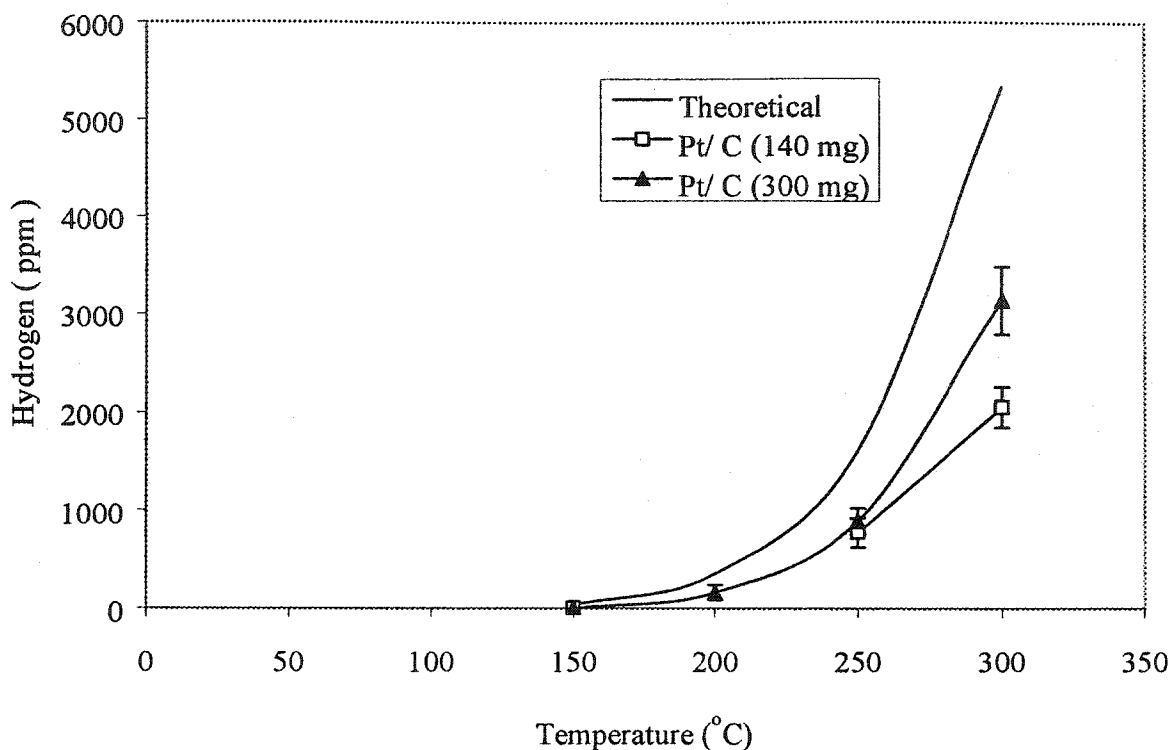
Figure 5-26 Variation of hydrogen produced from dehydrogenation reaction of C_3H_8 with temperatures at 1 atm pressure with different catalyst loadings.
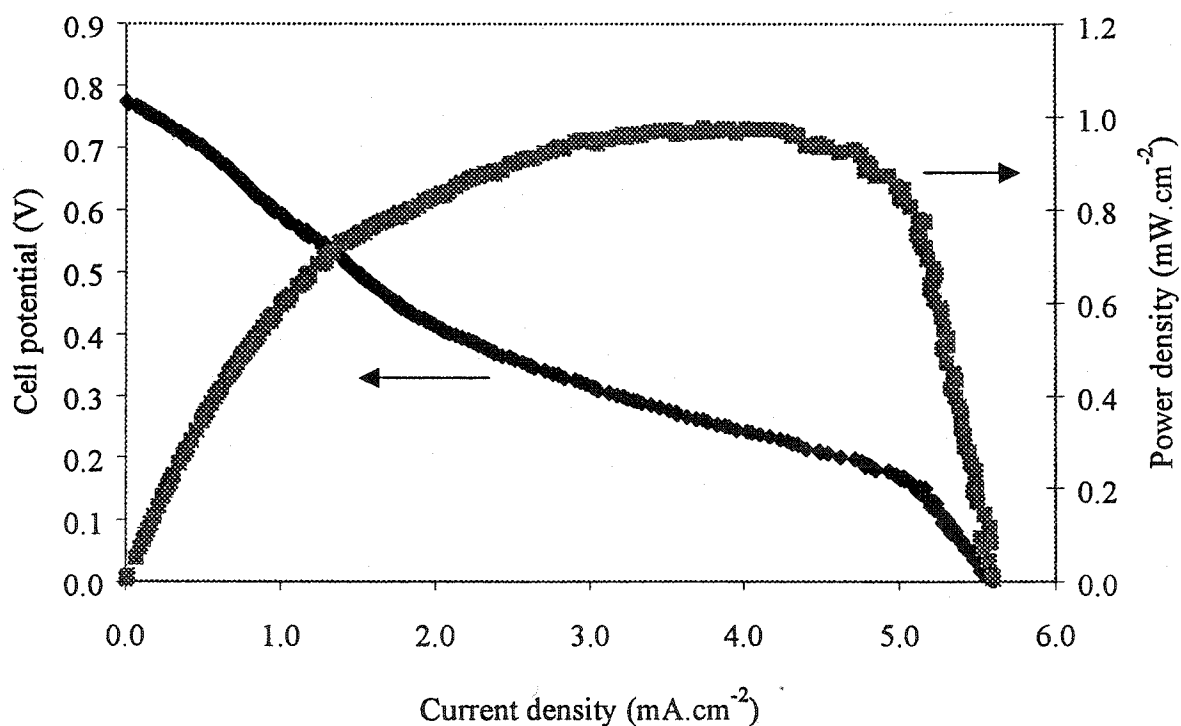
Figure 5-27 Polarization curve of C_3H_8-O_2 fuel cells at 215°C (anhydrous conditions) after applying two layers of platinum on different sides of anode (I.R. was 0.33 Ohm).

123

Figure 5-27 shows that there was an improvement in current density under anhydrous condition, compared to results shown in Figure 5-19. The sustainability of current flow was poor, as shown in Figure 5-28. When fuel cells were operated at OCV, formation of propylene was observed, using G.C. analysis. But, during operation at 200 mV, the propylene produced from the catalytic reaction diminished. This confirmed that, during fuel cell operation, propylene produced was retained strongly on the platinum surface by forming stable intermediate species.
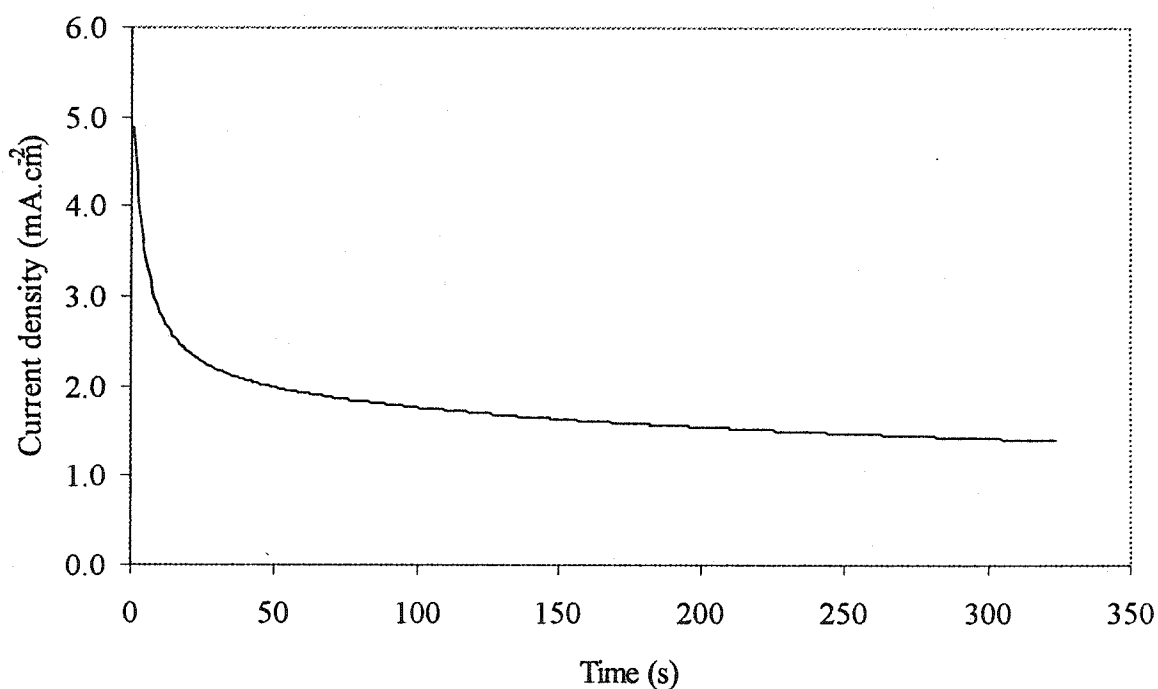
Figure 5-28 Sustainability of current flow at 200 mV during the C_3H_8-O_2 fuel cell operation at 215°C and 1 atm pressure.

The above results were consistent with the proposal that low temperature hydrocarbon fuel cells cannot produce large current flow (> 100 mA/ cm^2) because of the formation of very stable intermediate species on the catalyst surface. Thus the intermediate species had a poisoning effect, and blocked other reactants from adsorbing onto the catalyst surface.

Another cause of low current flow is a result of the equilibrium limitation. As shown in Figure 5-26, 5500 ppm of hydrogen is the maximum concentration that can be produced under equilibrium conditions by thermal dehydrogenation of propane at 300°C. Mass transport limitations as well as ionic resistance of membranes reduce the rate of

124

conversion of hydrogen. Mass transport limitation occurs because of equilibrium gradients established between bulk concentration and concentration of hydrogen near the catalyst surface.

Performance of an alkane fuel cell is a function of partial pressure of hydrogen, as shown by the Nernst equation for the half-cell reaction at the anode side for propane:

$$\Delta U_{Anode} = \Delta U^o_{Anode} - \frac{RT}{2F} \ln\left(\frac{P_{H_2} P_{C_3H_6}}{P_{C_3H_8}}\right) \qquad (5.9)$$

Dilution of hydrogen produced from the dehydrogenation process by incoming propane, which predominate in the anode atmosphere, further reduces the current flow of fuel cells. So, to improve the kinetics, high temperature fuel cell is preferred, in which thermal dehydrogenation can produce higher amounts of hydrogen. Hydrogen is more reactive than propane or propylene and thus, it will be selectively and rapidly adsorbed onto the catalyst surface. This adsorbed hydrogen will be oxidized to form protons, thus leaving propylene as the product.

Figures 5-29 and 5-30 show the effect of hydrogen partial pressure on the amount of electricity generated. Dilution with N_2 gas was used to mimic hydrocarbon fuel cells operation. Figure 5-29 shows a mass control region at current densities over 25.0 mA.cm^{-2} for a stream containing 2% H_2. Figure 5-30 shows that the onset of a mass controlling region occurred at higher current density, approximately 170 mA.cm^{-2} for a stream containing 13% H_2. Explicitly, higher concentration of hydrogen resulted in higher current flow. It should be noted that all hydrogen may not have been consumed during the fuel cell operations. For the experiment shown in Figure 5-29, about 80% (nearly 1.6% of H_2 was consumed out of 2% present initially) of hydrogen was consumed at values before the mass transfer region. In total, approximately 90% of hydrogen was consumed (only 0.2% of H_2 in tailing gas out of 2% initially). For the Figure 5-30, 73% of hydrogen was consumed (only 3.5% of H_2 in tailing gas) at values before the mass transport region. In total, about 84% of hydrogen was consumed (2% of H_2 in tailing gas out of 13% H_2 present initially) to produce that large current flow. These experiments showed that high temperature fuel cells can be used to generate large current flow and obtain value-added products by conversion of alkane feed because thermal dehydrogenation of propane can produce high amount of hydrogen.

125
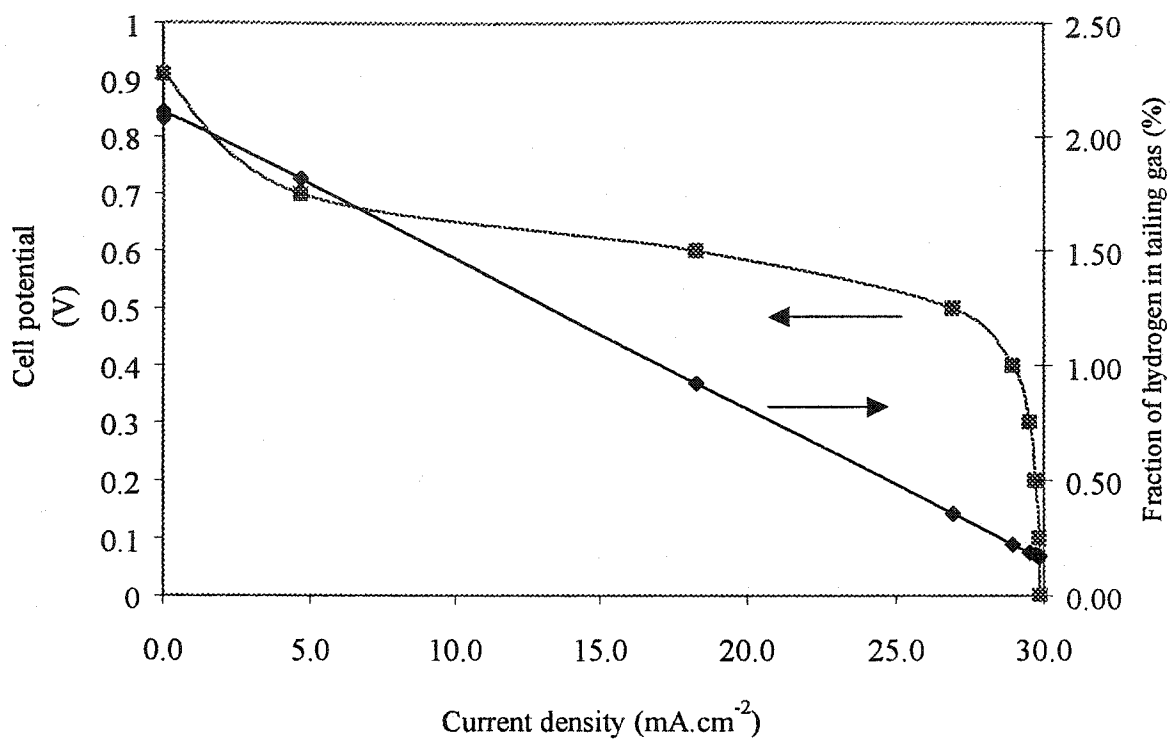
Figure 5-29 Polarization curve of hydrogen (2 vol%) diluted with nitrogen at 150°C, and the concentration of hydrogen in tailing gas (I.R. was 0.36 Ohm).
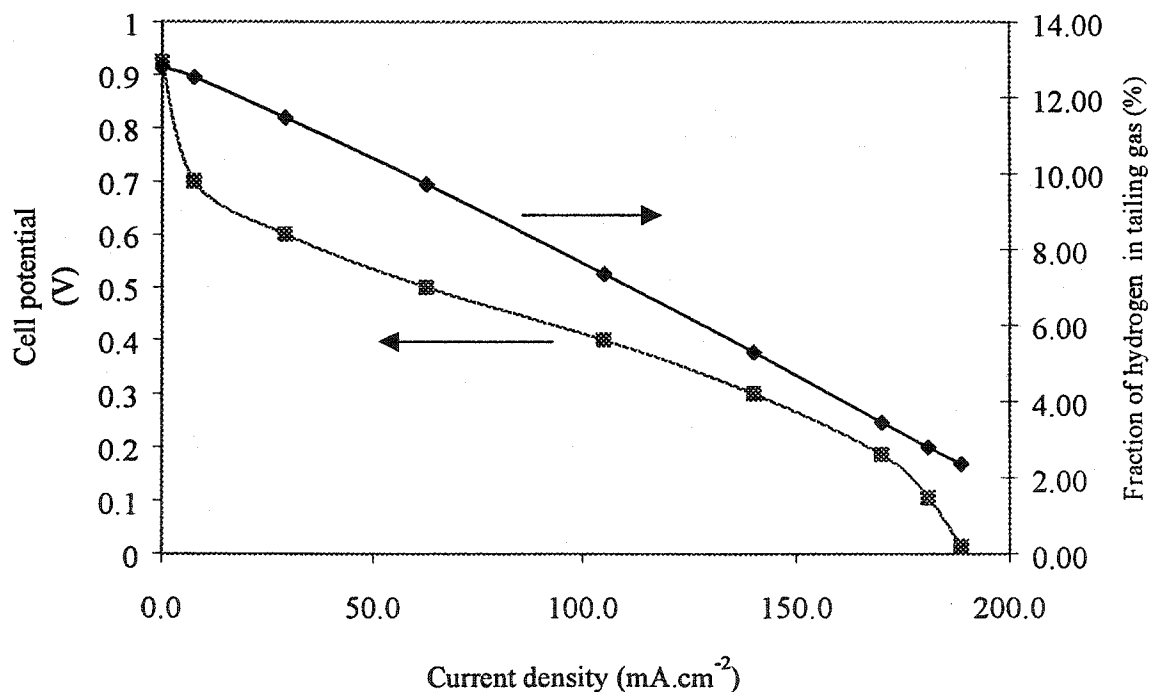
Figure 5-30 Polarization curve of hydrogen (13 vol%) diluted with nitrogen at 150°C, and the concentration of hydrogen in tailing gas (I.R. was 0.36 Ohm).

126

Figure 5-31 shows the linear relationship between H_2 concentrations in the inlet stream and current flow. The equation obtained can be used to predict the current density of hydrocarbon fuel cells operated at high temperatures, at which dehydrogenation of propane can produce significant amounts of hydrogen.
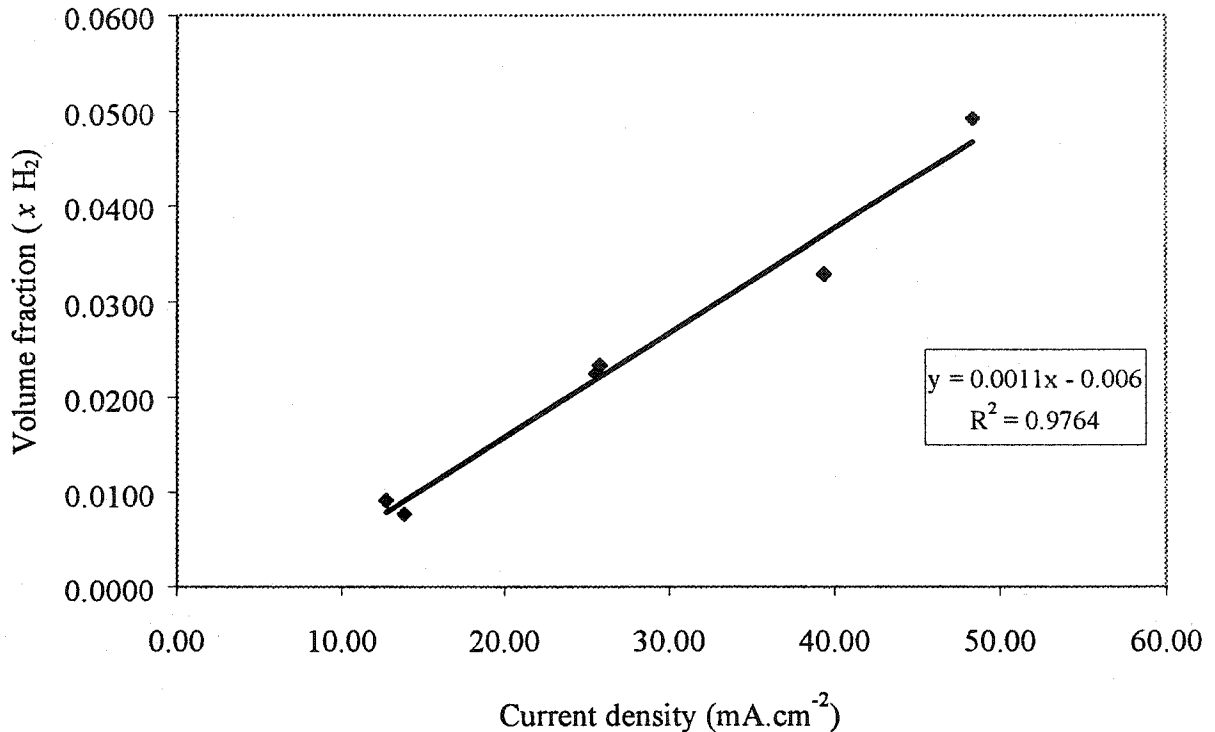
Figure 5-31 Effect of H_2 concentration on current density at 150°C under anhydrous conditions. (I.R. was 0.38 Ohm).

Figure 5-32 shows the effect of theoretical hydrogen concentration produced from the dehydrogenation of C_3H_8 with reaction temperature at 1 atm pressure. Obviously, high temperature favor production of H_2. At temperatures approaching 900°C, nearly all propane will be dehydrogenated to form approximately equimolar amounts of H_2 and C_3H_6, with smaller amounts of by-products. If the same conditions are as shown in Figure 5-31, then the derived equation can be used to predict the current density, assuming a constant I.R. of 0.38 Ohm. Apparently, an operating temperature lower than 500°C is not sufficient to produce a high enough H_2 concentration to generate a current density larger than 100 $mA.cm^{-2}$. The fraction of H_2 at temperatures over 500°C is at least 0.14 and the current density that can be generated increases to about 500 $mA.cm^{-2}$ at 900°C. Thus the

127

equation derived from data in Figure 5-31 suggests that, with appropriate catalysts, high current densities can be achieved using high temperature fuel cells for conversion of alkanes using thermal dehydrogenation reactions.
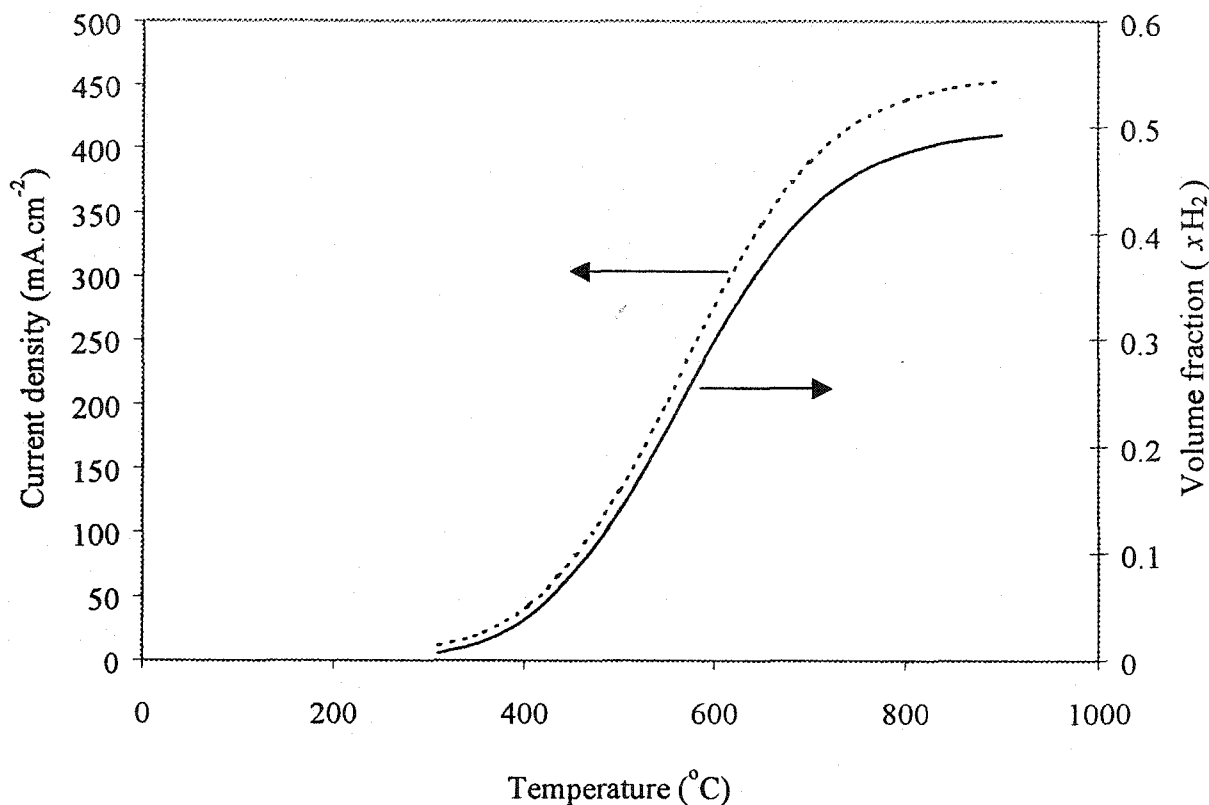
Figure 5-32 Predicted values for hydrogen concentration produced from dehydrogenation of C_3H_8 and current density, assuming conditions presented in Figure 5-30.

CONCLUSIONS

Conversion of ethane and propane to the corresponding alkenes in low temperature fuel cell using H_3PO_4 doped PBI polymer membranes was not feasible under anhydrous conditions. Under these conditions, formation of very stable intermediate species poisoned the surface of noble metal catalysts. The intermediate species could not react further into desorbable final products, thus preventing further electrochemical reactions. As a result, the stable intermediate species, which were retained strongly by platinum, remained on the catalyst surface and blocked further access by fresh paraffins. So, a small and unsustainable current flow was obtained.

In the presence of water, electrochemical reactions, especially at the anode side, allowed further reaction to form CO and CO_2 as products that were easily detached from the catalyst surface. Thus, fresh reactant was continuously chemisorbed onto the catalyst surface, resulting in significantly higher and sustainable current density. It was also shown from operation of a H_2-C_2H_4 fuel cell that adsorption of C_2H_6 was poor especially below 300 mV.

High temperature fuel cells can generate larger current flows and produced olefins as value-added products. Thermodynamically, high temperatures are more suitable for thermal dehydrogenation of paraffins.

REFERENCES

[1]   Smith, J.M., H.C. van Ness and M.M. Abbott, "Introduction to Chemical Engineering Thermodynamic", 5th Edition, McGraw-Hill International Editions, Singapore (1996), pp. 638.

[2]   Otsuka, T., T. Ina and I. Yamanaka, "The partial oxidation of methanol using a fuel cells reactor", Appl. Catal. A: General, 247, 219 – 229 (2003).

[3]   Bodke, A.S., D.A. Olschki, L.D. Schmidt and E. Ranzi, "High selectivities to ethylene by partial oxidation of ethane', Science, 285, 712 – 715 (1999).

[4]   Gorer, A., "Platinum-Ruthenium-Nickel alloy for use as a fuel cells catalyst", U. S. Patent #6,517,965 (2003).

[5]   Uzio, D., B. Didillon and E. Pellier, "Catalyst comprising an element from groups 8, 9 or 10 with good accessibility, and its use in a paraffin dehydrogenation process", U. S. Patent #6,498,280 (2002).

[6]   Savadogo, O., and F.J.R. Varela, "Low-temperature direct propane polymer electrolyte membranes fuel cells (DPFC)", J. New Mat. Electrochem. Systems, 4, 93 – 97 (2000).

[7]   Zarea, F., "Probing catalytic reactions at surface", Prog. in Surf. Sci., 69, 1 – 98 (2001).

[8]   Kemball, C., and H.S. Taylor, "The catalytic decomposition of ethane and ethane-hydrogen mixtures", J. Am. Chem. Soc., 70 (1), 345 – 351 (1948).

[9]   Wade, Jr.L.G., "Alkenes: Structure and synthesis", in "Organic chemistry", Prentice-Hall, Inc., Englewood Cliffs, NJ (1987), pp. 241.

[10]   Fahmi, A., and R.A. van Santen, "Density functional study of ethylene adsorption on palladium clusters", J. Phys. Chem., **100**, 5676 – 5680 (1996).

CHAPTER 6

CONCLUSIONS AND RECOMMENDATIONS
FOR FUTURE WORK

6.1 CONCLUSIONS

H_3PO_4 doped PBI membranes have been prepared using a high molecular weight PBI polymer powder, and have been shown to be suitable for use in both low and intermediate temperature fuel cells.

The solution casting method with mild heat treatment was used to prepare membranes having a PBI matrix with a dense microstructure, as determined using optical microscope analysis for comparison of PBI and Nafion™ membranes. Both membranes exhibited the same microstructure morphology, with only tiny micropores.

Doping with H_3PO_4 was performed using the immersion method. H_3PO_4 was chosen as electrolyte. It is a very hygroscopic material, and self-dissociates under anhydrous conditions. Hence, by loading H_3PO_4 onto PBI matrix, membranes were fabricated that were capable of being operated under anhydrous conditions or with very low levels of humidification. Doping time was reduced appreciably by increasing the temperature, to provide membranes with good ionic conductivity, comparable to that of membranes doped at room temperature for extended periods of 3 to 10 days reported earlier by other authors.

It was also shown that these PBI membranes remained active during operation over several days at temperatures up to 250°C. The stability of the ionic conductivity was ensured by operation under conditions of very low humidification, or by partial retention of water generated during continuous running of fuel cells. Furthermore, prolonged operation at 250°C in severely oxidizing and reducing environments, as found in H_2-O_2

131

fuel cells, caused no chemical decomposition of these PBI membranes. DSC analysis of used and new membranes showed that no thermal or chemical degradation occurred during use of H_3PO_4 doped PBI membranes.

H_3PO_4 doped PBI membranes also provided better resistance to gas permeation than commercial Nafion™ membranes, particularly to hydrogen and oxygen, at all temperatures tested. Thus PBI membranes prepared using the solution casting method had superior morphology as well as superiour thermal and chemical stability when compared to Nafion™ membranes.

H_3PO_4 doped PBI membranes prepared from high M.W. PBI performed well in H_2-O_2 and hydrocarbon-O_2 fuel cells. Large current densities and high open circuit potential were obtained using H_2-O_2 fuel cells under anhydrous conditions. This confirmed that the design of the single cell constructed in house was satisfactory, and that the design and materials used prevented gas leakage. The performance of these fuel cells was enhanced through the production of water vapor at the cathode side. Water vapor kept the membranes hydrated through adsorbtion by the hygroscopic phosphoric acid component of the PBI matrix.

Hydrocarbon-O_2 fuel cells developed good cell potentials, typically in the range of 600 to 700 mV, over a range of conditions. However, the product slate depended on temperature. At low temperatures, the current density was low and the OCV was small under anhydrous conditions. In contrast, a significant current flow was obtained when the anode feed was slightly humidified. High humidification was undesirable, due to the highly hygroscopic nature of H_3PO_4. At temperatures below 200°C, oxidation of paraffins at the anode side in the presence of H_2O produced only CO and CO_2, the proportions of each depending on the temperature and potential of the cell. The mechanism under these conditions appeared to involve formation of strongly bound hydrocarbon fragments at surface active sites, followed by reaction with water to 'clean' the surface of the noble metal catalyst, and thereby generate fresh sites for reaction with hydrocarbon. Without participation of water in the electrochemistry reaction, negligible current flow was obtained. Thus, at low temperatures the system behaved as a direct hydrocarbon fuel cell.

In contrast, when the same fuel cell was operated with propane as feed at high temperatures with two layers of catalyst applied at the anode side, current density has improved. However, it was not sustainable over prolonged operating time.

6.2 RECOMMENDATIONS FOR FUTURE WORK

It is recommended that the present work be extended to the investigation of conversion of light hydrocarbons in high temperature fuel cells, for sustainable co-generation of electrical power and olefins.

Operation at high temperature permits utilization of metal catalysts other than noble metals for effective dehydrogenation of light paraffins, particularly for conversion of ethane and propane. This may reduce capital costs associated with fuel cell manufacture, since noble metals that are normally employed in low temperature fuel cells, including platinum, ruthenium and palladium, are expensive.

Operating costs will be reduced by utilization of heat energy of the high temperature effluent, which is impractical for low temperature systems.

Lower temperature fuel cells normally utilize strong acid or polymers having acidic substituents as the electrolyte. The acidic environment hinders desorption of olefins from catalyst surface. The π bond of olefins, which is rich in electrons, binds strongly to the resulting electron deficient catalyst sites. As a result, intermediate species will form that are strongly bound to the active sites, thereby blocking the catalyst surface from further adsorption of fresh reactants. The strong catalyst-intermediate interaction may also be a factor in cracking the $C - C$ bonds of the hydrocarbon feed to form C_1 fragments, leading to formation of CO and CO_2 at low temperatures. In contrast, high temperature fuel cells normally use ceramic proton conductors. In these systems, there are no strong acid effects. A more basic metal catalyst may be preferred, capable of extracting hydrogen from paraffins. Another advantage would accrue because basic materials are rich in electrons, leading to reduced propensity for disruption of the original carbon backbone structure of the feed hydrocarbon, thus retaining that structure in the olefin product, and promoting desorption of that product.

133

From thermodynamic considerations, higher temperatures, especially greater than 500°C, provide favorable conditions for production of unsaturated hydrocarbon products in a thermal dehydrogenation step. Hydrogen has been identified as mostly responsible species for large current flow because of its high reactivity. It is selectively oxidized to protons at the anode side, thus driving the reaction and sustaining current flow. Therefore, high temperature fuel cells are expected to generate higher current density concurrently with conversion of hydrocarbon feed to value-added products.

134

APPENDIX A1

Table A1-1 Experimental results for O_2 permeating through dry, untreated Nafion™ membranes.

Temperature °C	Membrane Area, m^2	Membrane thickness, m	ΔP O_2 (Pa)	Molar Flux O_2 (mol sec.$^{-1}$cm^{-1})	Permeability of O_2 (mol sec^{-1}m^{-1}Pa^{-1})
25	0.000314	0.0002	101349.5	2.26E-11	2.23E-14
25	0.000314	0.0002	137891.9	2.28E-11	1.65E-14
25	0.000314	0.0002	176503.1	2.11E-11	1.20E-14
25	0.000314	0.0002	215803.7	1.98E-11	9.16E-15
50	0.000314	0.0002	101349.2	2.42E-11	2.39E-14
50	0.000314	0.0002	133755.2	2.15E-11	1.61E-14
50	0.000314	0.0002	182708.3	2.14E-11	1.17E-14
50	0.000314	0.0002	215113.1	2.56E-11	1.19E-14
80	0.000314	0.0002	101349.2	2.36E-11	2.33E-14
80	0.000314	0.0002	141339.2	2.31E-11	1.63E-14
80	0.000314	0.0002	177881.1	2.59E-11	1.45E-14
80	0.000314	0.0002	219940.2	2.13E-11	9.67E-15
120	0.000314	0.0002	101349	2.51E-11	2.47E-14
120	0.000314	0.0002	133063.9	3.19E-11	2.39E-14
120	0.000314	0.0002	173742.8	3.39E-11	1.95E-14
120	0.000314	0.0002	207525	4.82E-11	2.32E-14

135

Table A1-2 Experimental results for H_2 permeating through dry, untreated Nafion™ membranes.

Temperature °C	Membrane Area, m²	Membrane thickness, m	Δ P H₂ (Pa)	Molar Flux H₂ (mol sec.⁻¹cm⁻¹)	Permeability of H₂ (mol sec.⁻¹m⁻¹Pa⁻¹)
25	0.0001	0.0002	101350.81	1.99208E-11	1.96553E-14
25	0.0001	0.0002	137547.99	2.38604E-11	1.73469E-14
25	0.0001	0.0002	172710.51	3.0639E-11	1.77401E-14
40	0.0001	0.0002	101349.16	3.16872E-11	3.12654E-14
40	0.0001	0.0002	135132.68	3.90541E-11	2.89006E-14
40	0.0001	0.0002	178224.28	4.58843E-11	2.57453E-14
60	0.0001	0.0002	101347.19	4.59909E-11	4.53795E-14
60	0.0001	0.0002	137887.61	6.1192E-11	4.43782E-14
60	0.0001	0.0002	172016.62	6.18325E-11	3.59456E-14
80	0.0001	0.0002	101344.99	6.27669E-11	6.19339E-14
80	0.0001	0.0002	140298.2	7.92953E-11	5.65191E-14
80	0.0001	0.0002	176835.57	1.17309E-10	6.63378E-14
100	0.0001	0.0002	101341.29	9.27866E-11	9.15585E-14
100	0.0001	0.0002	138566.65	1.38877E-10	1.00224E-13
100	0.0001	0.0002	169577.51	2.48243E-10	1.46389E-13
120	0.0001	0.0002	101333.96	1.43844E-10	1.4195E-13
120	0.0001	0.0002	134410.14	2.77028E-10	2.06107E-13
120	0.0001	0.0002	177113.33	3.14532E-09	1.77588E-12
130	0.0001	0.0002	101298.36	3.99038E-10	3.93923E-13

136

Table A1-3 Experimental results for O_2 permeating through treated PBI membranes.

Temperature °C	Membrane Area, m^2	Membrane thickness, m	ΔP O_2 (Pa)	Molar Flux O_2 (mol sec.$^{-1}$cm^{-1})	Permeability of O_2 (mol sec.$^{-1}$m^{-1}Pa^{-1})
25	0.0002268	0.0001	101350.01	1.37044E-11	1.35219E-14
25	0.0002268	0.0001	135823.72	1.44976E-11	1.06738E-14
25	0.0002268	0.0001	177192.76	1.3591E-11	7.67018E-15
25	0.0002268	0.0001	206840.52	1.36101E-11	6.58E-15
50	0.0002268	0.0001	101349.4	1.5755E-11	1.55453E-14
50	0.0002268	0.0001	137202.61	1.50444E-11	1.09651E-14
50	0.0002268	0.0001	172366.24	1.46374E-11	8.49204E-15
50	0.0002268	0.0001	204771.53	1.54873E-11	7.56319E-15
80	0.0002268	0.0001	101349.73	1.4765E-11	1.45684E-14
80	0.0002268	0.0001	139271.34	1.37039E-11	9.8397E-15
80	0.0002268	0.0001	171677.07	1.30411E-11	7.59628E-15
80	0.0002268	0.0001	209597.8	1.55802E-11	7.43339E-15
120	0.0002268	0.0001	101349.33	1.59379E-11	1.57257E-14
120	0.0002268	0.0001	139271.08	1.46335E-11	1.05072E-14
120	0.0002268	0.0001	175124.82	1.17054E-11	6.68406E-15
120	0.0002268	0.0001	217182.68	1.32577E-11	6.10441E-15
150	0.0002268	0.0001	101349.59	1.52558E-11	1.50526E-14
150	0.0002268	0.0001	137202.6	1.47765E-11	1.07698E-14
150	0.0002268	0.0001	173745.07	1.46944E-11	8.45748E-15
150	0.0002268	0.0001	209598.27	1.40414E-11	6.69922E-15
166	0.0002268	0.0001	101350.17	1.31262E-11	1.29513E-14
180	0.0002268	0.0001	101350	1.37824E-11	1.35988E-14
190	0.0002268	0.0001	101345.45	3.1377E-11	3.09604E-14
200	0.0002268	0.0001	101344.37	3.54069E-11	3.49372E-14
200	0.0002268	0.0001	101328.84	9.68342E-11	9.55643E-14
200	0.0002268	0.0001	101320.84	1.26129E-10	1.24485E-13

Table A1-4 Experimental results for H_2 permeating through treated PBI membranes.

Temperature °C	Membrane Area, m^2	Membrane thickness, m	ΔP H_2 (Pa)	Molar Flux H_2 (mol sec.$^{-1}$cm^{-1})	Permeability of H_2 (mol sec.$^{-1}$m^{-1}Pa^{-1})
25	0.00011314	0.000275	101352.1	1.32537E-11	1.30769E-14
25	0.00011314	0.000275	133756.5	2.29563E-11	1.71628E-14
25	0.00011314	0.000275	165470.5	4.16653E-11	2.51799E-14
25	0.00011314	0.000275	101351.4	1.95727E-11	1.93117E-14
50	0.00011314	0.000275	101351.7	1.62725E-11	1.60554E-14
50	0.00011314	0.000275	140306.0	2.72156E-11	1.93973E-14
80	0.00011314	0.000275	101350.0	3.11464E-11	3.07315E-14
80	0.00011314	0.000275	132722.1	2.46425E-11	1.8567E-14
80	0.00011314	0.000275	180294.7	3.90506E-11	2.16593E-14
120	0.00011314	0.000275	101348.9	4.12207E-11	4.0672E-14
120	0.00011314	0.000275	134787.9	4.81138E-11	3.56959E-14
120	0.00011314	0.000275	202701.2	5.15923E-11	2.54524E-14
150	0.00011314	0.000275	101350.4	2.74772E-11	2.71111E-14
150	0.00011314	0.000275	143750.5	5.29517E-11	3.68358E-14
150	0.00011314	0.000275	181671.1	6.05693E-11	3.33401E-14
170	0.00011314	0.000275	101350.6	2.70168E-11	2.66567E-14
170	0.00011314	0.000275	144442.8	2.96784E-11	2.05468E-14
170	0.00011314	0.000275	151337.8	2.71477E-11	1.79385E-14
170	0.00011314	0.000275	155474.7	2.72523E-11	1.75284E-14
200	0.00011314	0.000275	101346.6	6.05438E-10	5.9776E-13

138

APPENDIX A2

<u>1st Calculations Method: Assuming electrochemical reaction in series at anode side</u>

Sample calculations are shown here for C_2H_6-O_2 fuel cell:

For inlet volumetric flowrate, $\dot{V} = 1.0 \times 10^{-6}$ $m^3.s^{-1}$ at STP

From Ideal Gas Law; $P\dot{V} = nRT$

where R = Gas constant

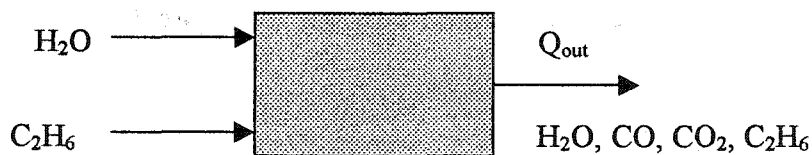T = Absolute temperature (K)

P = Pressure of C_2H_6

n = Molar flowrate

Thus; $n = 4.08968942 \times 10^{-5}$ $mol.s^{-1}$

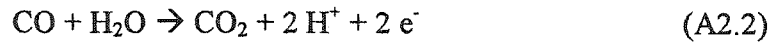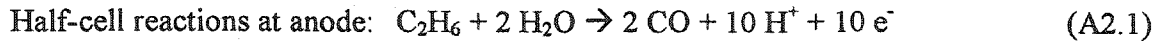<u>Performing mass balance at anode side:</u>

For example, from G.C. analysis:

[CO] = 780 ppm

[CO_2] = 440 ppm

<u>Assumptions made:</u>

i)   Amount of water is negligible and is excluded from mass balance calculations.

ii)   The following half-cell reactions, (A2.1) and (A2.2) happened at the anode side with further assumption that C_2H_6 was first converted to CO and part of CO later on reacted to produce CO_2.

139

Half-cell reactions at anode: $C_2H_6 + 2\ H_2O \rightarrow 2\ CO + 10\ H^+ + 10\ e^-$ (A2.1)

$$CO + H_2O \rightarrow CO_2 + 2\ H^+ + 2\ e^-$$ (A2.2)

Perform atomic balance on C atom:

Atom C_{in} = Atom C_{out}

$2 \times n$ = {Molar fraction of CO at outlet $\times Q_{out}$} + {Molar fraction of $CO_2 \times Q_{out}$} + {Molar fraction of $C_2H_6 \times Q_{out}$}

{$2 \times 4.08968942 \times 10^{-5}$ mol.s^{-1}} = $0.78 \times 10^{-3} Q_{out} + 0.44 \times 10^{-3}\ Q_{out}$ + {$2 \times (1 - 0.78 \times 10^{-3} - 0.44 \times 10^{-3}) \times Q_{out}$

{$2 \times 4.08968942 \times 10^{-5}$ mol.s^{-1}} = $0.78 \times 10^{-3} Q_{out} + 0.44 \times 10^{-3}\ Q_{out}$ + {$2 \times 0.99878 \times Q_{out}$}

$Q_{out} = 4.09219 \times 10^{-5}$ mol.s^{-1}

Thus; $(C_2H_4)_{out} = Q_{out} \times 0.99878$

$= 4.0872 \times 10^{-5}$ mol.s^{-1}

$(C_2H_4)_{converted}\ = n - 4.08719 \times 10^{-5}$ mol.s^{-1}

$= 2.496 \times 10^{-8}$ mol.s^{-1}

$(CO)_{generated} = 2 \times (C_2H_4)_{converted} = 4.992 \times 10^{-8}$ mol.s^{-1}

$(CO_2)_{generated} = 0.44 \times 10^{-3} \times 4.09219 \times 10^{-5}$ mol.s$^{-1} = 1.8 \times 10^{-8}$ mol.s^{-1}

Calculations for current flow:

Current flow = Current produced by (A2.1) + Current produced by (A2.2)

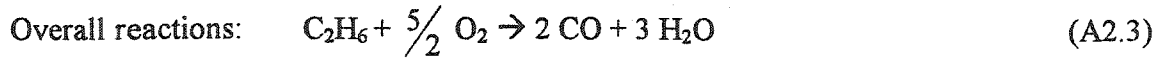= {No. of electrons produced by (A2.1) $\times F \times (C_2H_4)_{converted}$} + {No. of electrons produced by (A2.2) $\times F \times (CO_2)_{generated}$

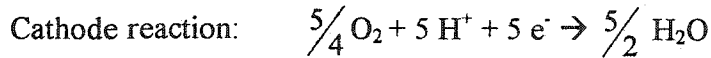= $96500 \times 10 \times 2.496 \times 10^{-8} + 96500 \times 2 \times 1.8 \times 10^{-8}$

= **27.56 mA**

2nd Calculations Method: Assuming parallel reactions at anode side

Unlike first case where we assume the reactions are in series, in this case, we assume that electrochemistry reactions took place were parallel reactions where CO and CO_2 are competing with each other to get converted from C_2H_6.
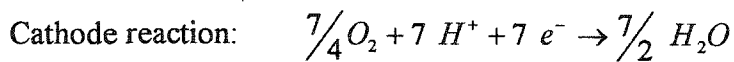
140

Overall reactions: $\quad C_2H_6 + \frac{5}{2} O_2 \rightarrow 2\ CO + 3\ H_2O$ $\qquad\qquad$ (A2.3)

$\qquad\qquad\qquad\qquad C_2H_6 + \frac{7}{2} O_2 \rightarrow 2\ CO_2 + 3\ H_2O$ $\qquad\qquad$ (A2.4)

Half-cell reaction for (A2.3):

Cathode reaction: $\quad \frac{5}{4} O_2 + 5\ H^+ + 5\ e^- \rightarrow \frac{5}{2} H_2O$

Anode reaction: $\quad$ If cathode reaction needs 5 mol of proton, the reaction at the anode must release 5 H^+.

Half-cell reaction for (A2.4):

Cathode reaction: $\quad \frac{7}{4} O_2 + 7\ H^+ + 7\ e^- \rightarrow \frac{7}{2} H_2O$

Anode reaction: $\quad$ As in reaction (A2.3), 7 mol of H^+ are needed to accomplish this reaction.

Remarks: $\quad$ The written overall reactions are based on 2 mol of CO and CO_2 produced. As for the half-cell reactions, they are based on 1 mol of CO and CO_2 generated.

Calculations for current flow:

Early calculations have shown that conversion is low, so, for simplicity, we can just assume that basically, Q_{out} is equal to the inlet $Q_{C_2H_6}$

Thus;

CO produced $\quad = 0.00078 \times 4.08968942 \times 10^{-5}\ mol.s^{-1}$

$\qquad\qquad\qquad = 3.19 \times 10^{-8}\ mol/\ s$

CO_2 produced $= 0.00044 \times 4.08968942 \times 10^{-5}\ mol.s^{-1}$

$\qquad\qquad\qquad = 1.80 \times 10^{-8}\ mol/\ s$

Current flow $\quad =$ Total current produced by both reactions in parallel

$\qquad\qquad\qquad = (96500 \times 3.19 \times 10^{-8} \times 5) + (96500 \times 1.80 \times 10^{-8} \times 7)$

$\qquad\qquad\qquad = \mathbf{27.55\ mA}$

141